



January 2018

Novel Bio-Kinetic Modeling And 2,3-Butanediol Productivity Optimization Of Clostridium Autoethanogenum

Timothy Taylor

Follow this and additional works at: <https://commons.und.edu/theses>

Recommended Citation

Taylor, Timothy, "Novel Bio-Kinetic Modeling And 2,3-Butanediol Productivity Optimization Of Clostridium Autoethanogenum" (2018). *Theses and Dissertations*. 2361.
<https://commons.und.edu/theses/2361>

This Thesis is brought to you for free and open access by the Theses, Dissertations, and Senior Projects at UND Scholarly Commons. It has been accepted for inclusion in Theses and Dissertations by an authorized administrator of UND Scholarly Commons. For more information, please contact zeinebyousif@library.und.edu.

NOVEL BIO-KINETIC MODELING AND 2,3-BUTANEDIOL
PRODUCTIVITY OPTIMIZATION OF CLOSTRIDIUM
AUTOETHANOGENUM

by

Timothy Micheal Taylor
Bachelor of Science, University of North Dakota, 2018

A Thesis

Submitted to the Graduate Faculty

of the

University of North Dakota

in partial fulfillment of the requirements

for the degree of

Master of Science

Grand Forks, North Dakota

August
2018

This thesis, submitted by Timothy Taylor in partial fulfillment of the requirements for the Degree of Master of Science from the University of North Dakota, has been read by the Faculty Advisory Committee under whom the work has been done and is hereby approved.



Dr. Ali Alshami



Dr. Michael Mann



Dr. Edward Kolodka

This thesis is being submitted by the appointed advisory committee as having met all of the requirements of the School of Graduate Studies at the University of North Dakota and hereby is approved.



Dr. Grant McGimpsey
Dean of the School of Graduate Studies

July 24, 2018
Date

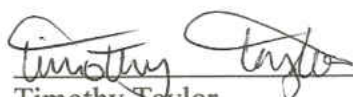
Permission

Title NOVEL BIO-KINETIC MODELING AND 2,3-BUTANEDIOL
PRODUCTIVITY OPTIMIZATION OF CLOSTRIDIUM
AUTOETHANOGENUM

Department Chemical Engineering

Degree Master of Science

In presenting this thesis in partial fulfillment of the requirements for a graduate degree from the University of North Dakota, I agree that the library of this University shall make it freely available for inspection. I further agree that permission for extensive copying for scholarly purposes may be granted by the professor who supervised my thesis work or, in his absence, by the Chairperson of the department or the dean of the School of Graduate Studies. It is understood that any copying or publication or other use of this thesis or part thereof for financial gain shall not be allowed without my written permission. It is also understood that due recognition shall be given to me and the University of North Dakota in any scholarly use which may be made of any material in my thesis.



Timothy Taylor

07/27/2018

Date

Acknowledgments

I wish to express my sincere appreciation to the members of my advisory committee; Dr. Ali Alshami, Dr. Michael Mann, and Dr. Edward Kolodka, for their guidance and support during my time at the University of North Dakota. Deep admiration goes to the Institute of Energy Studies for their consistent help with the gasification system. I would like to thank Marc Kurz, from the Energy and Environmental Research Center in Grand Forks, ND, for his generosity with the initial gas chromatography readings. I would like to thank Dave Hirschmann for his help with setting up the compression system and for sharing his safety knowledge and lessons. Other graduate students and personnel that I would like to personally thank for their assistance are Kris Keller, Junior Nesah, Harry Feilen, Srikanth Vijjamarrri, and Tanner Pearson

Table of Contents

Chapter 1 State of the Art and Perspective of Biologically Producing 2,3-BDO via Coal to Liquid (CTL) Fermentation Technology	1
1.1 Introduction	1
1.2 Syngas Fermentation	2
1.2.a Advantages	2
1.2.b State of the Art.....	3
1.3 Future Direction	5
1.4 Syngas Production from Coal Gasification	6
1.5 Biochemistry of Gas Fermentation	7
1.6 Organisms and Products.....	9
1.7 Derivatives of 2,3-BDO	10
1.8 Optimization.....	12
1.9 Product Recovery	15
1.10 Summary	17
References	19
Chapter 2 Biological Kinetics on Carbon Monoxide and D-xylose of a 2,3-Butanediol Producing Bacterium: Clostridium autoethanogenum.....	24
Abstract	24
2.1 Introduction	25

2.2 Materials, Methods, and Equipment	26
2.2.a Microorganism.....	26
2.2.b Inoculation and Growth Curve	27
2.2.c Spectrophotometer Calibration Curve	28
2.3 Theory and Calculation	28
2.3.a Growth Kinetics	28
2.3.b Statistical Treatment of Experimental Data	31
2.4 Results and Analysis	31
2.4.a Spectrophotometer Calibration Curve	31
2.4.b Growth Kinetics with D-xylose: No Inhibition.....	32
2.4.c Dual Substrate Growth: D-xylose and Carbon Monoxide.....	35
2.4.d Growth Kinetics with D-xylose: Inhibition.....	36
2.5 Discussion	38
2.6 Conclusions	39
References	40
Chapter 3 Syngas Formation, Compression, and Products with <i>C. autoethanogenum</i>	44
Abstract	44
3.1 Introduction	44
3.2 Materials, Method, and Equipment.....	45
3.2.a Overview of Whole Process	45
3.2.b Overall Gasification System.....	45
3.1.b Gasification Operation.....	47
3.1.c Compression System	48

3.1.d Medium Preparation, Bioreactor Set-up, and Inoculation.....	49
3.1.e Growth Curve and Product Analysis	50
3.2 Results and Discussion.....	51
3.2.a Syngas Production	51
3.3.b C. autoethanogenum Growth Curve.....	52
3.3.c 2,3-BDO and Ethanol Rate of Formation Analyses	53
3.4 Conclusion.....	55
References	56
Chapter 4 Product Formation with Design of Experimental Analysis	58
Abstract	58
4.1 Introduction	58
4.2 Materials, Method, and Equipment.....	60
4.2.a Microorganism.....	60
4.2.b Bioreactor Inoculation and Set-up.....	60
4.2.c Bioreactor Fractional Factorial Design.....	61
4.2.d Product Analytic Methods	63
4.3 Results and Discussion.....	65
4.3.a Fractional Factorial Design.....	65
4.3.b Optimum Product Production.....	69
4.3.c 2,3-BDO Rate of Formation Analysis	72
4.3.d Ethanol Rate of Formation Analysis	72
4.4 Conclusion.....	73
Chapter 5 Conclusions and Prospects.....	78

Appendix A Raw Data and Figures A-1

List of Figures

Figure 1-1: Reaction pathway from hexoses, pentoses, hydrogen and carbon dioxide, and carbon monoxide to Acetyl-CoA[27].	8
Figure 1-2: Wood-Ljungdahlii pathway to produce 2,3-BDO, lactate, ethanol, and acetate[13].....	9
Figure 1-3: 2,3-BDO derivatives through dehydration, dehydrogenation, ketalization, and esterification[3].	11
Figure 1-4: Optimal temperature range for bacteria[40].....	14
Figure 1-5: Reaction equation of n-butylaldehyde and 2,3-BDO[49].	16
Figure 1-6: Reaction distillation and separation process of 2,3-BDO[49].	17
Figure 2-1: Non-linear regression calibration curve of cell concentration versus OD ₆₀₀	32
Figure 2-2: D-xylose growth curves of 0.01 g/L (●), 0.05 g/L (▲), and 0.10 g/L (■).	33
Figure 2-3: D-xylose growth curves of 0.50 g/L (●), 0.90 g/L (▲), and 1.30 g/L (■).	33
Figure 2-4: D-xylose growth curves of 1.75 g/L (●), 3.50 g/L (▲), and 5.25 g/L (■).	33
Figure 2-5: Specific growth rates from 0 g/L to 5.25 g/L of D-xylose with the Monod (dotted curve) and predicted (solid curve) model.	34
Figure 2-6: Carbon monoxide growth curves with 0.00 g/L (●), 1.00 g/L (▲), and 2.00 g/L (■) of D-xylose.....	35
Figure 2-7: Carbon monoxide growth curves with 3.00 g/L (●), 4.00 g/L (▲), and 5.00 g/L (■) of D-xylose.....	35

Figure 2-8: Specific growth rates of carbon monoxide with 0.00 g/L to 5.00 g/L of D-xylose with a modified Monod and predicted model.....	36
Figure 2-9: Models fitted to the experimental data with. A) Predicted B) Monod C) Webb D) Levenspiel.....	37
Figure 3-1: Overall process to covert coal to saleable bio-products.....	45
Figure 3-2: Original gasification design by Robert Mota[1].	46
Figure 3-3: New gasification design with compression system where J-101 is a screw feeder, R-101 is the fluidized bed reactor, F-101 are bag house filters, E-101 is a condenser, C-101 is a compressor, V-101 is an inflatable storage bag, and D-101 is a storage tank.	46
Figure 3-4: Bioreactor schematic.....	50
Figure 3-5: Growth curve of synthesis gas in bioreactor.....	53
Figure 4-1: Bioreactor schematic.....	61
Figure 4-2: Pareto Chart of parameters effect on the formation of 2,3-BDO.....	67
Figure 4-3: Pareto Chart of parameters effect on the formation of 2,3-BDO with 95% confidence.	67
Figure 4-4: Pareto Chart of parameters effect on the formation of 2,3-BDO with 80% confidence.	68
Figure 4-5: Pareto Chart of parameters effect on the formation of 2,3-BDO.....	69
Figure 4-6: Pareto Chart of parameters effect on the formation of ethanol.....	70
Figure 4-7: 2,3-BDO and ethanol production over 96 hours.	71

Figure A-1: Calibration run of 30% 2,3-BDO, 30% methanol, and 40% water by volume.	A-1
Figure A-2: Calibration run of 30% ethanol, 30% butanol, and 40% water by volume.	A-1
Figure A-3: 2,3-BDO GC analysis standard run order #1.	A-2
Figure A-4: 2,3-BDO GC analysis standard run order #2.	A-2
Figure A-5: 2,3-BDO GC analysis standard run order #3.	A-3
Figure A-6: 2,3-BDO GC analysis standard run order #4.	A-3
Figure A-7: 2,3-BDO GC analysis standard run order #5.	A-4
Figure A-8: 2,3-BDO GC analysis standard run order #6.	A-4
Figure A-9: 2,3-BDO GC analysis standard run order #7.	A-5
Figure A-10: 2,3-BDO GC analysis standard run order #8.	A-5
Figure A-11: 2,3-BDO GC analysis standard run order #9.	A-6
Figure A-12: 2,3-BDO GC analysis standard run order #10.	A-6
Figure A-13: 2,3-BDO GC analysis standard run order #11.	A-7
Figure A-14: 2,3-BDO GC analysis standard run order #12.	A-7
Figure A-15: 2,3-BDO GC analysis standard run order #13.	A-8
Figure A-16: 2,3-BDO GC analysis standard run order #14.	A-8
Figure A-17: 2,3-BDO GC analysis standard run order #15.	A-9
Figure A-18: 2,3-BDO GC analysis standard run order #16.	A-9
Figure A-19: Ethanol GC analysis standard run order #1.....	A-10
Figure A-20: Ethanol GC analysis standard run order #2.....	A-10
Figure A-21: Ethanol GC analysis standard run order #3.....	A-11
Figure A-22: Ethanol GC analysis standard run order #4.....	A-11

Figure A-23: Ethanol GC analysis standard run order #5.....	A-12
Figure A-24: Ethanol GC analysis standard run order #6.....	A-12
Figure A-25: Ethanol GC analysis standard run order #7.....	A-13
Figure A-26: Ethanol GC analysis standard run order #8.....	A-13
Figure A-27: Ethanol GC analysis standard run order #9.....	A-14
Figure A-28: Ethanol GC analysis standard run order #10.....	A-14
Figure A-29: Ethanol GC analysis standard run order #11.....	A-15
Figure A-30: Ethanol GC analysis standard run order #12.....	A-15
Figure A-31: Ethanol GC analysis standard run order #13.....	A-16
Figure A-32: Ethanol GC analysis standard run order #14.....	A-16
Figure A-33: Ethanol GC analysis standard run order #15.....	A-17
Figure A-34: Ethanol GC analysis standard run order #16.....	A-17
Figure A-35: 2,3-BDO GC analysis from syngas at 24 hours.	A-18
Figure A-36: Ethanol GC analysis from syngas at 24 hours.	A-18

List of Tables

Table 1-1: Organic reactions that occur within gasification[25,26].	7
Table 1-2: Mesophilic and Thermophilic microorganisms and their products from syngas[16].	10
Table 1-3: Rate of mass transfer for gas-liquid reactors[37].	13
Table 2-1: Biokinetic inhibition models with constants for <i>C. autoethanogenum</i>	36
Table 2-2: Biokinetic inhibition models with constants for <i>C. autoethanogenum</i>	37
Table 3-1: Ultimate analysis of lignite coal.	47
Table 3-2: Volume composition of syngas before and after compression.	52
Table 4-1: Coded and uncoded parameter values.	62
Table 4-2: Non-randomized fractional factorial design with optimized experimental runs.	63
Table 4-3: Concentrations of 2,3-BDO and ethanol for a six factor fractional factorial design.	66
Table 4-4: Production of 2,3-BDO from previous researchers.	72
Table 4-5: Production of ethanol from previous researchers.	73

Chapter 1

State of the Art and Perspective of Biologically Producing 2,3-BDO via Coal to Liquid (CTL) Fermentation Technology

1.1 Introduction

2,3-Butanediol (2,3-BDO) is a high-value, low-volume commodity chemical with extensive industrial applications that can be biologically produced via bacterial fermentation of synthesis gas (syngas) from coal gasification processes. Biological production of 2,3-BDO was initially discovered as a by-product from *Klebsiella pneumonia*, also known as *Aerobacter aerogenes*, in 1906 by Harden and Walpole[1]. Many other organisms since then have been shown to produce 2,3-BDO, but the primary industrially-relevant producers were *K. pneumonia*, *K. oxytoca*, *Bacillus polymyxa* (reclassified as *Paenibacillus polymyxa*)[2], *Enterobacter aerogenes*, and *Serratia marcescens*[3,4]. These organisms were capable of producing 150, 130, 36.9, 110, and 152 $\frac{g}{L}$ of 2,3-BDO, respectively, on common sugar-containing substrates, such as glucose and sucrose[3]. *P. polymyxa* is a more versatile organism because it is actively diastatic; therefore, fermentation may be done from starchy raw materials such as corn and wheat as well as sugar-containing substrates[5]. These organisms require costly substrates and nitrogen sources such as yeast extract. Additionally, these organisms, except *P. polymyxa*, are all categorized by the World Health Organization (WHO) as hazard group 2 pathogenic

species[6]; hence, rendering their use problematic and costly, especially for commercial-scale production.

In 2011, Köpke et al. gave evidence of three organisms from the nonpathogenic *Clostridium* genus; *C. autoethanogenum*, *C. ljungdahlii*, and *C. ragsdalei*, that produce 2,3-BDO without yeast extract and on steel mill waste gas[7]. This development marked almost a new revival in the possibility of fermentative production of 2,3-BDO in commercial quantities.

The objective of this work is to elucidate the viable significance and technological implications for the fermentative production of 2,3-BDO from syngas by researching the following: derivation of a novel bio-kinetic model with substrate inhibition, analyzing product formation with the use of syngas from coal, and conducting an experimental design for potential significant factors that affect product formation. A critical review and analysis of the state-of-the-art developments for gas to liquid (GTL) technologies and syngas formation from coal are provided.

1.2 Syngas Fermentation

1.2.a Advantages

The primary advantage of fermentation via syngas from coal is the ability for certain microbes to produce a variety of fuels or saleable commodities; such as ethanol, 2,3-BDO, butanol, acetate, and others, which are discussed in Section 1.5. Conventionally, the Fischer-Tropsch (FT) synthesis is used to convert bio-based syngas to biofuels by the use of metal catalysts such as nickel, cobalt, iron, and ruthenium which has a large distribution of products[8]. Possible products that may be formed are olefins, paraffins,

alcohols, aldehydes, acids, and ketones. This large array of product distribution makes the selectivity of biomass syngas fermentation highly advantageous.

From a past literature review, the comparison between thermochemical synthesis and gas fermentation to ethanol showed that gas fermentation produced 220% more fuel, had a 39% higher carbon to fuel efficiency, and required 28% less energy[9]. Therefore, the gas fermentation process also produced less carbon dioxide than that of the thermochemical process. Microbial biomass that is separated from the liquid product stream can further be utilized as a feedstock to an anaerobic digestive system, whereby biogas can be produced and mixed with the syngas that is formed from coal[10]. Biogas is made up of carbon dioxide and methane and will further increase carbon efficiency.

1.2.b State of the Art

Research and development activities involving bulk biochemical production has been cyclical and closely, yet oppositely, follows the cycles of crude oil pricing. Interest and demand for developing alternative technologies that are both green and sustainable for producing chemicals that are conventionally petroleum-based always increase when crude oil prices reach unattractively high levels. Once crude prices start diminishing, so does interest in biochemical developments. This is simply because biochemical routes of producing bulk chemicals do not remain cost-effective when compared to conventional thermal cracking of crude oil. Nevertheless, recent advances in biotechnology and associated bioprocessing the past decade seem to have made it possible for biochemical developments to remain active and competitive regardless of crude oil prices.

In the recent past, 2,3-BDO has been formed from a variety of substrates, such as carbon monoxide, fructose, and steel mill gas, which contains carbon monoxide, nitrogen,

carbon dioxide, and hydrogen. However, the concentration of 2,3-BDO is relatively low compared to the pathogenic bacteria discussed in Section 1.1[7,11,12,13].

As of today, the technology to produce high value chemicals (e.g. 2,3-BDO) exists and has been performed in many lab scale environments, but not much has been done to perform fermentation with syngas from coal. Commercializing 2,3-BDO fermentation is costly due to the capital investment and manufacturing costs required. The fixed capital investment and manufacturing cost, as of 2013, while using molasses as the substrate are \$38.3 million and \$11.2 million per year, respectively[14]. With these costs, the minimum selling price of 2,3-BDO would have to be between \$7.70 and \$9.90 per kilogram[14]. However, molasses is a relatively costly substrate compared to syngas from coal. Companies, including Coskata Inc., were leading the current efforts toward the commercialization of 2,3-BDO from syngas fermentation before closing and re-emerging as Synata Bio, Inc. [15].

So far, only a few companies and research groups have tried to improve and commercialize syngas fermentation for high value chemical products. LanzaTech Inc. USA has been able to produce liquid fuels (e.g. ethanol) and chemicals (e.g. 2,3-BDO) on an industrial scale using effluent waste gas from steel mills in Shanghai, China[17]. Additionally, LanzaTech's research and development laboratories located in Auckland, New Zealand are currently in the process of developing other processes in which other high value chemicals can be produced via fermentation (e.g. butyrate, n-butanol, and i-propanol)[18]. The SNYPOL project platform, a conglomeration of partners from academic institutions and industry, have produced polyhydroxyalkanoates, hydroxybutyrate, butanediol, and succinate from syngas fermentation within R&D

laboratories[18]. Finally, Coskata Inc., USA have been able to produce ethanol in a demonstration plant located in Madison, PA using natural gas, industrial gases, and syngas from coal[19]. Furthermore, Coskata Inc. has produced propanol, butanol, butanediol, hexanol, organic acids, and fatty acids on a lab scale at their facility in Warrenville, IL[18].

1.3 Future Direction

Even though many optimization experiments, which are discussed in Section 1.8, have been conducted, still more remains to be done with the fermentation process. First and foremost, on the genetic and microbiology side of fermentation, research needs to be carried out in genetic modification. Much of the improvement in the fermentation process lies with genetic restructuring of the genes to produce desired, high-value chemicals. On the engineering side of fermentation, maximization of fermentation products can be studied by attempting to optimize the various fermentation operating process conditions. First, there have been experiments to show that gas-to-liquid (GTL) mass transfer is rate limiting during fermentation[20]. Therefore, a factorial experimental design assessing the effects of substrate concentration by changing syngas flow rates to the reactor, temperature at which fermentation is carried out, the agitation induced by the reactor's impellers, and the reactor pressure can be conducted to make improvements to the GTL mass transfer rates. By increasing the GTL mass transfer rates, studies can be carried out to determine if carbon monoxide from coal can be used as the sole substrate for fermentation. One study by Gaddy et al. (2013) showed that products formed from *C. ljungdahlii* were mostly produced from fructose during dual substrate, CO and fructose, fermentation and was well supported by the low uptake efficiency of CO[21]. Secondly, varying constituents within the medium could be further studied for economic feasibility and the effects on growth and product

formation, where media cost is about 70% of the manufacturing cost[9]. Most studies currently are trying to improve product ratios. For example, one study showed that the addition of selenium and/or vitamins to the growth medium did not improve the ethanol/acetic acid ratio when compared to a control medium without such additions; furthermore, an enhanced 2,3-BDO/acetic acid ratio was obtained with the presence of tungsten, but not with selenium[12]. Another study showed that a maximum concentration of ethanol was obtained when higher L-cysteine·HCl (a reducing agent) and lower yeast extract concentrations were used[23]. Although no studies have showed the effects of omitting constituents of the growth medium on the fermentation process, this is a subject that could be explored further.

1.4 Syngas Production from Coal Gasification

Syngas composition from coal can vary greatly depending on the feed to the reactor, the type of reactor used, and the energy supplied. There are many types of reactors for gasification but the most common types are fluidized bed, moving bed, and entrained flow reactors. A more detailed description of these type of reactors can be found in a review by Breault (2010)[24]. In these reactors, many different reactions can occur in the gasification process, such as combustion reactions as well as steam gasification, Boudouard, water-gas shift, methanation, hydro-gasification, and steam methane reforming reaction[25,26]. These reactions are summarized in Table 1-1. When gasifying coal, an energy and mass balance is required around the system to optimize the operating temperature and feed concentrations. If too much energy and oxygen are added then more carbon dioxide will be present in the syngas when it is desirable to have high concentrations of carbon monoxide and hydrogen.

Table 1-1: Organic reactions that occur within gasification[25,26].

	Reactions	$\Delta H \left(\frac{BTU}{lb-mol} \right)$
Combustion	$C + O_2 \rightarrow CO_2$	-16,900
	$C + \frac{1}{2} O_2 \rightarrow CO$	-47,600
	$CO + \frac{1}{2} O_2 \rightarrow CO_2$	-121,700
Steam Gasification	$C + H_2O \rightarrow CO + H_2$	56,490
Boudouard	$CO_2 + C \leftrightarrow 2CO$	74,200
Water Gas Shift	$CO + H_2O \leftrightarrow CO_2 + H_2$	-17,700
Methanation	$CO + 3H_2 \rightarrow CH_4 + H_2O$	-88,700
Hydro-gasification	$2H_2 + C \rightarrow CH_4$	-32,200
Steam Methane Reforming	$CH_4 + H_2O \leftrightarrow CO_2 + H_2$	88,600

There are also inorganic reactions that occur in gasification because coal is a blend of carbon, hydrogen, sulfur, nitrogen, oxygen, water, and metals. With limiting the presence of oxygen concentrations, the sulfur typically reacts into hydrogen sulfide and small amounts of carbonyl sulfide. Nitrogen fed into the system typically stays as nitrogen except for some ammonia formation and hydrogen cyanide[26]. The syngas produced from coal has many impurities that are not found in biogas or steel mill gas. Gasification reactions and the impurities within the coal are of importance to microbial growth because of thermodynamic limitations, discussed in Section 1.8, as well as the impurities may be toxic.

1.5 Biochemistry of Gas Fermentation

Understanding the metabolic pathways for product formation by a bacterium is crucial for enzymatic manipulation and metabolic shifts. The reaction pathway for this

microorganism is shown in Figure 1-1 and Figure 1-2[13,27]. Figure 1-1 details the metabolic pathway for carbohydrates with the use of *C. autoethanogenum* up to Acetyl-CoA. The products after Acetyl-CoA can be found in Figure 1-2. Figure 1-2 details the full Wood-Ljungdahlii pathway with gaseous substrates where 2,3-BDO, lactate, ethanol, and acetate are all by-products. Figure 1-1 is important to understand because it shows the different enzymatic steps and energy requirements by utilizing carbohydrates or GTL technology while Figure 1-2 focuses on the products formed by *C. autoethanogenum* after Acetyl CoA. In many previous studies, *C. autoethanogenum* has been shown to be able to utilize carbon dioxide and hydrogen as substrates through the carbonyl branch or with just carbon monoxide through the methyl branch[7,11,12,13].

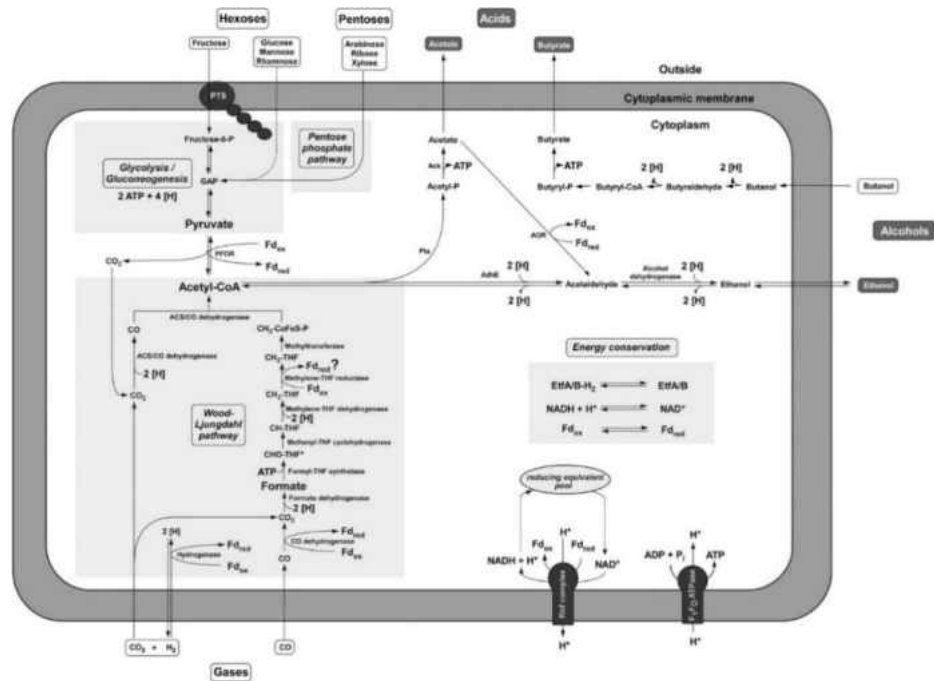


Figure 1-1: Reaction pathway from hexoses, pentoses, hydrogen and carbon dioxide, and carbon monoxide to Acetyl-CoA[27].

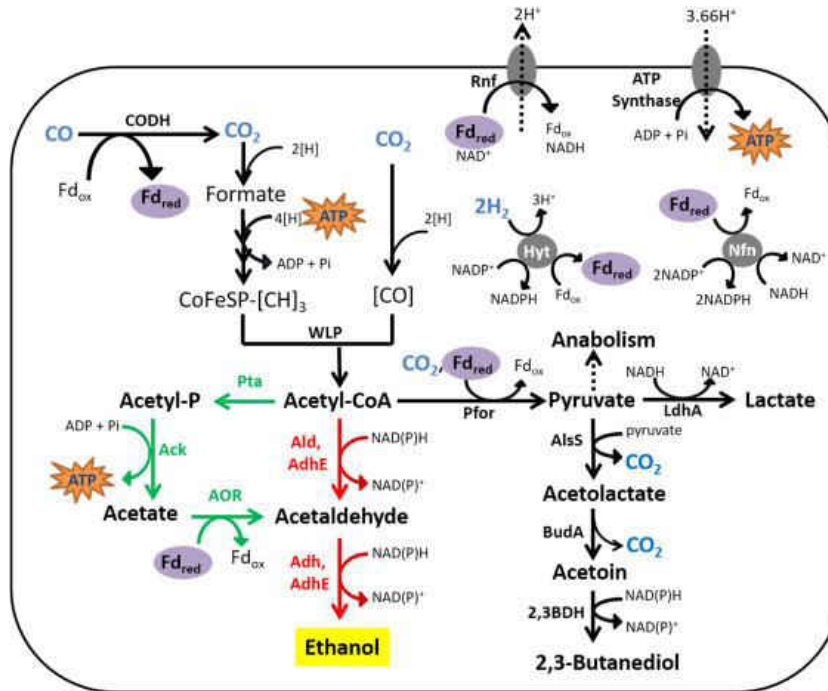


Figure 1-2: Wood-Ljungdahlii pathway to produce 2,3-BDO, lactate, ethanol, and acetate[13].

1.6 Organisms and Products

Many mesophilic and thermophilic microorganisms have been known to ferment a mixture of carbon monoxide and hydrogen (syngas) and these organisms have a range of products which are shown in Table 1-2[16].

Table 1-2: Mesophilic and Thermophilic microorganisms and their products from syngas[16].

Species	Products
Mesophilic Microorganisms	
<i>Acetobacterium woodii</i>	Acetate
<i>Butyribacterium methylotrophicum</i>	Acetate, Ethanol, Butyrate, Butanol, Pyruvate
<i>Clostridium aceticum</i>	Acetate
<i>Clostridium autoethanogenum</i> *	Acetate, Ethanol, Lactate, 2,3-BDO
<i>Clostridium carboxidivorans</i>	Acetate, Ethanol, Butyrate, Butanol
<i>Clostridium leatocellum</i> SG6	Acetate, Lactate, Ethanol
<i>Clostridium ljungdahlii</i> *	Acetate, Ethanol, Lactate, 2,3-BDO
<i>Clostridium ragsdalei</i> *	Acetate, Ethanol, Lactate, 2,3-BDO
<i>Eubacterium limosum</i>	Acetate
Mesophilic <i>Bacterium</i> P7	Acetate, Ethanol, Butyrate, Butanol
<i>Oxabactor pfennigii</i>	Acetate, n-butyrate
<i>Peptostreptococcus productus</i>	Acetate
Thermophilic Microorganisms	
<i>Carboxydocella sporoproducens</i>	H ₂
<i>Clostridium thermocellum</i>	Acetate
<i>Desulfotomaculum thermobenzoicum</i> subsp.	Acetate, H ₂ S
<i>Thermosyntrophicum</i>	
<i>Moorella thermoacetica</i> (<i>Clostridium thermoaceticum</i>)	Acetate
<i>Moorella thermoautotrophica</i>	Acetate

* From Köpke et al. (2011)[7]

From Table 1-2 there are only three microorganisms, *C. autoethanogenum*, *C. ljungdahlii*, and *C. ragsdalei*, known so far that can produce 2,3-BDO from syngas fermentation. To increase product formation and yield it may be useful to use a mixture of bacteria.

1.7 Derivatives of 2,3-BDO

2,3-BDO is a precursor to many different chemicals such as methyl ethyl ketone (MEK), butadiene, diacetyl, acetone 2,3-butanediol ketal, and 2,3-BDO diester. The versatility of 2,3-BDO is of importance to note because the chemicals mentioned are used

in everyday activities; therefore, cheaper production of 2,3-BDO is desired. Figure 1-3 summarizes the overall reactions to convert biomass to the chemicals previously mentioned. The typical production methods and/or the common uses of these chemicals are briefly discussed.

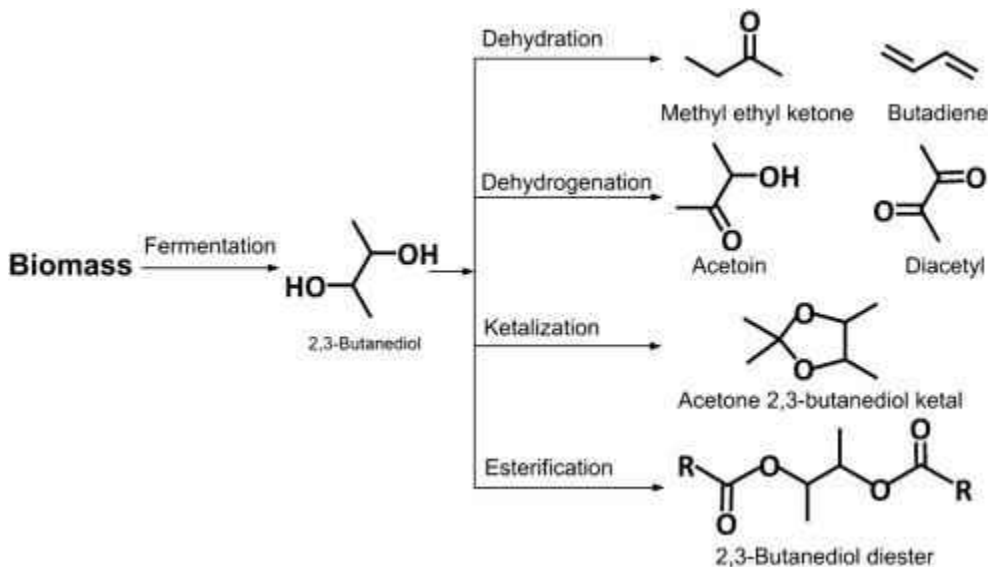


Figure 1-3: 2,3-BDO derivatives through dehydration, dehydrogenation, ketalization, and esterification[3].

2,3-BDO can be dehydrated into MEK and butadiene. MEK is typically produced with subcritical water and transitional metal sulfates such as CuSO_4 [28]. MEK has many applications, such as surface coatings, adhesives, printing inks, and as a solvent, and is expected to have a \$4.01 billion market by 2024[29]. Butadiene is also formed through dehydration with transition metals but the most common one is $\gamma\text{-Al}_2\text{O}_3$ [30]. Butadiene is primarily used for synthetic rubber but is also used to make acrylonitrile butadiene styrene, styrene butadiene rubber, nitrile butadiene rubber, SB latex, and hexamethylenediamine[31].

Acetoin and diacetyl are produced by the dehydrogenation of 2,3-BDO and is used as flavoring. Diacetyl specifically is typically used as a butter flavoring; however, both are used in the manufacturing of caramel, butterscotch, pina colada, strawberry and many other flavors. There are also trace amounts of acetoin and diacetyl in electronic cigarettes as well which may cause severe respiratory diseases[32].

The ketalization and esterification process of 2,3-BDO results in a methyl tert-butyl ether (MTBE) and a diester, respectively. MTBE is used as a fuel additive and the 2,3-BDO diester is a precursor used in the synthesis of cosmetics, drugs, and thermoplastic polymers[33].

1.8 Optimization

Many optimization experiments, such as altering media substituents[19,34,35], changing process parameters[19], enzyme removal[13], and gas composition[35], have been carried to improve carbon monoxide fermentation in the hopes to produce desired chemicals. Such experiments and research seek to improve many aspects that pertain to the gasification, fermentation, and separation parts of the process. Most of the recent research, however, is focused on optimizing the fermentation process to produce sufficient amounts of ethanol. Of the factors that have been studied, the following factors appear to be the most significant: inhibitory compounds in syngas streams, GTL mass transfer, reactor type, temperature, pH of the growth media, constituents of growth media, and the types of microbes used in the fermentation process[4,16]. A detailed review of the inhibition factors that affect the anaerobic digestion process is described in a journal article called “Inhibition of anaerobic digestion process: A review” by Ye Chen et al. (2008)[36].

Inhibitory compounds in the syngas such as tars, ash, nitric oxide, sulfur compounds, and others affect the efficiency of the fermentation process by shifts in metabolic pathways, cell dormancy, and inhibition of enzymatic activity which results in low cell growth and product yield[16]. Most often, tar reforming and scrubbing as well as a gas purification process will bring the syngas to the standards that must be met for clean syngas.

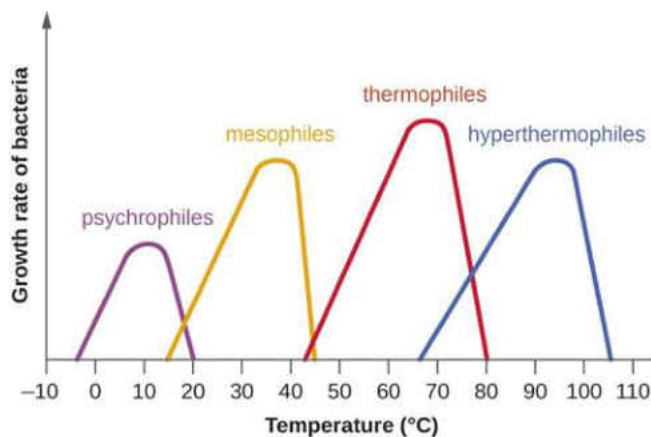
Reactor type is strongly correlated to the mass transfer limitations of the gaseous substrate. The rate of mass transfer is compared experimentally by the mass transfer coefficient multiplied by the GTL interface surface area unit per volume, $k_L\alpha$, which has the units of inverse hours[37]. The mass transfer performance of different commercialized reactor types can be seen in Table 1-3. From Table 1-3, packed columns have the highest rate of mass transfer followed by spray columns then continuously stirred tank reactors (CSTRs); although, CSTRs are the most common type of bioreactors due to the price, versatility, and constructability[16,38].

Table 1-3: Rate of mass transfer for gas-liquid reactors[37].

Reactor Type	$k_L\alpha$ (hr⁻¹)
Packed Countercurrent Column	1.4 – 250
Packed Cocurrent Column	1.4 – 3,670
Bubble Cap Plate Column	36 – 720
Sieve Plate Column	36 – 1,400
Horizontal and Coiled Tube Reactor	18 – 2,500
Vertical Tube Reactor	72 – 3,600
Spray Column	2.5 – 54
Continuously Stirred Tank Reactor	11 – 2,900

The temperature of the reactor has two major effects on syngas fermentation processes. One main effect is that temperature plays an important role on microbial growth (substrate utilization). The other effect is the solubility of the gaseous substrate within the medium[39]. Both effects can negatively and positively affect microbial

growth. Microbes have an optimum growth temperature and these temperatures can vary widely depending on the type of bacterium. The categories of bacteria range from psychrophiles (-15°C and lower) to hyperthermophiles (60°C and above); however, all categories of bacteria have an optimum temperature which can be visually seen in Figure



1-4[40]. Temperature and gas solubility in liquids are inversely proportional; therefore, psychrophiles will be more suitable to consume gaseous substrates than hyperthermophiles.

Figure 1-4: Optimal temperature range for bacteria[40].

Furthermore, pH is an important parameter for the optimal activity of microbial catalysts. The optimum pH for syngas fermenting microbes varies between 5.5 and 7.5 depending on the species. For example, *C. ljungdahlii* has an optimum pH of 5.8–6.0[16]. Shifting the pH during fermentation can strain enzymatic pathways to increase productivity[22,41].

The culture media in which the reaction takes place affects the fermentation process greatly. The growth media provides the microbes with all essential nutrients including minerals, trace elements, vitamins, and reducing agents for their maximal growth[16]. The growth media constituents vary greatly based on the selection of the fermenting microbe.

Many factorial experiments have analyzed optimal mineral, vitamin, and metal content for growth media for a variety of microbes[42,43].

Finally, microbe selection is extremely important yet perplexing choice for syngas fermentation. Of the many syngas fermenting bacteria, the most common are strict mesophilic anaerobes such as *C. ljungdahlii*, *C. acetivum*, *A. woodii*, *C. autoethanogenum*, and *C. carboxydeviron*[16]. Additionally, on the microbiological scale, scientists are attempting to engineer microorganisms used in the fermentation process to selectively produce desired products by genetic engineering techniques.

To optimize these parameters more research needs to be done for each bacterium or a mixture of bacteria until a suitable culture produces sufficient quantities. In general the medium for each bacterium is provided by the distributor, but by supplying nutrients in excess or scarce amounts will strain the bacterium and could retard or accelerate productivity.

1.9 Product Recovery

As of date, the single principal challenge to economically produce 2,3-BDO seems to be the separation and purification of the product from the fermentation broth in an efficient and cost-effective manner[44].

A promising candidate method is liquid-liquid extraction with n-butanol as the solvent with a polydimethylsiloxane (PDMS) membrane. Water and n-butanol are more permeable through the PDMS than 2,3-BDO which makes the concentration of 2,3-BDO more concentrated in the retentate with only the membrane. This system achieved a concentration solution of 2,3-BDO of 98+ weight percent with low energy usage but requires a substantial amount of solvent[45,46].

Another method is using an aqueous two-phase extraction (ATPE) using an ethanol and ammonium sulfate system. The recovery of 2,3-BDO was 97% and the ATPE system effectively removed cells, glucose, and protein impurities simultaneously. This system requires large amounts of salts and loses about 3% of the salt during recycling[47].

The most recent type of separation for 2,3-BDO from fermentation broth is reactive distillation. Xiang et al. (2001) suggests that reactive distillation is the most effective way to separate a complicated system[48]. N-butylaldehyde (BA) has been used as a reactant with 2,3-BDO to form 2-propyl-4,5-dimethyl-1,3-dioxalane (PDD) which is immiscible with water[14,48]. This reaction is summarized in Figure 1-5[49].

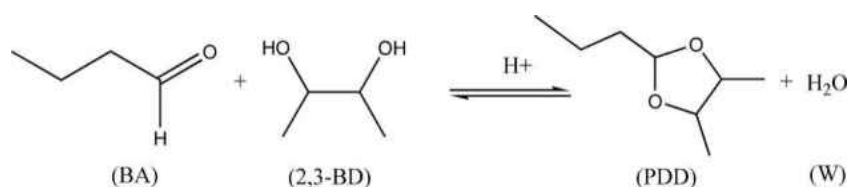


Figure 1-5: Reaction equation of n-butylaldehyde and 2,3-BDO[49].

The study done by Xiang et al. (2001) used a broth that was pretreated to remove biomass and proteins before separating the aqueous and organic phases. This treated broth enters a reactive extraction unit where the 2,3-BDO in the broth joined and reacted with recycled BA to form PDD. The dilute PDD stream enters a settler where the aqueous phase was removed and the organic phase was sent to a reactive distillation column. An acid solution was added to the reactive distillation column as a catalyst. The 2,3-BDO solution exits the bottom of the column where the BA and unreacted PDD was recycled to the reactive extraction unit. This process is summarized in Figure 1-6[49].

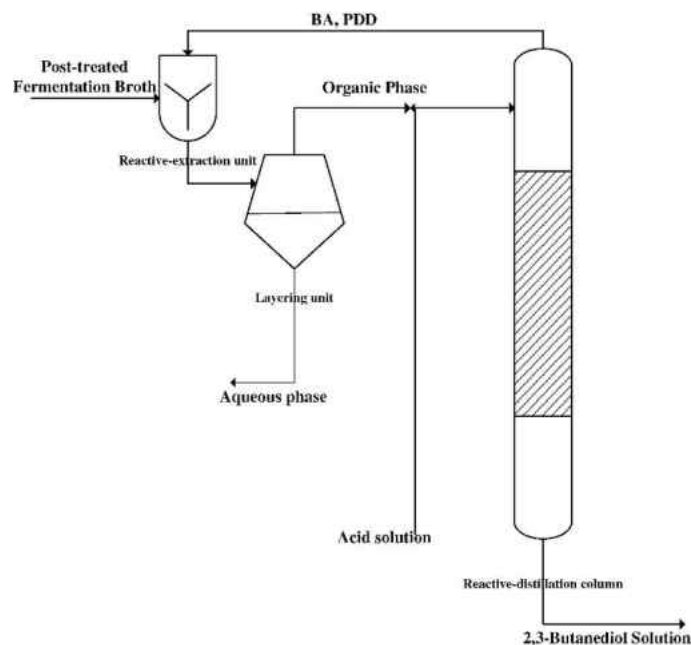


Figure 1-6: Reaction distillation and separation process of 2,3-BDO[49].

Hydrochloric acid exhibited less loss of PDD, BA, and 2,3-BDO of the two catalytic acids, sulfuric and hydrochloric acid, used. This process had a yield rate and a purity of 2,3-BDO of more than 90% and 99%, respectively. The major downfall of this process is recycling of the acid solution so the author suggested that the acid solution should be neutralized after reactive-distillation[49].

1.10 Summary

Fermentation processes that produce valuable chemicals are sustainable, but there are many hurdles that need to be explored at bench/pilot scale before commercialization. The primary hurdles are to optimize product formation that will counteract the costs associated with plant operations. Economic and plant designs need to be assessed for the use of non-pathogenic bacteria to make high-value chemicals with the optimized conditions, where pH, temperature, media composition, and mass transfer are the primary conditions that affect microbial productivity. An additional consideration with plant

operation is whether to use the biomass produced by the process for biogas, for animal feed, or for a combination of both. From the literature review the most efficient, up to date, way to separate 2,3-BDO from a fermentation broth is by reactive distillation with an aldehyde and an acid catalyst.

There are three major research topics related to *C. autoethanogenum* addressed within this thesis. The first topic is the kinetics with carbon monoxide and D-xylose. A novel inhibition model with D-xylose as the substrate and the derivation is included. The second topic researched the growth and product formation with the use of syngas derived from lignite coal. The last topic considered optimizing process conditions to increase 2,3-BDO and ethanol productivity.

References

- [1] Magee, R. L., & Kosaric, N. (1987). The microbial production of 2,3-butanediol. *Advanced Applied Microbiology*, 32, 89-161.
- [2] Ash, C., Priest, F., & Collins, M. (1993). Molecular identification of rRNA group 3 bacilli (ash, farrow, wallbanks and collins) using a PCR probe test. proposal for the creation of a new genus paenibacillus. *Antonie Van Leeuwenhoek*, 64(3-4), 253-260.
- [3] Ji, X., Huang, H., & Ouyang, P. (2011). Microbial 2, 3-butanediol production: A state-of-the-art review. *Biotechnology Advances*, 29(3), 351-364.
- [4] Celińska, E., & Grajek, W. (2009). Biotechnological production of 2, 3-butanediol—current state and prospects. *Biotechnology Advances*, 27(6), 715-725.
- [5] Long, S. K., & Patrick, R. (1963). The present status of the 2,3-butylene glycol fermentation. *Advances in Applied Microbiology*, 5, 135-155.
- [6] Health and Safety Executive. (2016). The approved list of biological agents. Retrieved 6/24, 2018, from <http://www.hse.gov.uk/pubns/misc208.pdf>
- [7] Köpke, M., Mihalcea, C., Liew, F., Tizard, J. H., Ali, M. S., Conolly, J. J., et al. (2011). 2,3-butanediol production by acetogenic bacteria, an alternative route to chemical synthesis, using industrial waste gas. *Applied and Environmental Microbiology*, 77(15), 5467-5475. doi:10.1128/AEM.00355-11 [doi]
- [8] Bashir, A., Divakaransantha, B., Poudel, P., & Kelifa, S. (2015). Fisher-tropsch process. *Department of Chemical and Bio Molecular Engineering, University of Maryland*.
- [9] Wei, L., Pordesimo, L., Igathinathane, C., & Batchelor, W. (2009). Process engineering evaluation of ethanol production from wood through bioprocessing and chemical catalysis. *Biomass and Bioenergy*, 33(2), 255-266.
- [10] Griffin, D. W., & Schultz, M. A. (2012). Fuel and chemical products from biomass syngas: A comparison of gas fermentation to thermochemical conversion routes. *Environmental Progress & Sustainable Energy*, 31(2), 219-224.
- [11] Mock, J., Zheng, Y., Mueller, A. P., Ly, S., Tran, L., Segovia, S., et al. (2015). Energy conservation associated with ethanol formation from H₂ and CO₂ in *Clostridium autoethanogenum* involving electron bifurcation. *Journal of Bacteriology*, 197(18), 2965-2980. doi:10.1128/JB.00399-15 [doi]
- [12] Kracke, F., Viridis, B., Bernhardt, P. V., Rabaey, K., & Krömer, J. O. (2016). Redox dependent metabolic shift in *Clostridium autoethanogenum* by extracellular electron supply. *Biotechnology for Biofuels*, 9(1), 249.

- [13] Liew, F., Henstra, A. M., Köpke, M., Winzer, K., Simpson, S. D., & Minton, N. P. (2017). Metabolic engineering of *Clostridium autoethanogenum* for selective alcohol production. *Metabolic Engineering*, 40, 104-114.
- [14] Koutinas, A., Yapez, B., Kopsahelis, N., Freire, D., Castro, M., Papanikolaou, S., et al. (2015). Techno-economic evaluation of a complete bioprocess for 2,3-butanediol production from renewable resources. *Bioresource Technology*, 204, 55-64.
- [15] Loris, N. (2017). Time to eliminate energy cronyism in the farm bill The Heritage Foundation.
- [16] Munasinghe, P. C., & Khanal, S. K. (2010). Biomass-derived syngas fermentation into biofuels: Opportunities and challenges. *Bioresource Technology*, 101(13), 5013-5022.
- [17] Chemicals Technology. (2018). LanzaTech 2,3-butanediol demonstration plant. Retrieved 6/24, 2018, from <https://www.chemicals-technology.com/projects/lanzatech23butanedio/>
- [18] Drzyzga, O., Revelles, O., Durante-Rodríguez, G., Díaz, E., Daniell, J., & Datar, R. P. (2015). New challenges for syngas fermentation: Towards production of biopolymers. *Chemical Technology and Biotechnology*, 90(10), 1735-1751.
- [19] Coskata and Advanced Biofuels. (2011). Syngas fermentation: The third pathway for cellulosic ethanol. Retrieved 6/24, 2018, from <https://advancedbiofuelsusa.info/wp-content/uploads/2011/06/3rd-Pathway-Revision-FINAL-6-17-11.pdf>
- [20] Bredwell, M. D., Srivastava, P., & Worden, M. R. (1999). Reactor design issues for synthesis-gas fermentations. *Biotechnology Progress*, 15(5), 834-844.
- [21] Gaddy, J., Gang, S., Ro, H., Lee, M., Choi, W., Hong, S., et al. (2013). Tracing carbon monoxide uptake by *clostridium ljungdahlii* during ethanol fermentation using ¹³C-enrichment technique. *Bioprocess and Biosystems Engineering*, 36(5), 591-595.
- [22] Abubackar, H. N., Bengelsdorf, F. R., Dürre, P., Veiga, M. C., & Kennes, C. (2016). Improved operating strategy for continuous fermentation of carbon monoxide to fuel-ethanol by clostridia. *Applied Energy*, 169, 210-217.
- [23] Abubackar, H. N., Veiga, M. C., & Kennes, C. (2012). Biological conversion of carbon monoxide to ethanol: Effect of pH, gas pressure, reducing agent and yeast extract. *Bioresource Technology*, 114, 518-522.
- [24] Breault, R. (2010). Gasification processes old and new: A basic review of the major technologies. *Energies*, , 216-240.

- [25] Mota, R. (2013). Design and construction of a fluidized bed. *Umi*, #1552207
- [26] Hightman, C., & Burgt, M. (2008). *Gasification* (2nd ed.) Elsevier Inc.
- [27] Köpke, M., Held, C., Hujer, S., Liesegang, H., Wiezer, A., Wollherr, A., et al. (2010). *Clostridium ljungdahlii* represents a microbial production platform based on syngas. *Proceedings of the National Academy of Sciences of the USA*, 107(29), 13087-13092.
- [28] Vogel, H. and Soler, A. *Dehydration of 2,3-butanediol to methyl ethyl ketone in sub- and supercritical water*. Darmstadt, Germany: 12th European Meeting on Supercritical Fluids: Poster presentation.
- [29] Market Research Report. (2016). *MEK market size projected to reach \$4.01 billion by 2024* (Electronic No. 978-1-68038-209-9)Grand View Research.
- [30] Liu, X., Fabos, V., Taylor, S., Knight, D., & Whiston, K. (2016). One-step production of 1,3-butadiene from 2,3-butanediol dehydration. *Chemistry A European Journal*, 22(35), 12290-12294.
- [31] Market Research Report. (2015). *1,3-butadiene (BD) market analysis by application (butadiene rubber, ABS, SBR, SB latex, NBR, hexamethylenediamine), bio-based opportunities and segment forecasts to 2020* (Electronic No. 978-1-68038-200-6)Grand View Research.
- [32] Allen, J., Flanigan, S., LeBlanc, M., Vallarino, J., MacNaughton, P., & Stewart, J. (2016). Flavoring chemicals in E-cigarettes: Diacetyl, 2,3-pentanedione, and acetoin in a sample of 51 products, including fruit-, candy-, and cocktail-flavored E-cigarettes. *Environmental Health Perspectives*, 124(6), 733-739.
- [33] Okonkwo, C., Ujor, V., Mishra, P., & Ezeji, T. (2017). Process development for enhanced 2,3-butanediol production by *paenibacillus polymyxa* DSM 365. *Fermentation MDPI*.
- [34] Guo, Y., Xu, J., Zhang, Y., Xu, H., Yuan, Z., & Li, D. (2010). Medium optimization for ethanol production with *clostridium autoethanogenum* with carbon monoxide as sole carbon source. *Bioresource Technology*, 101(22), 8784-8789.
- [35] Xu, H., Liang, C., Yuan, Z., Xu, J., Hua, Q., & Guo, Y. (2017). A study of CO/syngas bioconversion by *clostridium autoethanogenum* with a flexible gas-cultivation system. *Enzyme and Microbial Technology*, 101, 24-29.
- [36] Chen, Y., Cheng, J. J., & Creamer, K. S. (2008). Inhibition of anaerobic digestion process: A review. *Bioresource Technology*, 99(10), 4044-4064.

- [37] Charpentier, J. C. (1981). Mass-transfer rates in gas-liquid absorbers and reactors. *Advances in Chemical Engineering*, 11, 1-133.
- [38] Chaplin, M. (2016). Continuous flow stirred tank reactors. Retrieved 6/24, 2018, from <http://www1.lsbu.ac.uk/water/enztech/cstr.html>
- [39] Shen, Y. (2013). *Attached-growth bioreactors for syngas fermentation to biofuel. (dissertation. Iowa State University)*. Unpublished Doctorate, Iowa State University.
- [40] lumen: Microbiology. Temperature and microbial growth. Retrieved 6/15, 2018, from <https://courses.lumenlearning.com/microbiology/chapter/temperature-and-microbial-growth/>
- [41] Singh, V., Hague, S., Niwas, R., Srivastave, A., Pasupuleti, M., & Tripathi, C. (2016). Strategies for fermentation medium optimization: An in-depth review. *Frontiers in Microbiology*, 7
- [42] Wetzel, K., Cao, J., Kothe, E., & Kohler, M. J. (2015). Changing growth behavior of heavy-metal tolerant bacteria: Media optimization using droplet based microfluidics. *Engineering in Life Sciences*, 15(3), 327-332.
- [43] Abubackar, H. N., Fernández-Naveira, Á., Veiga, M. C., & Kennes, C. (2016). Impact of cyclic pH shifts on carbon monoxide fermentation to ethanol by *Clostridium autoethanogenum*. *Fuel*, 178, 56-6
- [44] Voloch, M., Jansen, N., Ladisch, M., Tsao, G., Narayan, R., & Rodwell, V. 2,3-butandiol from purdue university. *Industrial Chemical, Biochemicals, and Fuels*, , 933-947.
- [45] Shao, P. and Kumar, A. (2008). Recovery of 2,3-butanediol from water by a solvent extraction and pervaporation separation scheme. *Journal of Membrane Science*, 329(1), 160-168.
- [46] Harvianto, G., Haider, J., Hong, J., Long, N., Shim, J., Cho, M., et al. (2018). Purification fo 2,3-butanediol from fermentation broth: Process development and techno-econmonic analysis. *Biotechnology for Biofuels*
- [47] Li, Z., Teng, H., & Xiu, Z. (2009). Aquesour two-phase extraction of 2,3-butanediol from fermentation broths using an ethanol/ammonium sulfate system. *Process Biochemistry*, 45(5), 731-737.
- [48] Xiang, B., Chen, S., & Liu, D. (2001). Extraction of 1,3-prpanediol in dilute fermentation broth. *Journal of Tsinghua University*, 41(12), 53-55.

- [49] Li, Y., Wu, Y., Zhu, J., Liu, J., & Shen, Y. (2016). Separating 2,3-butanediol from fermentation broth using n-butylaldehyde. *Journal of Saudi Chemical Society*, 20(1), S495-S502.

Chapter 2

Biological Kinetics on Carbon Monoxide and D-xylose of a 2,3-Butanediol Producing Bacterium: *Clostridium autoethanogenum*

Abstract

Clostridium autoethanogenum has recently emerged as a strong nonpathogenic potential candidate for producing 2,3-butanediol in significant quantities using carbon monoxide as the sole carbon substrate. Success of this bacterium, however, remains elusive due to lack of understanding of the kinetics of its growth and the effects of substrate inhibition. This study reports on experimental and theoretical study of the growth kinetics of *C. autoethanogenum* on single and dual substrates as well as their inhibitory effects. This was accomplished by growing the bacterium on a simple sugar, D-xylose, and a mixture of carbon monoxide and D-xylose. Key findings include specific growth rates at different substrate concentrations, maximum biomass, and relevant biokinetic parameters. The maximum growth rate while utilizing carbon monoxide, D-xylose, and dual substrate was $0.45 \pm 0.10 \frac{g}{L}$, $0.42 \pm 0.01 \frac{g}{L}$, and $0.64 \pm 0.08 \text{ hr}^{-1}$, respectively, with a Monod constant of $7.0 \pm 0.79 \frac{mg}{L}$. Additionally, a new simplified model is proposed that accounts D-xylose growth and inhibition. Non-linear regression of the proposed model with the experimental model was done to verify the precision of the model and was compared to previous models. The proposed model out performed many of the previous models with less parameters.

2.1 Introduction

In recent years, growing attention has been drawn to a strict anaerobic bacterium from the Clostridium genus, *C. autoethanogenum*, due to its exquisite capability of utilizing carbon monoxide (CO) as the sole nutrient for fermentation[1,2,3]. Additional desirable attributes of this bacterium are that it is non-pathogenic and produces a high-value, low-volume by-product, 2,3-butanediol (2,3-BDO), in the stationary phase along with ethanol, lactate, acetate, and an intermediate product, acetoin, through the Wood-Ljungdahlii pathway[3,4,5,6,7,8].

A vast amount of research and resources have been devoted to maximizing the yield of ethanol to acetate ratios by manipulating various system and/or process parameters, while little has been done to maximize the more valuable 2,3-BDO product. Within the last ten years, many parameters such as gas flow rate, medium composition, pressure, pH, external electron donation, and enzyme inactivation have been manipulated by Cotter et al.[5,6], Guo et al.[9], Abubackar et al.[1,2,7], Krack et al.[10], Liew et al.[3], and Xu et al.[8] in an effort to increase ethanol production while suppressing all other by-products. Abrini et al. (1994) discovered various carbon sources that can be utilized by *C. autoethanogenum* which are: carbon monoxide, carbon dioxide and hydrogen, D-xylose, arabinose, D-fructose, rhamnose, and L-glutamate[11]. The current prices of these carbohydrates per gram from SigmaAldrich (2017) are \$0.40, \$2.92, \$0.36, \$3.44, and \$0.90, respectively. Economically, the carbohydrates of interests would be the carbohydrates with the lowest price, D-fructose and D-xylose. In this study D-xylose was used as the substrate of choice for growth kinetics and for dual substrate growth with carbon monoxide.

Other researchers have been primarily interested in the microbiological aspects of the growth mechanism such as enzymatic functions, metabolic pathways, and metabolite formation such as Koepke et al.[4] and Mock et al.[12].

There exists little to no information on the growth kinetics of the microorganism and the maximum biomass density that can be achieved. This information is vital to determine the economic feasibility of a commercial fermentation process, as well as for studies concerning process simulation, control, and optimization.

This study aimed at investigating and quantifying the bacterial growth and biokinetics of substrate utilization by *C. autoethanogenum*, as well as, developing a novel rate kinetic law based on elementary reactions. The new and simplified developed model was experimentally verified and its performance was contrasted to existing literature models. In addition to the quantification of biokinetic parameters, a calibration curve was generated to convert optical density at 600 nm (OD₆₀₀) to milligrams per liter.

2.2 Materials, Methods, and Equipment

2.2.a Microorganism

Bacterial freeze-dried pellets of *C. autoethanogenum*, DSM 10061, were obtained from DSMZ (Deutsche Sammlung von Mikroorganismen und Zellkulturen GmbH, Braunschweig, Germany) and was revived in DSMZ medium 640 with 5.00 $\frac{g}{L}$ of D-xylose. Medium 640 contains, per liter, 0.90 g NH₄Cl, 0.90 g NaCl, 0.40 g MgCl₂ x 6 H₂O, 0.75 g KH₂PO₄, 1.50 g K₂HPO₄, 2.00 g tripticase peptone, 0.75 g L-cysteine-HCl x H₂O, 5.00 mg FeCl₃ x 6 H₂O, and 5.00 mL trace solution. The trace solution contains, per 990 mL, 10.00 mL HCl (7.7M), 1.50 g FeCl₂ x 4 H₂O, 70.00 mg ZnCl₂, 100.00 mg, MnCl₂ x 4 H₂O, 6.00 mg H₃BO₃, 190.00 mg CoCl₂ x 6 H₂O, 2.00 mg CuCl₂ x 2 H₂O,

24.00 mg NiCl₂ x 6 H₂O, and 36.00 mg Na₂MoO₄ x 2 H₂O. A Coy vinyl Type A anaerobic chamber (Coy Lab Products, Grass Lake, MI, USA) with a palladium catalyst and an oxygen concentration in the parts per billion with the balance nitrogen was used for reviving, culturing, and plating the bacteria. A Tuttnauer Ez10 autoclave was used to sterilize the media before inoculation. The medium was autoclaved at 250°F for the recommended length of time per mL of media by Iowa State University[13], and the initial pH of the medium was 6.4. To assure the sterility of the media, the media and all used glassware were subjected to UV-C light for approximately ten minutes within the anaerobic chamber before inoculation.

2.2.b Inoculation and Growth Curve

Freeze-dried pellets were thawed in the anaerobic chamber for 30 minutes, and 0.5 mL of media was added to the pellets. Half of the bacterial solution was spread on an agar plate (medium 640 with 15 $\frac{g}{L}$ of agar) and the other half was added to a broth vial. Growth trials were conducted in butyl rubber sealed 10 mL borosilicate glass vials, where 6 mL was occupied by the media. The growth vials were inoculated from a previous vial that was in the late exponential phase at $5.4 \times 10^8 \frac{CFU \text{ of Bacteria}}{mL \text{ of Media}}$. Experiments were conducted with concentrations of D-xylose ranging from 0.01 $\frac{g}{L}$ to 300 $\frac{g}{L}$ under 100% N₂, and with D-xylose from 1 $\frac{g}{L}$ to 5 $\frac{g}{L}$ under N₂ with approximately 1000 ppm_v of carbon monoxide (dual substrate growth). Biomass growth was monitored by turbidity with a UV-Vis Evolution 600 light spectrophotometer at an optical density of 600 nm (OD₆₀₀). All measurements were conducted in triplicates as a repeated measure to quantify instrumental error and experiments were replicated at least three times to account for overall experimental error. Due to the low initial cell concentration, it was assumed that

the initial absorbance was zero, and showed to be a viable assumption through an experimental measure of 0.017 ± 0.021 at an OD_{600} . All vials were placed in an incubator/shaker (Benchmark incu-shaker 10L) at 120 rpm and 30°C.

2.2.c Spectrophotometer Calibration Curve

Due to different conversion factors reported in the literature for *C. autoethanogenum*, a calibration curve was constructed. The curve was produced using six samples at 100 mL of inoculated media with $5.00 \frac{g}{L}$ of D-xylose, where each sample was removed at different times/ OD_{600} readings and then filtered using a Whatman Grade 4 filter paper. The filter paper was weighed before filtration and after six hours of drying in the shaker at 30°C.

2.3 Theory and Calculation

2.3.a Growth Kinetics

The Monod equation, Equation 2.1, is typically used to model the specific growth rate as a function of substrate concentration. This equation is an empirical expression based on the Michaelis-Menten model and is normally associated with enzyme kinetics and/or gas absorption. An inherent disadvantage of the Monod equation is that it assumes growth is limited by a single dominant substrate with no inhibitory effects. It has, nevertheless, become customary to modify the Monod equation for substrate, cell, and/or product inhibition[14][15].

$$\mu_m = \frac{\mu_{max} S}{K_m + S} \quad (2.1)$$

where μ_m is the Monod model growth rate, μ_{max} is the maximum specific growth rate, S is the concentration of the limiting substrate in the medium, D-xylose in $\frac{g}{L}$, and K_m is a system coefficient often referred to as the Monod constant in $\frac{g}{L}$, and/or half-velocity

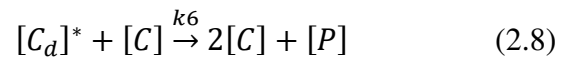
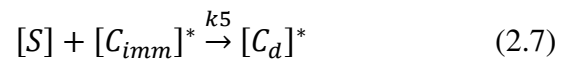
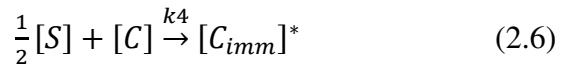
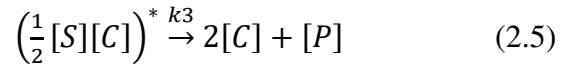
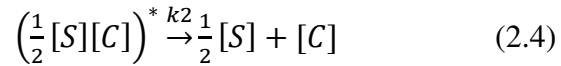
coefficient. The Monod constant is the concentration of substrate that yields a growth rate that is half of the maximum specific growth rate.

Derivation of the novel model consisted of many iterated trials until a viable and less complicated model that accounts for substrate inhibition was developed. The iterations consisted of varying the reaction coefficients and approximating the kinetic inhibition equations. Typically, an empirical inhibition coefficient, k_{obs} , is used with the Monod model for inhibition where the coefficient is shown in Equation 2.2[16]. This coefficient is also used in Hans and Levenspiel's model[15].

$$k_{obs} = \left(1 - \frac{S}{S_c}\right)^n \quad (2.2)$$

where S_c is the critical substrate concentration and n is an empirical constant. The critical substrate concentration is the assumed upper limit, above which cellular growth stops.

Elementary reactions were used to develop a new rate law that accounts for substrate inhibition. The elementary reactions are shown in Equations 2.3 to 2.8 where Equations 2.3 to 2.5 are for cellular division and Equations 2.6 to 2.8 account for substrate inhibition and cellular cannibalism, or cell-eat-cell phenomenon[17].



where starred concentrations, $[I]^*$, are for the inactive intermediates, $[S]$ is substrate concentration, $[C]$ is live cell concentration, $[P]$ is product concentration, $[C_{imm}]$ is immobilized cell concentrations, $[C_d]$ is dead cell concentrations, and k_1 - k_6 are the individual rate constants. By using the pseudo-steady state hypothesis (PSSH) the rate of cell generation and more importantly the specific growth rate can be determined for substrate inhibition with Equation 2.9.

$$\mu_{D,I} = \frac{(1-\frac{S}{S_c})\mu_{max}\sqrt{S}}{\sqrt{K_m}+\sqrt{S}} \quad (2.9)$$

where $\mu_{D,I}$ is the predicted model growth rate with substrate inhibition, $\mu_{max} =$

$$\frac{k_1k_3k_5}{k_2k_4+k_3k_4}, K_m = \left(\frac{k_2k_5+k_3k_5}{k_2k_4+k_3k_4}\right)^2, \text{ and } S_c = \frac{k_6C_{tot}}{k_4} \text{ for } C_{tot} \text{ is the total cell concentration}$$

measured. If substrate inhibition is not present then the elementary Equations 2.6 to 2.8 are omitted, which leads to Equation 2.10.

$$\mu_D = \frac{\mu_{max}\sqrt{S}}{\sqrt{K_m}+\sqrt{S}} \quad (2.10)$$

where μ_D is the predicted model growth rate without substrate inhibition, $\mu_{max} = k_3$ and

$$C_m = \frac{k_2+k_3}{k_1}.$$

To represent dual substrate growth, an empirical constant, μ_{mix} , is added to the rate equations to account for the growth from carbon monoxide which shifts the maximum specific growth rate by μ_{mix} . Dual substrate growth is represented by Equation 2.11.

$$\mu_{DS} = \mu_i + \mu_{mix} \quad (2.11)$$

where μ_{DS} is dual substrate growth rate without inhibition and μ_i is either the Monod or the predicted model.

The experimental specific growth rate is determined by Equation 2.12 during the exponential phase.

$$\mu = \frac{\ln(OD_{600,2}) - \ln(OD_{600,1})}{T_2 - T_1} \quad (2.12)$$

2.3.b Statistical Treatment of Experimental Data

Experimental results were compared using the t-value of the change in means to a critical t-value. The critical t-value was at 95% confidence for all data analysis. This 95% confidence interval accounts for the error among the replicate experiments and spectrophotometer readings. Non-linear regression was used to determine the rate constants for all models. Outlying data points for replicated data were assessed with box-plots. Data that fell outside the upper or lower bounds were removed and more experiments were conducted. Other data that did not lie within the normal distribution curve were also replicated.

2.4 Results and Analysis

2.4.a Spectrophotometer Calibration Curve

Figure 2-1 is a calibration curve of cell concentration in $\frac{mg}{L}$ vs OD_{600} with non-linear regression against the experimental data. The model in Figure 2-1 appears to fit well with a R^2 value of 0.994.

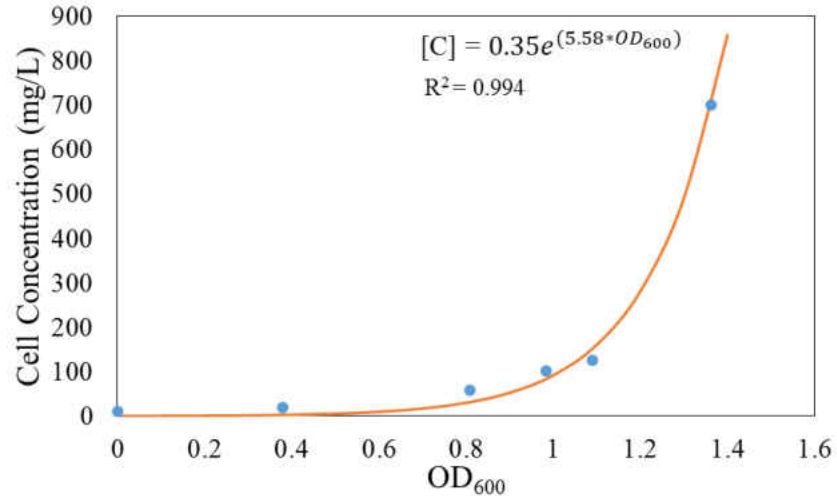


Figure 2-1: Non-linear regression calibration curve of cell concentration versus OD₆₀₀.

The differences between the generated curve and literature values are unknown.

Mock et al. (2015)[12] had $0.4 \frac{g \text{ of dry cells}}{L}$ and Cotter et al. (2009)[6] had $0.317 \frac{g \text{ of dry cells}}{L}$ at an OD₆₀₀ of 1 which is much greater than the predicted model. The corresponding OD₆₀₀ from the model to achieve $0.4 \frac{g \text{ of dry cells}}{L}$ and $0.317 \frac{g \text{ of dry cells}}{L}$ would be 1.26 and 1.22, respectively. Currently, there are no other published literature that have a calibration curve for *C. autoethanogenum* that correlates cell concentration and optical density.

2.4.b Growth Kinetics with D-xylose: No Inhibition

Modeling elementary processes for cellular growth can lead to improved process control and provide reliable methods for interpreting process parameters such as product formation. Cell density is a function of time; consequently, the growth curves while utilizing D-xylose at concentrations ranging from $0.01 \frac{g}{L}$ to $5.25 \frac{g}{L}$ as a function of time are represented in Figures 2-2 through 2-4 at 95% confidence.

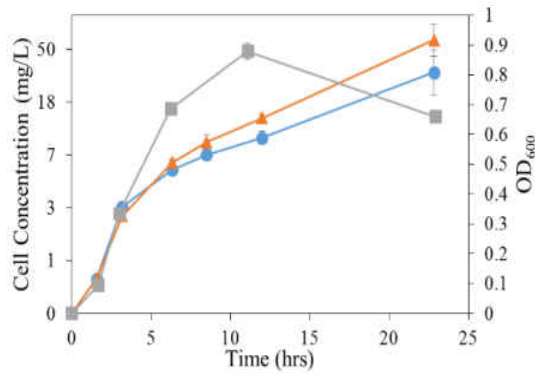


Figure 2-2: D-xylose growth curves of 0.01 g/L (●), 0.05 g/L (▲), and 0.10 g/L (■).

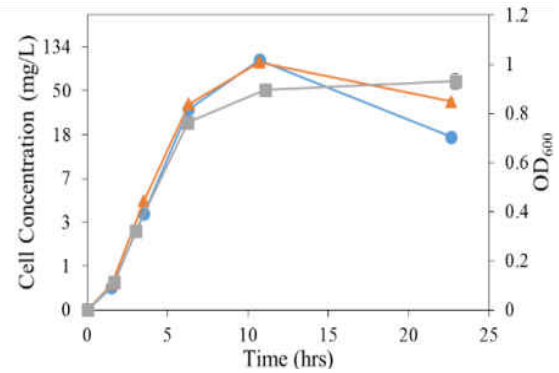


Figure 2-3: D-xylose growth curves of 0.50 g/L (●), 0.90 g/L (▲), and 1.30 g/L (■).

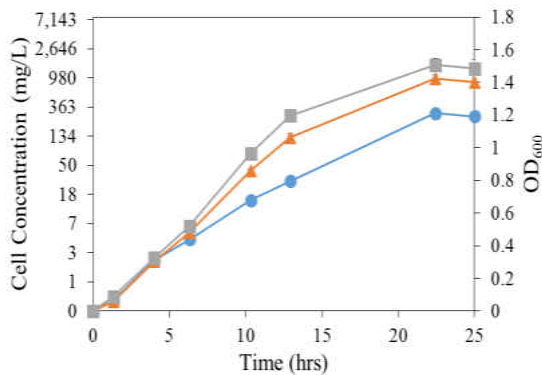


Figure 2-4: D-xylose growth curves of 1.75 g/L (●), 3.50 g/L (▲), and 5.25 g/L (■).

The decreasing concentration at extended growth times indicates that cellular cannibalism may be occurring or that the standard vials may not have been sterile during these trials which caused inaccurate readings. Either case would not affect the growth rate calculation because Equation 2.12

was used at $t_1 = 1.3$ hours and $t_2 = 6.3$ hours. The specific growth rate with 95% confidence are shown in Figure 2-5, along with the Monod model and the predicted model.

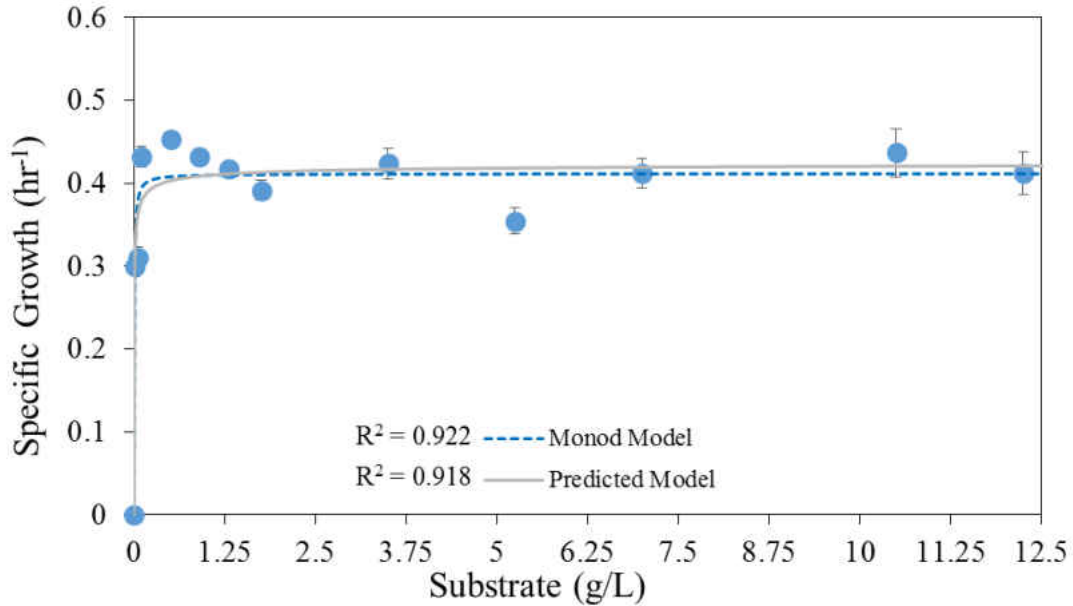


Figure 2-5: Specific growth rates from 0 g/L to 5.25 g/L of D-xylose with the Monod (dotted curve) and predicted (solid curve) model.

Figure 2-5 reveals that there is not a significant statistical difference between the two models; consequently, either model would be sufficient when there is no inhibition.

The Monod model parameters, μ_{\max} and K_m , are 0.41 hr^{-1} and $4.4 \frac{\text{mg}}{\text{L}}$, respectively,

whereas, the predicted model has a μ_{\max} of 0.43 hr^{-1} and a K_m of $1.7 \frac{\text{mg}}{\text{L}}$. The experimental maximum specific growth rate is $0.42 \pm 0.01 \text{ hr}^{-1}$ with a Monod constant, K_m , of $7.0 \pm 1.0 \frac{\text{mg}}{\text{L}}$ with 95% confidence. That is with the experimental Monod constant determined by

linear interpolation. The experimental and modelled Monod constants are significantly different at the 95% confidence level. This discrepancy is unknown, but the Monod

model has a better representation for K_m when substrate inhibition is not a factor;

however, further experiments at these values should be conducted to verify the

approximated K_m .

2.4.c Dual Substrate Growth: D-xylose and Carbon Monoxide

Dual substrate experiments were conducted to understand the impact on the growth rate when carbon monoxide and D-xylose, where utilized simultaneously. Figures 2-6 and 2-7 show the growth curves with carbon monoxide in the headspace at concentrations approximately to 1000 ppm_v and D-xylose concentrations from 0 $\frac{g}{L}$ to 5 $\frac{g}{L}$ at 1 $\frac{g}{L}$ increments with 95% confidence.

Equation 2.12 was used to compute the specific growth rates at each concentration of D-xylose with carbon monoxide. The dual substrate models, Equation 2.11, with the same Monod constants as growth on D-xylose and the experimental data at 95% confidence are represented in Figure 2-8. The dual substrate models with the parameters are shown in Table 2-1.

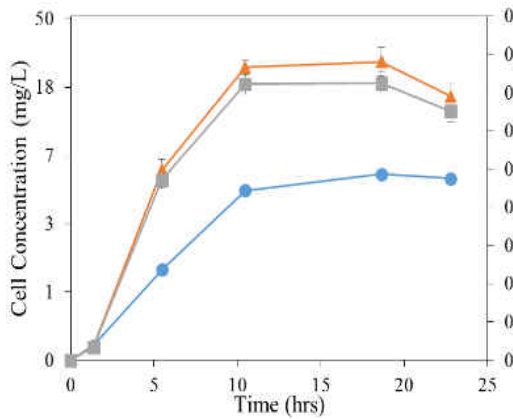


Figure 2-6: Carbon monoxide growth curves with 0.00 g/L (●), 1.00 g/L (▲), and 2.00 g/L (■) of D-xylose.

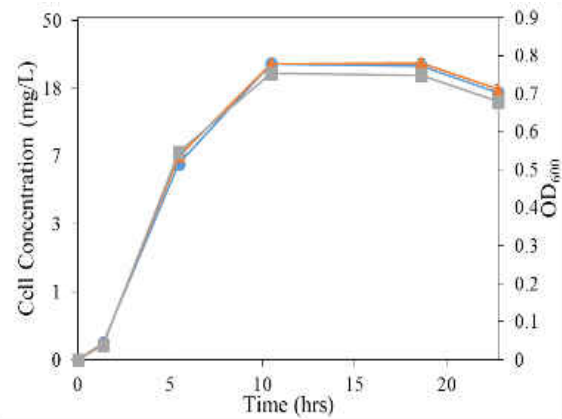


Figure 2-7: Carbon monoxide growth curves with 3.00 g/L (●), 4.00 g/L (▲), and 5.00 g/L (■) of D-xylose.

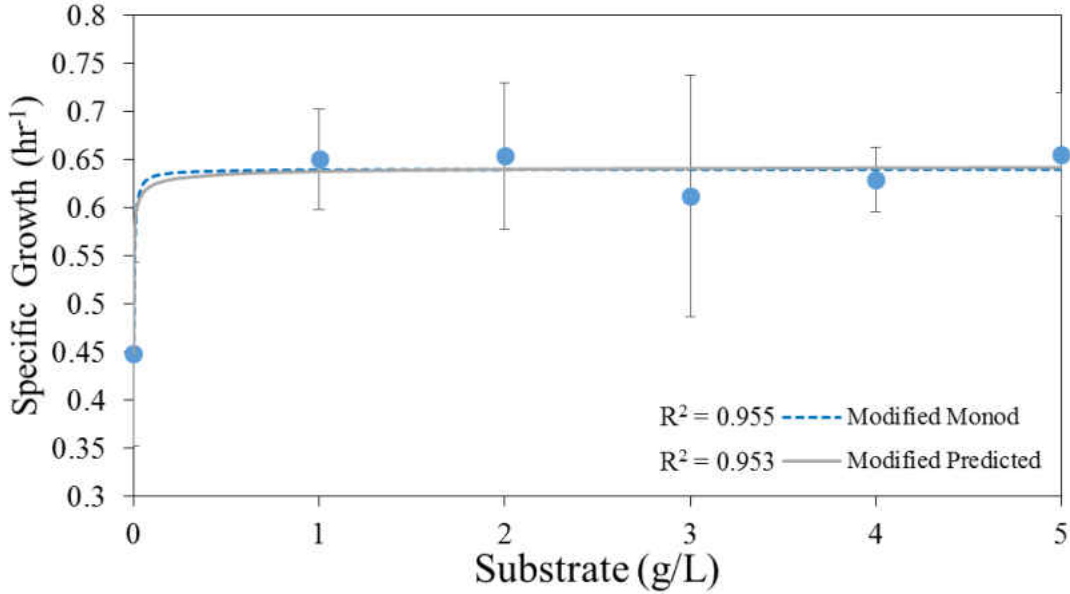


Figure 2-8: Specific growth rates of carbon monoxide with 0.00 g/L to 5.00 g/L of D-xylose with a modified Monod and predicted model.

Table 2-1: Biokinetic inhibition models with constants for *C. autoethanogenum*.

Model	Equation	Constants
Monod	$\mu = \frac{\mu_{max}S}{K_m + S} + \mu_{mix}$	$\mu_{max} = 0.19 \text{ hr}^{-1}$ $\mu_{mix} = 0.45 \text{ hr}^{-1}$ $K_m = 4.36 \frac{mg}{L}$
Predicted	$\mu = \frac{\mu_{max}\sqrt{S}}{\sqrt{K_m} + \sqrt{S}} + \mu_{mix}$	$\mu_{max} = 0.20 \text{ hr}^{-1}$ $\mu_{mix} = 0.45 \text{ hr}^{-1}$ $K_m = 1.58 \frac{mg}{L}$

2.4.d Growth Kinetics with D-xylose: Inhibition

The same process that was used in Section 2.4.b was used for the inhibition model. Experimental specific growth rates for concentrations from 0 $\frac{g}{L}$ to 300 $\frac{g}{L}$ are shown in Figure 2-9 with 95% confidence along with the predicted, Monod, Han and Levenspiel[18], and Webb[18] inhibition models. Table 2-2 shows the model equations with the inhibition parameters. Other inhibition models such as Tseng and Wayman[19], Haldane[20], Tessier[18], Yano[21], Aiba[22], and Andrews[23] were used, but these models did not fit the data as well.

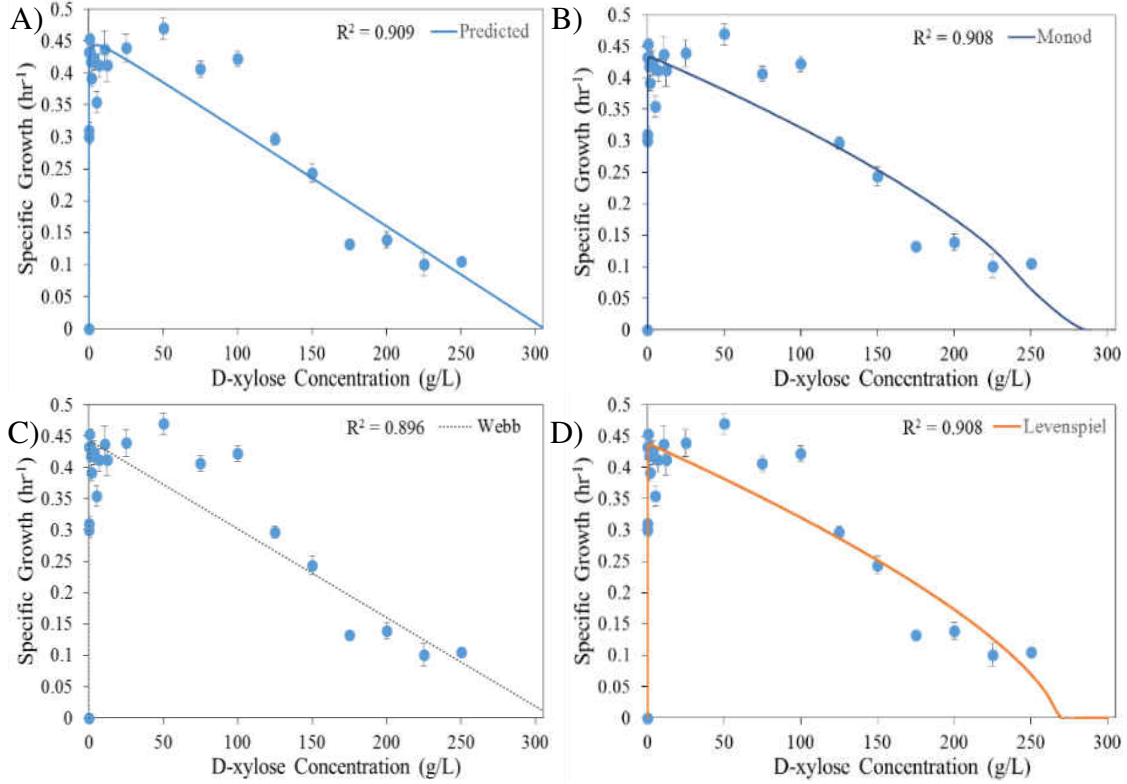


Figure 2-9: Models fitted to the experimental data with. A) Predicted B) Monod C) Webb D) Levenspiel.

Table 2-2: Biokinetic inhibition models with constants for *C. autoethanogenum*.

Model	Equation	Constants
Han and Levenspiel[18]	$\mu = \left[\left(1 - \frac{S}{S_c} \right)^n \right] \frac{\mu_{max} S}{S + K_m \left(1 - \frac{S}{S_c} \right)^m}$	$\mu_{max} = 0.44 \text{ hr}^{-1}$ $K_m = 5.75 \frac{\text{mg}}{\text{L}}$ $S_c = 268 \frac{\text{g}}{\text{L}}$ $n = 0.677$ $m = 0.641$
Webb[18]	$\mu = \frac{\mu_{max} S \left(1 + \frac{KS}{K_s} \right)}{S + K_m + \frac{S^2}{K_s}}$	$\mu_{max} = 0.44 \text{ hr}^{-1}$ $K_m = 6.62 \frac{\text{mg}}{\text{L}}$ $K = -306,000 \frac{\text{g}}{\text{L}}$ $K_s = 95,770,000 \frac{\text{g}}{\text{L}}$
Monod	$\mu = \left(1 - \frac{S}{S_c} \right)^n \frac{\mu_{max} S}{K_m + S}$	$\mu_{max} = 0.44 \text{ hr}^{-1}$ $K_m = 6.00 \frac{\text{mg}}{\text{L}}$ $S_c = 265 \frac{\text{g}}{\text{L}}$ $n = 0.649$
Predicted	$\mu = \left(1 - \frac{S}{S_c} \right) \frac{\mu_{max} \sqrt{S}}{\sqrt{K_m} + \sqrt{S}}$	$\mu_{max} = 0.46 \text{ hr}^{-1}$ $K_m = 4.46 \frac{\text{mg}}{\text{L}}$ $S_c = 306 \frac{\text{g}}{\text{L}}$

The Monod and Webb model half-velocity constant, K_m , agreed within the experimental value of $7.0 \pm 1.0 \frac{mg}{L}$, whereas the predicted and Levenspiel models predicted lower values. However, all models overestimate the measured maximum growth rate of $0.42 \pm 0.01 \text{ hr}^{-1}$. The predicted model is a less complicated model because less variable parameters have to be fitted with the experimental data to achieve similar or superior results.

2.5 Discussion

The growth rates experienced during this research are much greater than previous literature values. Köpke et al. (2011) had an approximate specific growth rate of 0.06 hr^{-1} on steel mill gas[4]. Mock et al. (2015) experienced a specific growth rate of 0.021 hr^{-1} , 0.046 hr^{-1} , and 0.14 hr^{-1} on a mixture of hydrogen and carbon dioxide, fructose, and steel mill gas, respectively[12]. Lastly, Kracke et al. (2016) had a specific growth rate of 0.053 hr^{-1} on D-fructose[10].

These differences may be speculated to the type of medium used (nutrients supplied) and/or oxygen concentrations present. For the former, all three researchers mentioned used a different medium, ATCC 1754, which is a modified medium of DSMZ 879. Medium DSMZ 879 is the suggested medium to cultivate *C. ljungdahlii*[24]. Köpke et al. (2011)[4] and Mock et al. (2015)[12] did not use yeast extract in their media, whereas Kracke et al. (2016)[10] used double the recommended amount of yeast extract. As for the latter, the oxygen concentration for all literature values were not listed and a few acknowledged that there was a possibility of oxygen being present during the experiments[1,5,8]. For this research, the oxygen meter within the anaerobic chamber had a minimum value of 0 ppm_v, and all experiments were conducted at this steady reading.

When substrate inhibition is not a factor the Monod model should be chosen because the Monod model fits the data slightly better and had a closer Monod constant to the experimental value. However, if substrate inhibition is a factor the proposed model is superior because the proposed model fits the data better, requires less parameters to model, and had a closer critical substrate constant compared to the experimental value. To verify the validity of the proposed model it is recommended for the model to be compared to other organisms that experienced substrate inhibition.

From Figure 2-5 and 2-8 *C. autoethanogenum* appears to have a higher affinity for carbon monoxide over D-xylose. The specific growth rate with a 1000 ppm_v of carbon monoxide, μ_{mix} , is greater than the maximum specific growth rate with D-xylose, μ_{max} . A beneficial trait that *C. autoethanogenum* has is that there is not an inhibition carbon monoxide concentration. In fact, 2,3-BDO productivity favors higher carbon monoxide concentration at standard pressures[25].

2.6 Conclusions

The following conclusions can be drawn from this work. *C. autoethanogenum* can utilize carbon monoxide and D-xylose simultaneously, which increases the overall maximum specific growth rate. This bacterium may prefer carbon monoxide over D-xylose as indicated by a higher growth rate with carbon monoxide compared to D-xylose. The maximum experimental growth rates with D-xylose, carbon monoxide, and a mixture of both were $0.42 \pm 0.01 \text{ hr}^{-1}$, $0.45 \pm 0.1 \text{ hr}^{-1}$, and $0.64 \pm 0.08 \text{ hr}^{-1}$ with 95% confidence, respectively. Substrate inhibition for *C. autoethanogenum* can be modeled more precisely with less parameters by the proposed model. Lastly, the maximum biomass and growth rate on D-xylose can be reached at concentrations of 7 and $0.10 \frac{g}{L}$, respectively.

References

- [1] Abubackar, H. N., Bengelsdorf, F. R., Dürre, P., Veiga, M. C., & Kennes, C. (2016). Improved operating strategy for continuous fermentation of carbon monoxide to fuel-ethanol by clostridia. *Applied Energy*, *169*, 210-217.
- [2] Abubackar, H. N., Fernández-Naveira, Á., Veiga, M. C., & Kennes, C. (2016). Impact of cyclic pH shifts on carbon monoxide fermentation to ethanol by clostridium autoethanogenum. *Fuel*, *178*, 56-62.
- [3] Liew, F., Henstra, A. M., Winzer, K., Köpke, M., Simpson, S. D., & Minton, N. P. (2016). Insights into CO₂ fixation pathway of clostridium autoethanogenum by targeted mutagenesis. *Mbio*, *7*(3), 10.1128/mBio.00427-16.
doi:10.1128/mBio.00427-16 [doi]
- [4] Köpke, M., Mihalcea, C., Liew, F., Tizard, J. H., Ali, M. S., Conolly, J. J., et al. (2011). 2,3-butanediol production by acetogenic bacteria, an alternative route to chemical synthesis, using industrial waste gas. *Applied and Environmental Microbiology*, *77*(15), 5467-5475. doi:10.1128/AEM.00355-11 [doi]
- [5] Cotter, J. L., Chinn, M. S., & Grunden, A. M. (2009). Ethanol and acetate production by clostridium ljungdahlii and clostridium autoethanogenum using resting cells. *Bioprocess and Biosystems Engineering*, *32*(3), 369-380.
- [6] Cotter, J. L., Chinn, M. S., & Grunden, A. M. (2009). Influence of process parameters on growth of clostridium ljungdahlii and clostridium autoethanogenum on synthesis gas. *Enzyme and Microbial Technology*, *44*(5), 281-288.

- [7] Abubackar, H. N., Veiga, M. C., & Kennes, C. (2012). Biological conversion of carbon monoxide to ethanol: Effect of pH, gas pressure, reducing agent and yeast extract. *Bioresource Technology*, *114*, 518-522.
- [8] Xu, H., Liang, C., Yuan, Z., Xu, J., Hua, Q., & Guo, Y. (2017). A study of CO/syngas bioconversion by *Clostridium autoethanogenum* with a flexible gas-cultivation system. *Enzyme and Microbial Technology*, *101*, 24-29.
- [9] Guo, Y., Xu, J., Zhang, Y., Xu, H., Yuan, Z., & Li, D. (2010). Medium optimization for ethanol production with *Clostridium autoethanogenum* with carbon monoxide as sole carbon source. *Bioresource Technology*, *101*(22), 8784-8789.
- [10] Kracke, F., Viridis, B., Bernhardt, P. V., Rabaey, K., & Krömer, J. O. (2016). Redox dependent metabolic shift in *Clostridium autoethanogenum* by extracellular electron supply. *Biotechnology for Biofuels*, *9*(1), 249.
- [11] Abrini, J., Naveau, H., & Nyns, E. (1994). *Clostridium autoethanogenum*, sp. nov., an anaerobic bacterium that produces ethanol from carbon monoxide. *Archives of Microbiology*, *161*(4), 345-351.
- [12] Mock, J., Zheng, Y., Mueller, A. P., Ly, S., Tran, L., Segovia, S., et al. (2015). Energy conservation associated with ethanol formation from H₂ and CO₂ in *Clostridium autoethanogenum* involving electron bifurcation. *Journal of Bacteriology*, *197*(18), 2965-2980. doi:10.1128/JB.00399-15 [doi]
- [13] Iowa State University (2006). Guide to Sterilization Times. Retrieved from <http://agron-www.agron.iastate.edu/cpandp/SOPs/Equipment/GuidetoSterilizationTimes.pdf>

- [14] Kim, D., Park, J. M., Song, H., & Chang, Y. K. (2016). Kinetic modeling of substrate and product inhibition for 2, 3-butanediol production by *Klebsiella oxytoca*. *Biochemical Engineering Journal*, 114, 94-100.
- [15] Han, K., & Levenspiel, O. (1988). Extended monod kinetics for substrate, product, and cell inhibition. *Biotechnology and Bioengineering*, 32(4), 430-447.
- [16] Fogler, H. S. (2006). *Bioreactors. Elements of chemical reaction engineering* (4th ed., pp. 424). Westford, MA: Pearson Education.
- [17] Kale, A. P. (2015). Cellular cannibalism. *Journal of Oral and Maxillofacial Pathology*, 19(1), 7-9.
- [18] Han, K., & Levenspiel, O. (1988). Extended monod kinetics for substrate, product, and cell inhibition. *Biotechnology and Bioengineering*, 32(4), 430-447.
- [19] Velizarov, S. and Beschkov, V. (1998). Biotransformation of glucose to free gluconic acid by *Gluconobacter oxydans*: Substrate and product inhibition situations. *Process Biochemistry*, 33(5), 527-534.
- [20] Haldane, J. B. S. (1965). *Enzymes* The MIT Press.
- [21] Yano, T., Nakahara, T., Kamiyama, S., & Yamada, K. (1966). Kinetic studies on microbial activities in concentrated solutions. *Agricultural and Biological Chemistry*, 30(1), 42-48.
- [22] Aiba, S., Shoda, M., & Nagatani, M. (1968). Kinetics of product inhibition in alcohol fermentation. *Biotechnology and Bioengineering*, 10(6), 845-864.
- [23] Andrews, J. F. (1968). A mathematical model for the continuous culture of microorganisms utilizing inhibitory substrates. *Biotechnology and Bioengineering*, X, 707-723.

- [24] Tanner, R. S., Miller, L. M., & Yang, D. (1993). *Clostridium ljungdahlii* sp. nov., an acetogenic species in clostridial rRNA homology group I. *International Journal of Systematic and Evolutionary Microbiology*, 43(2), 232-236.

Chapter 3

Syngas Formation, Compression, and Products with *C. autoethanogenum*

Abstract

Fermentation of acetogenic bacteria have been shown to produce valuable products such as 2,3-butanediol from carbon monoxide. The carbon monoxide previously supplied was synthetic or from a steel mill which does not contain impurities such as NO_x, H₂S, and many others found in synthesis gas from coal. Here we demonstrate the use of synthesis gas from lignite coal to produce fermentation products, 2,3-butanediol and ethanol, with *C. autoethanogenum* at pilot scale. The productivity of 2,3-butanediol in the stationary phase and ethanol over 24 hours are 0.36 and $41.6 \frac{mg}{L-hr}$, respectively.

3.1 Introduction

Many bacteria can generate fuels and chemicals from bio-based synthesis gas (syngas) such as *Clostridium autoethanogenum*, *Butyribacterium methylotrophicum*, and Mesophilic *bacterium* P7 to name a few[1]. Bio-based syngas can be formed by gasification of a variety of lignocellulosic sources like switchgrass[2], pine wood chips[3], willow[4], cacao shells[4], dairy biomass[5], bluegrass straw[6], and paper residue[4]. Certain organisms can utilize this bio-based syngas due to the metabolic pathway, acetyl-CoA, used and possess carbon monoxide dehydrogenase. It is suggested that anaerobic bacteria are the only type that can utilize the acetyl-CoA pathway[7]. Bio-based syngas is a usable substrate for fuels, but a cheaper and well established feedstock

for the production of syngas is coal[8,9] However, coal has impurities like sulfur and mercury which may impact cellular growth and product formation. Currently the only coal fermentation known to the authors is the use of methane producing bacteria in enriched methanogenus mine water[10,11]. This study looked into how the impurities from coal affect product and cellular formation with an acetogenic bacterium *C. autoethanogenum*.

3.2 Materials, Method, and Equipment

3.2.a Overview of Whole Process

The process to make syngas from coal and to ferment with this syngas is a cumbersome process. The primary processes are gasification of the coal, storage of the syngas, fermentation with the syngas, and analyzing products. The block flow diagram of this process is shown in Figure 3-1.

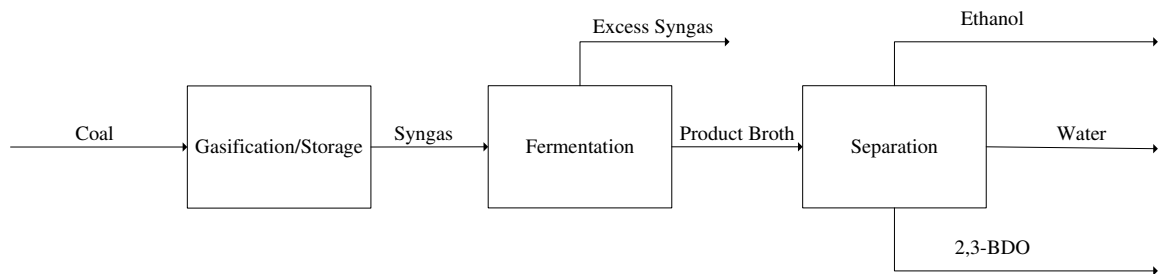


Figure 3-1: Overall process to convert coal to saleable bio-products.

3.2.b Overall Gasification System

The original design of the fluidized bed gasification system was done by Robert Mota (2013)[12], which had a coal feeder, an air pre-heater, a steam generator, a heated fluidized bed (fluidized with nitrogen and oxygen), a cyclone, two condensers, and a laser gas analyzer (LGA). The modified design now has two bag filters replacing the cyclone and a single condenser. To store the synthesis gas (syngas) formed from coal a compression system was designed after the condenser. A more detailed description of the

compression system can be found in Section 3.2.c. The original design can be seen in Figure 3-2 and the new design can be found in a process flow diagram shown in Figure 3-3.



Figure 3-2: Original gasification design by Robert Mota[1].

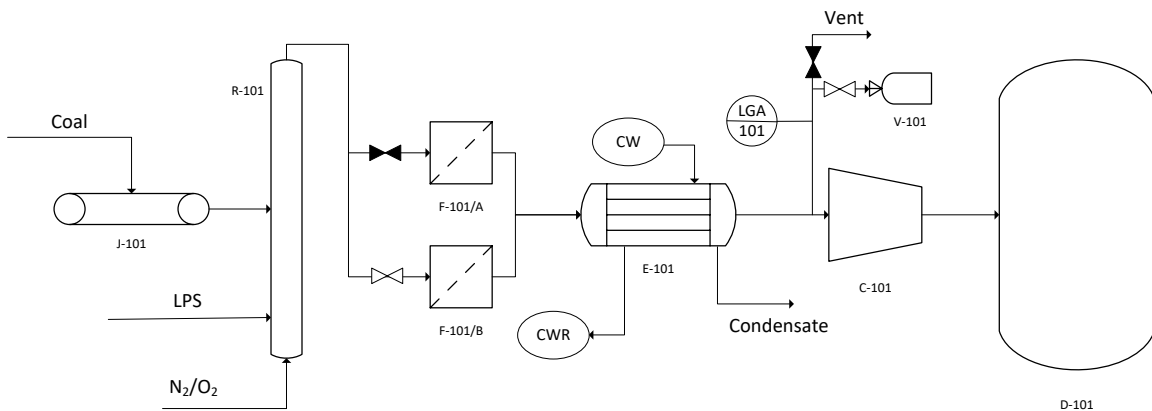


Figure 3-3: New gasification design with compression system where J-101 is a screw feeder, R-101 is the fluidized bed reactor, F-101 are bag house filters, E-101 is a condenser, C-101 is a compressor, V-101 is an inflatable storage bag, and D-101 is a storage tank.

As shown in Figure 3-3, the bag filters, Part PEMFXL1.0P1S, are ran in parallel with one in operation. This redundancy is used to clean the filter without shutting down production. A pressure differential between the fluidized bed and the product stream is used to determine if the bag filter needs replacing. The bag house, unlike the cyclone, has dual roles; to filter the char from the gaseous stream and to remove tar that condenses at room temperature. Low pressure steam (LPS) is used for steam gasification which produces carbon monoxide and hydrogen. The reactions associated with gasification can be found in Section 1.4.

3.1.b Gasification Operation

The fluidized bed gasifier was charged with two pounds of sand that was between 20 and 40 mesh and 12.5 weight percent of limestone as the starting bed material. Limestone was added to remove sulfur components that are generated from the lignite coal. Lignite coal between 18-60 mesh was added at a rate of approximately $0.5 \frac{lbs}{hr}$ at the screw feeder (J-101). The ultimate analysis of the coal used is shown in Table 3-1.

Table 3-1: Ultimate analysis of lignite coal.

	As Detected (%)	As Received (%)	Dry (%)	Dry/Ash Free (%)
Hydrogen	5.50	5.50	4.16	4.40
Carbon	51.88	51.88	64.09	67.83
Nitrogen	0.86	0.86	1.06	1.12
Sulfur	0.54	0.54	0.67	0.71
Oxygen	36.76	36.76	24.51	25.94
Ash	4.46	4.46	5.51	N/A
$\hat{H} \left(\frac{Btu}{lb} \right)$	8628	8628	10658	11280

By Table 3-1 the process requires $0.06 \frac{lbmol O_2}{lb-coal}$ to be added for complete combustion based on the reaction $C + O_2 \rightarrow CO_2$; however, this was not the actual amount of oxygen used because it was desirable to achieve high concentrations of carbon monoxide and

hydrogen in the syngas to utilize the methyl and carbonyl branch. Consequently, water and oxygen were fluctuated during the process because steady state was never reached. Water, when added, was entered at $0.5 \frac{mL}{min}$ while oxygen varied greatly by the operator. The gasifier was operated at 750°C with a gas pre-heater temperature of 400°C.

3.1.c Compression System

The compression system was designed for lab scale production. A three-gallon portable Fini air compressor from Menards, Model F3OL197N, was used as the in-line compressor. This compressor leaked around the piston head and partially pulled gas from the surrounding; therefore, a carbon dioxide blanket around the compressor was made by placing the compressor into a plastic storage container which was sealed with high temperature RTV silicone and slightly pressurized with carbon dioxide. This was done to maintain an oxygen concentration below 5 ppm_v which was needed for the anaerobic bacterium, *C. autoethanogenum*, to survive. An inflatable bag, Part 78917, was used to collect syngas that satisfied operation specifications prior to compression. The inflatable bag was used as a short-term storage container because the syngas flow rate exiting the condenser is at nearly atmospheric conditions and the compressor had an inlet gas flow rate greater than the production of syngas. The compressed syngas then flowed through a packed bed reactor that contained palladium, Pt, to react the hydrogen and the remaining oxygen by Equation 3.1 before entering a 120-gallon tank that was purchased from compressor world, Model 302423. The storage tank was compressed to 120 psi_g for a 24 hour experiment.



3.1.d Medium Preparation, Bioreactor Set-up, and Inoculation

Bacterial freeze-dried pellets of *C. autoethanogenum*, DSM 10061, were obtained from DSMZ (Deutsche Sammlung von Mikroorganismen und Zellkulturen GmbH, Braunschweig, Germany) and was revived in DSMZ medium 640 with D-xylose. Medium 640 contains, per liter, 0.90 g NH₄Cl, 0.90 g NaCl, 0.40 g MgCl₂ x 6 H₂O, 0.75 g KH₂PO₄, 1.50 g K₂HPO₄, 2.00 g trypticase peptone, 0.75 g L-cysteine-HCl x H₂O, 5.00 mg FeCl₃ x 6 H₂O, and 5.00 mL trace solution. The trace solution contains, per 990 mL, 10.00 mL HCl (7.7M), 1.50 g FeCl₂ x 4 H₂O, 70.00 mg ZnCl₂, 100.00 mg, MnCl₂ x 4 H₂O, 6.00 mg H₃BO₃, 190.00 mg CoCl₂ x 6 H₂O, 2.00 mg CuCl₂ x 2 H₂O, 24.00 mg NiCl₂ x 6 H₂O, and 36.00 mg Na₂MoO₄ x 2 H₂O. To revive the bacterium, a Coy vinyl anaerobic chamber with a palladium catalyst and an oxygen concentration in the parts per billion with the balance nitrogen was used. A Tuttnaurer Ez10 or Consolidated Mark II autoclave, depending on the volume required, was used to sterilize the media before inoculation. The medium was autoclaved at 250°F for the recommended length of time per mL of media by Iowa State University[13], and the initial pH of the medium was at 6.4.

A 14 L continuously stirred tank reactor (CSTR) from Eppendorf was utilized for growth and product formation by *C. autoethanogenum*. Temperature, dissolved oxygen (DO), agitation rate, gas flow rate, and pH were monitored throughout the experiment. A bioreactor schematic can be seen in Figure 3-4.

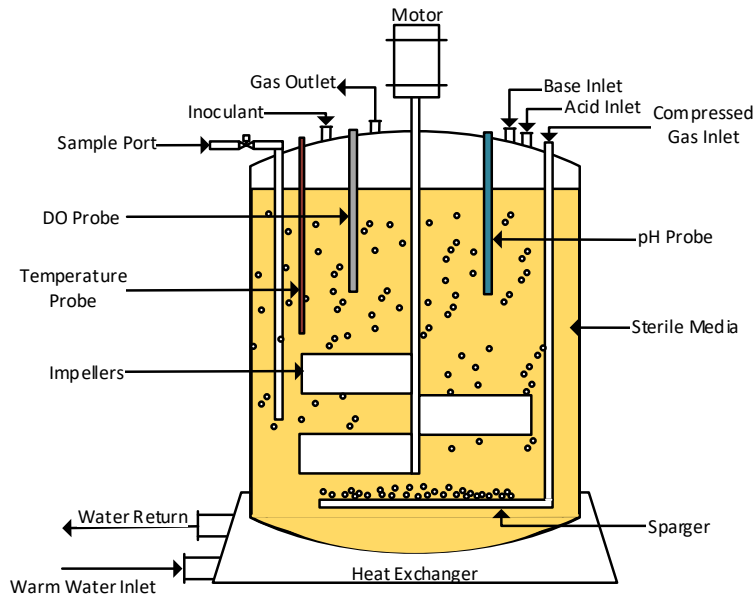


Figure 3-4: Bioreactor schematic.

The bioreactor contained 5L of DSMZ media 640 and was inoculated from a previous batch that was in the exponential phase at $5.4 \times 10^8 \frac{CFU \text{ of Bacteria}}{mL \text{ of Media}}$. A peristaltic pump with a Covidien 30 gauge hypodermic needle, Model 1188830340, and a Cilran transfer tube, Part C006021, was used to inoculate the bioreactor to insure anaerobic conditions and sterility.

3.1.e Growth Curve and Product Analysis

10 mL samples were removed periodically for a growth curve, whereas only a single 100 mL sample was removed after 24 hours for product analysis.

The turbidity of the 10 mL samples were monitored with a UV-Vis Evolution 600 at an optical density of 600 nm (OD_{600}). Due to low initial cell concentrations, it was assumed that the initial absorbance was zero, and showed to be a viable assumption through experiment with an OD_{600} reading of 0.017 ± 0.21 at 95% confidence. Cell

density conversion from OD₆₀₀ to $\frac{mg}{L}$ was determined according to a previously obtained calibration curve shown in Figure 2-1.

The single 100 mL sample was distilled through simple distillation until the low boiling point products (<100 °C) were removed to separate products and the distillate volume was recorded. The remaining high boiling point products (>100 °C) were collected and the volume was recorded. Metabolite concentrations of the two samples were determined using an Agilent 7890A gas chromatography (GC) machine equipped with a flame ionization detector (FID) and a fused-silica capillary column (SLB-5ms, 30 m x 0.25 mm x 0.25 μm). Nitrogen was used as the carrier gas at constant pressure of 12 psi_g with a split ratio of 1:10. Hydrogen, air, and makeup (helium) flow were 40, 400, and 30 $\frac{mL}{min}$, respectively. The injector and detector temperature were 250°C and 280°C, respectively. The initial oven temperature was 40°C. For analyzing 2,3-BDO, the oven temperature was increased after 2 minutes at a rate of 10 $\frac{°C}{min}$ until it reached 280°C. For analyzing ethanol, the oven temperature was increased after 2 minutes at a rate of 10 $\frac{°C}{min}$ until it reached 100°C.

3.2 Results and Discussion

3.2.a Syngas Production

Gasification products were produced at or near commercial grade syngas, but the carbon dioxide drastically increased after passing through the compression step due to the leaky piston. Table 3-2 shows the volume composition of the syngas entering the compressor and at the end of the operation.

Table 3-2: Volume composition of syngas before and after compression.

	Before Compression	After Compression
Carbon Monoxide (%)	20	5.44
Water (%)	4	3.82
Hydrogen Sulfide (ppm)	1000	226
Oxygen (ppm)	30	0
Hydrogen (%)	8	2.00
Carbon Dioxide (%)	20	63.35
Methane (ppm)	14,000	4610
Nitrogen (%)	50	23.38

The rate of gas pulled from the surroundings compared to the rate of syngas is approximately 2:1. That was determined by conducting a mass balance around the system with the surrounding gas being 86% carbon dioxide, 11% nitrogen and the balance oxygen. The water vapor concentration increased due to the reaction between hydrogen and oxygen on the palladium catalyst before storage.

From Table 3-2 it is clear that an in-line compressor from the local hardware store is insufficient to maintain commercial grade syngas. An alternative compressor that would better suit this operation is a Powermate single stage inline-twin compressor with cast iron cylinders, Model 040-0425RP. However, the inlet flow rate of the suggested compressor is much greater than the production rate for this system so a larger bladder bag may be required.

3.3.b C. *autoethanogenum* Growth Curve

The flow rate of syngas into the reactor was constant at $0.5 \frac{mL}{min}$ for 24 hours. Six samples were extracted at approximately four-hour intervals and the resulting growth curve is shown in Figure 3-4. *C. autoethanogenum* appeared to experience cellular cannibalism after 12 hours of growth which was not observed with steel mill gas[16]. This may be due to the use of a bioreactor with continuous substrate feed at atmospheric pressure or due to being in contact with hydrogen sulfide and other impurities. The

former is unlikely because the research conducted by Abubacker et al. (2016) was continuous fed batch as well and cellular cannibalism was not experienced to this extent[14]. The maximum biomass experienced is also lower than expected due to previous literature values. Cotter et al. (2009)[15], Köpke et al. (2011)[16], and Xu et al. (2017)[17] achieved cell concentrations of $150 \frac{mg}{L}$, $1.0 OD_{600}$, and $165 \frac{mg}{L}$, respectively, on synthetic syngas or steel mill gas. The primary hypothesis for the large differences in cell density is the impurities within the syngas formed from coal. Initially the differences between cell density was contributed to being a fed batch system; however, Cotter et al. (2009) utilized a fed batch system as well[15].

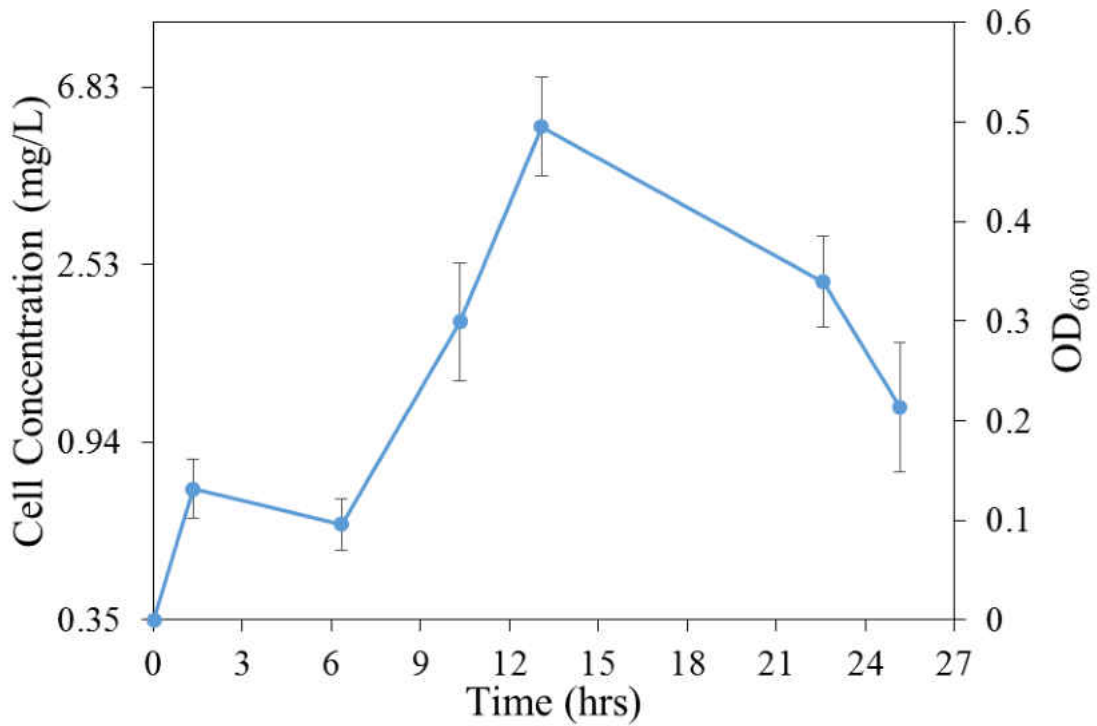


Figure 3-5: Growth curve of synthesis gas in bioreactor.

3.3.c 2,3-BDO and Ethanol Rate of Formation Analyses

The formation of 2,3-BDO and ethanol that was experienced was $4.30 \frac{mg}{L}$ and $1.00 \frac{g}{L}$, respectively. The productivity of 2,3-BDO in the stationary phase was $0.36 \frac{mg}{L-hr}$;

whereas, the productivity of ethanol over the 24 hour period was $41.6 \frac{mg}{L-hr}$. 2,3-BDO productivity was calculated after the stationary phase was achieved because the analysis conducted by Köpke et al. (2011) suggested that 2,3-BDO is not formed until the stationary phase[16]. The experimental data retrieved from the GC for 2,3-BDO and ethanol production at 24 hours are shown in Appendix A Figures A-37 and A-38, respectively.

Cotter et al. (2009)[15] and Xu et al. (2017)[17] either did not observe or did not measure 2,3-BDO formation; however, the normalized production rate of 2,3-BDO experienced by Köpke et al. (2011)[16] was $1.96 \frac{mg}{L-hr}$. The low production rate of 2,3-BDO, biomass production, and high cellular cannibalism experienced may be due to the impurities within the synthesis gas. This is the first known experiment that uses raw syngas from coal for production of 2,3-BDO; therefore, more experiments have to be conducted to further determine the effects of the impurities hydrogen sulfide, methane, trace metals, and other impurities.

Cotter et al (2009)[15], Köpke et al. (2011)[16], and Xu et al. (2017)[17] experienced an ethanol production rate of 5.35, 5.04, and $0.44 \frac{mg}{L-hr}$, respectively. In this study there was a huge increase in ethanol productivity, $41.6 \frac{mg}{L-hr}$. This large increase could be complementary to as why 2,3-BDO productivity dropped, which suggests that the impurities in the syngas suppress pyruvate:ferredoxin oxidoreductase. Again, further studies on varying concentrations of impurities need to be conducted to verify this hypothesis.

3.4 Conclusion

C. autoethanogenum can sustain life with the use of syngas generated by coal, but the bacterium does not thrive in the environment as shown by the cell density achieved. This is believed to be from the sulfur and potentially the untraceable amount of metals such as mercury within the syngas produced. In future studies hydrogen sulfide concentrations can be manipulated to determine if this bacterium will thrive better in a low sulfur coal. However, ethanol production with syngas was substantially higher than any other tests previously conducted. This suggests that these impurities may strain the bacterium and shift the metabolic pathway to produce less 2,3-BDO and more ethanol. 2,3-BDO was the original product of choice, but it may be useful to further study the production rates of ethanol at steady state operation for economic analysis.

References

- [1] Tirado-Acevedo, O., Chinn, M., & Grunden, A. (2010). Production of biofuels from synthesis gas using microbial catalysts. *Advances in Applied Microbiology*, 70, 57-92.
- [2] Datar, R., Shenkman, R., Cateni, B., Huhnke, R., & Lewis, R. (2004). *Fermentation of biomass-generated producer gas to ethanol*. Wiley InterScience,
- [3] Corella, J., Orio, A., & Aznar, P. (1998). Biomass gasification with air in fluidized bed: Reforming of the gas composition with commercial steam reforming catalysts. *Industrial Engineering Chemical Resources*, 37, 4617-4624.
- [4] van der Drift, A., van Doorn, J., & Vermeulen, J. W. (2001). Ten residual biomass fuels for circulating fluidized-bed gasification. *Biomass and Bioenergy*, 20(1), 45-56.
- [5] Gordillo, G., & Annamalai, K. (2010). Adiabatic fixedbed gasification of dairy biomass with air and steam. *Fuel*, 89(2), 384-391.
- [6] Boateng, A. A., Banowetz, G. M., Steiner, J. J., Barton, T. F., Taylor, D. G., Hicks, K. B., et al. (2007). Gasification of kentucky bluegrass (*Poa pratensis* L.) straw in a farm-scale reactor. *Biomass and Bioenergy*, 31(2-3), 153-161.
- [7] Henstra, A. M., Sipma, J., Rinzema, A., & Stams, A. J. (2007). Microbiology of synthesis gas fermentation for biofuel production. *Current Opinion in Biotechnology*, 18(3), 200-206.
- [8] Nguyen, M., Duddy, G., & Karam, C. (2015). Analysis of industrial syngas production from biomass. *Energy Science and Technology*,
- [9] Staffell, I. (2011). The energy and fuel data sheet

- [10] Gupta, P., & Gupta, A. (2014). Biogas production from coal via anaerobic fermentation. *Fuel*, 118(15), 238-242.
- [11] Xia, D., Zhang, H., Su, X., Liu, X., & Fu, C. (2017). Pilot test of a fermentation tank for producing coal methane through anaerobic fermentation. *Sains Malaysiana*, 46(11), 2083-2089.
- [12] Mota, R. (2013). Design and construction of a fluidized bed. Umi, #1552207
- [13] Iowa State University (2006). Guide to Sterilization Times. Retrieved from <http://agron-www.agron.iastate.edu/cpandp/SOPs/Equipment/GuidetoSterilizationTimes.pdf>
- [14] Abubackar, H. N., Bengelsdorf, F. R., Dürre, P., Veiga, M. C., & Kennes, C. (2016). Improved operating strategy for continuous fermentation of carbon monoxide to fuel-ethanol by clostridia. *Applied Energy*, 169, 210-217.
- [15] Cotter, J. L., Chinn, M. S., & Grunden, A. M. (2009). Influence of process parameters on growth of clostridium ljungdahlii and clostridium autoethanogenum on synthesis gas. *Enzyme and Microbial Technology*, 44(5), 281-288.
- [16] Köpke, M., Mihalcea, C., Liew, F., Tizard, J. H., Ali, M. S., Conolly, J. J., et al. (2011). 2,3-butanediol production by acetogenic bacteria, an alternative route to chemical synthesis, using industrial waste gas. *Applied and Environmental Microbiology*, 77(15), 5467-5475. doi:10.1128/AEM.00355-11 [doi]
- [17] Xu, H., Liang, C., Yuan, Z., Xu, J., Hua, Q., & Guo, Y. (2017). A study of CO/syngas bioconversion by clostridium autoethanogenum with a flexible gas-

Chapter 4

Product Formation with Design of Experimental Analysis

Abstract

A fractional factorial design was applied to determine which operating factors statistically affect 2,3-butanediol and ethanol formation by *C. autoethanogenum* with carbon monoxide as the primary substrate. 2,3-butanediol production is affected by two interaction terms: gas flow rate and D-xylose, and carbon monoxide and oxygen concentration. The optimal condition for 2,3-butanediol production is a pH of 5.75, a gas flow rate of $0.4 \frac{L}{min}$, a carbon monoxide concentration of 60 volume percent, a dissolved oxygen concentration of 0 percent, a temperature of 35°C, and no D-xylose. On the other hand, ethanol production was statistically unaffected at the 95% confidence level. The productivity of 2,3-butanediol in the stationary phase at the optimal conditions and the average productivity of ethanol over 24 hours was 3.0 and $100 \pm 80 \frac{mg}{L-hr}$.

4.1 Introduction

2,3-butanediol (2,3-BDO) is a valuable chemical and is used as a fuel additive, in certain gas chromatograph applications, and polymers. It is found naturally in sweet corn, fermented soybean curds, whole and ground grains, and rotten mussels[1]. 2,3-BDO is also produced through the hydrolysis of 2,3-epoxybutane[2]. It is desirable to find an economical and sustainable way to commercially produce this chemical with waste.

Certain bacterial strains can synthesize this product and production of this chemical was found by researching pathogenic bacteria such as *Klebsiella oxytoca*,

Enterobacter aerogenes, and *Bacillus lichiformis*[3]. *K. oxytoca* can lead to nosocomial outbreaks[4], *E. aerogenes* is an opportunistic bacterium that causes disease to patients with weakened immune systems[5], and *B. lichiformis* can cause food poisoning[6]. The pathogenic traits of these bacteria make it unfeasible to utilize them as a major source to produce 2,3-BDO.

In recent years, there has been discovery of non-pathogenic, strict anaerobic bacteria from the Clostridium family that can also synthesize 2,3-BDO. These bacteria are *C. autoethanogenum*, *C. ljungdahlii*, and *C. ragsdahlii*. All three strains have been shown to produce 2,3-BDO by utilizing carbon monoxide as the primary carbon source[7]. There has been a significant amount of research in optimizing the media and conditions to maximize the production of ethanol to acetate ratios while utilizing carbon monoxide as the primary substrate.

With this there has been little to no research on what factors may affect 2,3-BDO formation in batch form. A few researchers, Kracke et al. (2016)[8], Liew et al.(2017[9], and Abubacker et al (2016^{a,b})[10,11], have looked at the effect of external electron supply, changing enzymatic functions, and pH shifts, respectively, on 2,3-BDO production, but more research needs to be conducted. The primary factors that affect product formation from gaseous substrates are pH, temperature, media type, mass transfer, and reactor type[12]. Of these, this study considered pH, temperature, carbon monoxide concentration, oxygen concentration, gas flow rate, and the use of dual substrate.

4.2 Materials, Method, and Equipment

4.2.a Microorganism

Bacterial freeze-dried pellets of *C. autoethanogenum*, DSM 10061, were obtained from DSMZ (Deutsche Sammlung von Mikroorganismen und Zellkulturen GmbH, Braunschweig, Germany) and was revived in DSMZ medium 640 with D-xylose. Medium 640 contains, per liter, 0.90 g NH₄Cl, 0.90 g NaCl, 0.40 g MgCl₂ x 6 H₂O, 0.75 g KH₂PO₄, 1.50 g K₂HPO₄, 2.00 g trypticase peptone, 0.75 g L-cysteine-HCl x H₂O, 5.00 mg FeCl₃ x 6 H₂O, and 5.00 mL trace solution. The trace solution contains, per 990 mL, 10.00 mL HCl (7.7M), 1.50 g FeCl₂ x 4 H₂O, 70.00 mg ZnCl₂, 100.00 mg, MnCl₂ x 4 H₂O, 6.00 mg H₃BO₃, 190.00 mg CoCl₂ x 6 H₂O, 2.00 mg CuCl₂ x 2 H₂O, 24.00 mg NiCl₂ x 6 H₂O, and 36.00 mg Na₂MoO₄ x 2 H₂O. To revive the bacterium, a Coy vinyl anaerobic chamber with a palladium catalyst and an oxygen concentration in the parts per billion with the balance nitrogen was used. A Tuttnaurer Ez10 autoclave or Consolidated Mark II autoclave, depending on the volume required, was used to sterilize the media before inoculation. The medium was autoclaved at 250°F for the recommended length of time per mL of media by Iowa State University[13], and the initial pH of the medium was at 6.4. D-xylose was sterilized by filtration with a 0.22 μm polyvinylidene fluoride (PVDF) filter, Model SLGV013SL.

4.2.b Bioreactor Inoculation and Set-up

A 14 L continuously stirred tank reactor (CSTR) from Eppendorf was utilized for growth and product formation by *C. autoethanogenum*. Temperature, dissolved oxygen (DO), agitation rate, gas flow rate, and pH were monitored throughout the experiment. A bioreactor schematic can be seen in Figure 4-1.

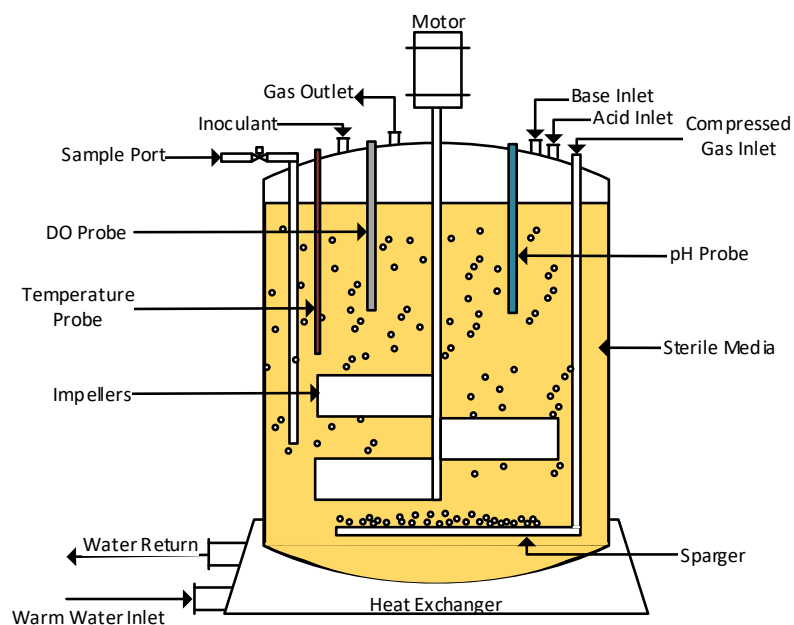


Figure 4-1: Bioreactor schematic.

The bioreactor contained 5L of DSMZ media 640 and was inoculated from a previous batch that was in the exponential phase at $5.4 \times 10^8 \frac{CFU \text{ of Bacteria}}{mL \text{ of Media}}$. A peristaltic pump with a Covidien 30 gauge hypodermic needle, Model 1188830340, and a Cilran transfer tube, Part C006021, was used to inoculate the bioreactor to insure anaerobic conditions and sterility.

4.2.c Bioreactor Fractional Factorial Design

A $\frac{1}{4}$ fractional factorial design was conducted to determine the most significant factors that affect the production of 2,3-BDO and ethanol. The agitation speed was constant at 40 rpm with an initial temperature of 30°C. Six parameters were varied for this experiment for a total of 16 runs. The six parameters varied were flow rate, carbon monoxide concentration, dual substrate growth with D-xylose, temperature shift, pH shift, and dissolved oxygen (DO) shift. The coded and uncoded values for the parameters are shown in Table 1.

Table 4-1: Coded and uncoded parameter values.

Parameter	Coded Value	Uncoded Value
pH	-1	4.5
	1	7
Flow	-1	0.4 Lpm
	1	2.0 Lpm
[CO]	-1	20 Vol. %
	1	100 Vol. %
[O ₂]	-1	0 DO %
	1	40 DO %
Temperature	-1	25°C
	1	45°C
D-xylose	-1	0.0 $\frac{g}{L}$
	1	0.1 $\frac{g}{L}$

Flow rate, carbon monoxide concentration, and initial D-xylose concentration were unadjusted throughout the 24 hour experiment, whereas the temperature, pH, and DO were changed after six hours to the appropriate condition for the screening design. Temperature, pH, and DO were not shifted at the beginning of the fermentation to prevent premature inhibition. An additional experiment was conducted to validate a coded regression model provided by the fractional factorial design. This additional experiment was a 96 hour experiment where samples were removed every 24 hours to relate time to the productivity of the bacterium. Table 4-2 represents the non-randomized $\frac{1}{4}$ fractional factorial design and the preliminary optimized experimental run.

Table 4-2: Non-randomized fractional factorial design with optimized experimental runs.

Std. Run Order	pH	Flow Rate (Lpm)	CO Conc. (Vol. %)	O ₂ Conc. (DO %)	Temperature (°C)	D-xylose ($\frac{g}{L}$)
1	-1	-1	-1	-1	-1	-1
2	1	-1	-1	-1	1	-1
3	-1	1	-1	-1	1	1
4	1	1	-1	-1	-1	1
5	-1	-1	1	-1	1	1
6	1	-1	1	-1	-1	1
7	-1	1	1	-1	-1	-1
8	1	1	1	-1	1	-1
9	-1	-1	-1	1	-1	1
10	1	-1	-1	1	1	1
11	-1	1	-1	1	1	-1
12	1	1	-1	1	-1	-1
13	-1	-1	1	1	1	-1
14	1	-1	1	1	-1	-1
15	-1	1	1	1	-1	1
16	1	1	1	1	1	1
Optimum	0	-1	0	-1	0	-1

Temperature and flow rate affect the mass transfer rate, while pH, dual substrate growth, carbon monoxide concentration and DO concentration was believed to affect enzymatic function. The addition of D-xylose was believed to be an important parameter because dual substrate biomass concentrations were greater than using single substrate[14]. DO concentration, carbon monoxide concentration, and pH were believed to affect the metabolic production by straining the bacterium[15].

4.2.d Product Analytic Methods

Samples were removed from the bioreactor after 24 hours and distilled through simple distillation until the low boiling point products (<100 °C) were removed and the distillate volume was recorded. The remaining high boiling point products (>100 °C) were collected and the volume was recorded. Metabolite concentrations of the two samples were determined using an Agilent 7890A gas chromatography (GC) machine

equipped with a flame ionization detector (FID) and a fused-silica capillary column (SLB-5ms, 30 m x 0.25 mm x 0.25 μm). Nitrogen was used as the carrier gas at constant pressure of 12 psi with a split ratio of 1:10. Hydrogen, air, and makeup (helium) flow were 40, 400, and 30 $\frac{mL}{min}$, respectively. The injector and detector temperature were 250°C and 280°C, respectively. The initial oven temperature was 40°C. For analyzing 2,3-BDO, the oven increased after 2 minutes and increased at a rate of 10 $\frac{°C}{min}$ until it reached 280°C. For analyzing ethanol, the oven increased after 2 minutes and increase at a rate of 10 $\frac{°C}{min}$ until it reached 100°C.

The high boiling point products used methanol as the internal standard due to the high boiling point products being extremely polar, whereas, the low boiling products used n-butanol as the internal standard. Both products were mixed with a 1:10 volume ratio of solvent to sample before injection into the GC. A blank run of dichloromethane (DCM) was injected between each GC run to flush the capillary column to prevent saturation. A single point internal standard method was used to determine the concentration of product within the sample[19]. The equation for this method is shown in Equation 4.1.

$$C_{SC} = \frac{V_{IS} * \rho_{IS} * A_{SC} * IRF_{SC} * V_{tot,P}}{A_{IS} * V_{med} * V_{Samp}} \quad (4.1)$$

where C_{SC} is the concentration of specific component in $\frac{mg}{\mu L}$, V_{IS} is volume of internal standard in μL , ρ_{IS} is the density of the internal standard in $\frac{mg}{\mu L}$, A_{SC} is the area of specific component, A_{IS} is the area of the internal standard, IRF_{SC} is the internal response factor, $V_{tot,P}$ is the total volume of low or high boiling point product in mL, V_{med} is the total volume extracted from the reactor in mL, and V_{samp} is the volume of the sample used for GC analysis in μL . With the internal standard and the sample constant at a 1:10 ratio then

$\frac{V_{IS}}{V_{Samp}} = 0.1$. The internal response factor of a specific component (IRF_{SC}) is determined

by Equation 4.2.

$$IRF_{SC} = \frac{A_{IS} * V_{SC} * \rho_{SC}}{A_{SC} * V_{IS} * \rho_{IS}} \quad (4.2)$$

where ρ_{SC} is the density of the internal standard in $\frac{mg}{\mu L}$.

4.3 Results and Discussion

4.3.a Fractional Factorial Design

A $\frac{1}{4}$ fractional factorial design was adopted to screen potential important fermentation parameters for the production of 2,3-BDO and ethanol. To get the concentration of the specific components an IRF was needed for calibration. Equation 4.2 was used with equal volumes of the internal standard and the specific component. The IRF for 2,3-BDO and ethanol are 1.72 and 1.78, respectively, and the GC IRF data can be found in Appendix A Figures A-1 and A-2, respectively. Raw GC data for each experimental run for 2,3-BDO can be found in Appendix A Figures A-3 to A-18 and raw GC data for each experimental run for ethanol can be found in Appendix A Figures A-19 to A-34. The concentrations of 2,3-BDO and ethanol for each experiment was determined from Equation 4.1 and is shown in Table 4-3.

Table 4-3: Concentrations of 2,3-BDO and ethanol for a six factor fractional factorial design.

Std. Run Order	2,3-BDO ($\frac{mg}{L}$)	Ethanol ($\frac{g}{L}$)
1	2.80	3.30
2	25.00	2.30
3	1.30	4.80
4	2.20	16.00
5	7.70	1.50
6	5.60	0.80
7	10.00	0.95
8	2.10	2.50
9	2.50	2.60
10	1.00	1.20
11	15.00	0.70
12	10.00	0.85
13	6.30	0.97
14	6.10	0.84
15	4.00	0.82
16	4.60	0.60

Minitab was used to determine which factors primarily affect the formation of 2,3-BDO and ethanol. A Pareto Chart at 95% confidence for 2,3-BDO and ethanol are shown in Figure 4-2 and 4-3, respectively.

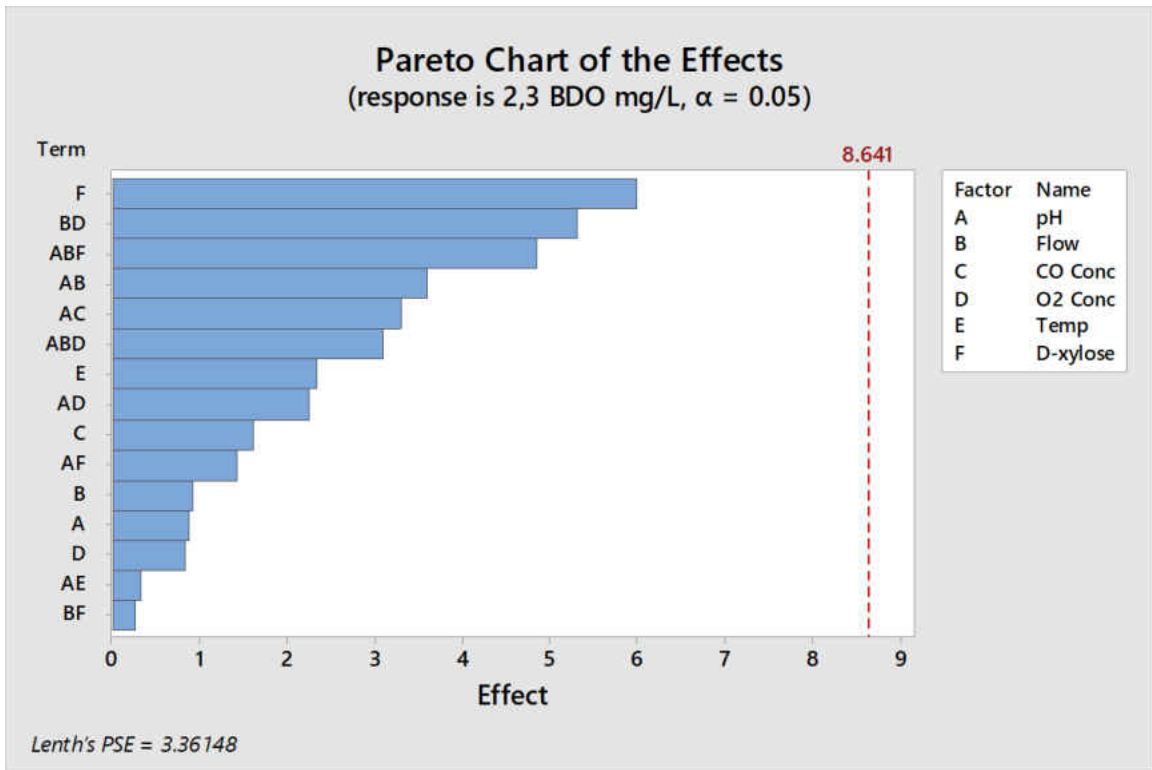


Figure 4-2: Pareto Chart of parameters effect on the formation of 2,3-BDO.

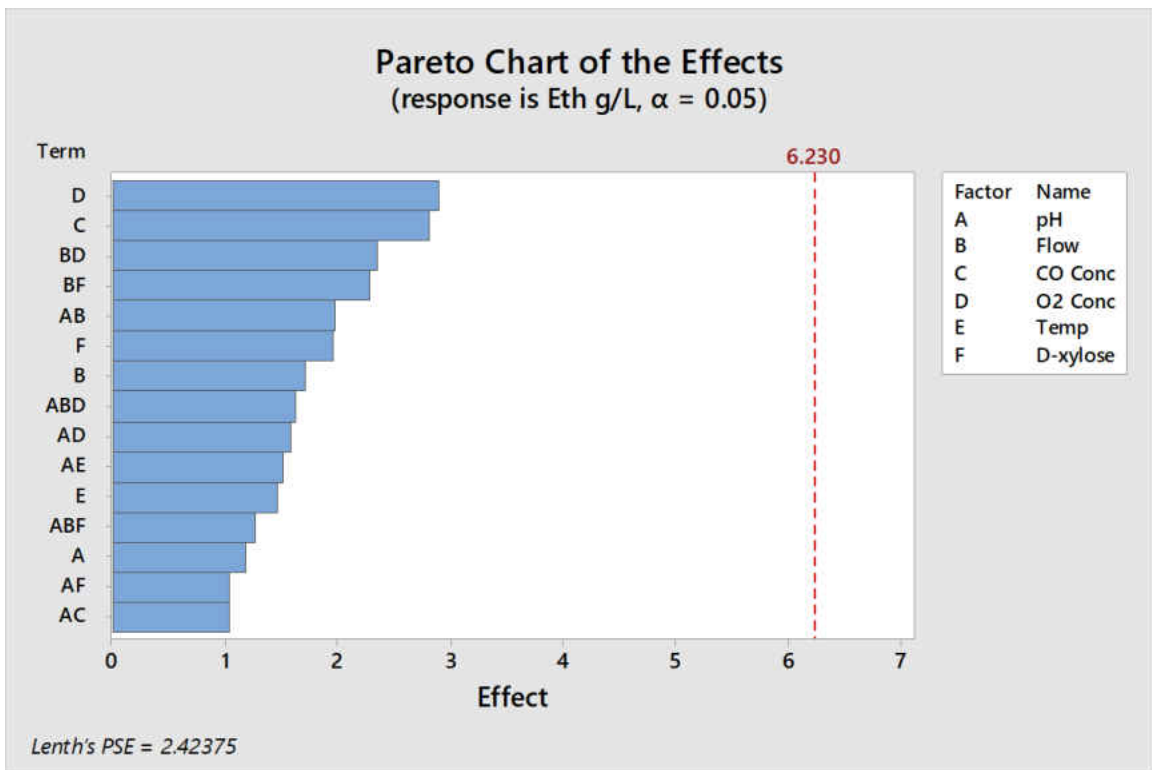


Figure 4-3: Pareto Chart of parameters effect on the formation of 2,3-BDO with 95% confidence.

None of the factors surpass the 95% confidence interval line on either Pareto Chart; however, if the confidence interval is lowered to 80% then D-xylose and the interaction reaction between flow and O₂ concentration significantly affect the formation of 2,3-BDO. This is represented in Figure 4-4. Lowering the confidence interval increases the chance that there is a Type II error.

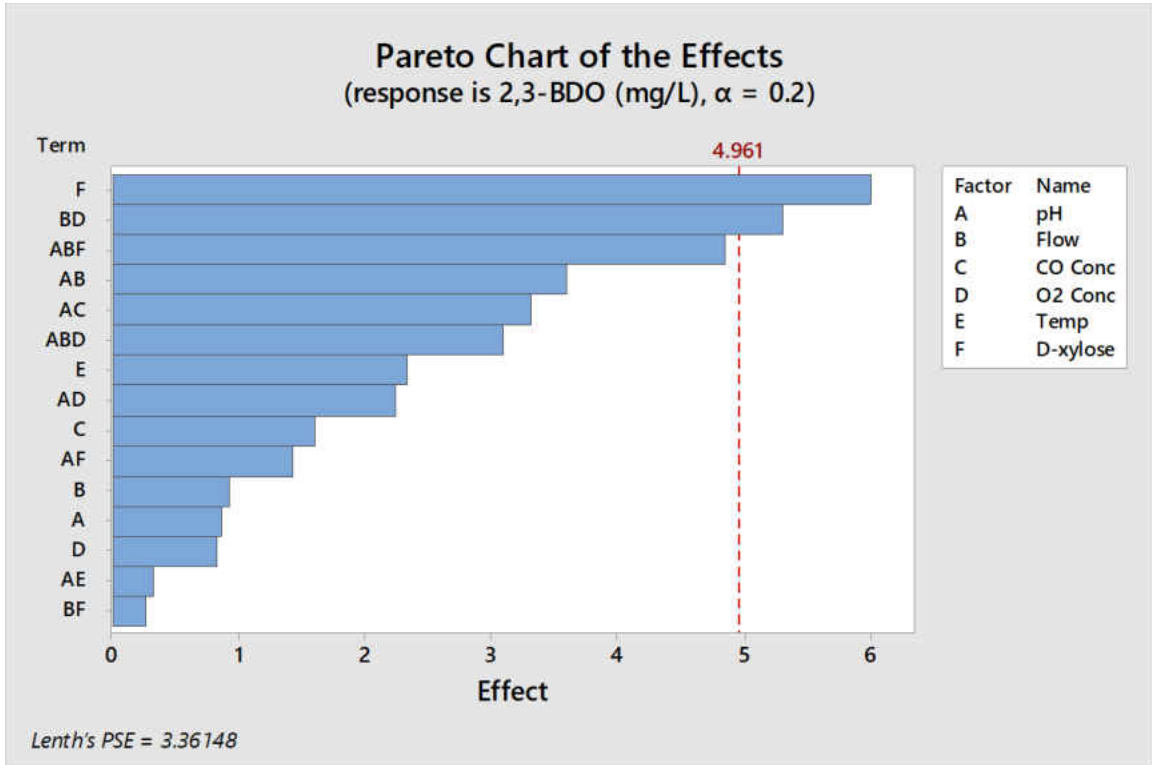


Figure 4-4: Pareto Chart of parameters effect on the formation of 2,3-BDO with 80% confidence.

Equation 4.3 is the coded regression model for the production of 2,3-BDO with D-xylose, flow, and O₂ concentrations as significant factors. From Equation 4.3, a maximum of $13 \frac{mg}{L}$ of 2,3-BDO can be formed in a 24 hour batch system with a pH of 5.75, a gas flow rate of $0.4 \frac{mL}{min}$, a carbon monoxide concentration of 60 volume percent, a temperature of 35°C, and no D-xylose.

$$[2,3BDO] = 6.60 - 0.462\dot{V}_{gas} - 0.4143[O_2] - 2.996*[S] + 2.652\dot{V}_{gas}[O_2] \quad (4.3)$$

where [2,3BDO] is 2,3-BDO concentration in $\frac{mg}{L}$, \dot{V}_{gas} is the coded value for gas flow rate, [S] is the coded value for substrate concentration, and [O₂] is the coded value for oxygen concentration.

None of the factors effected the production of ethanol at the 80% level, therefore a regression model could not be used. The average ethanol concentration over the 16 experimental runs is $2.6 \pm 2.0 \frac{g}{L}$ with 95% confidence.

4.3.b Optimum Product Production

The operating conditions from the previous section was used to check the validity of the model created and a time-based experiment was conducted to see how productivity changes over a 96 hour period. An updated Pareto Chart with the extra data point at 95% confidence for 2,3-BDO and ethanol are represented in Figure 4-5 and Figure 4-6, respectively.

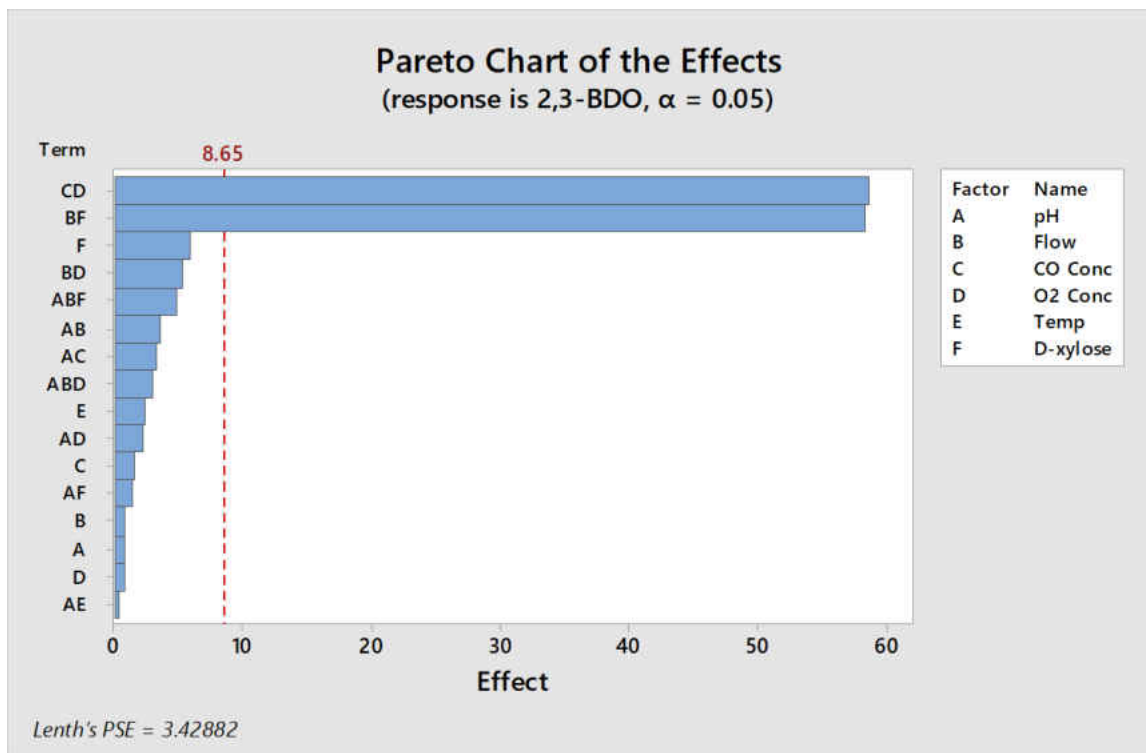


Figure 4-5: Pareto Chart of parameters effect on the formation of 2,3-BDO.

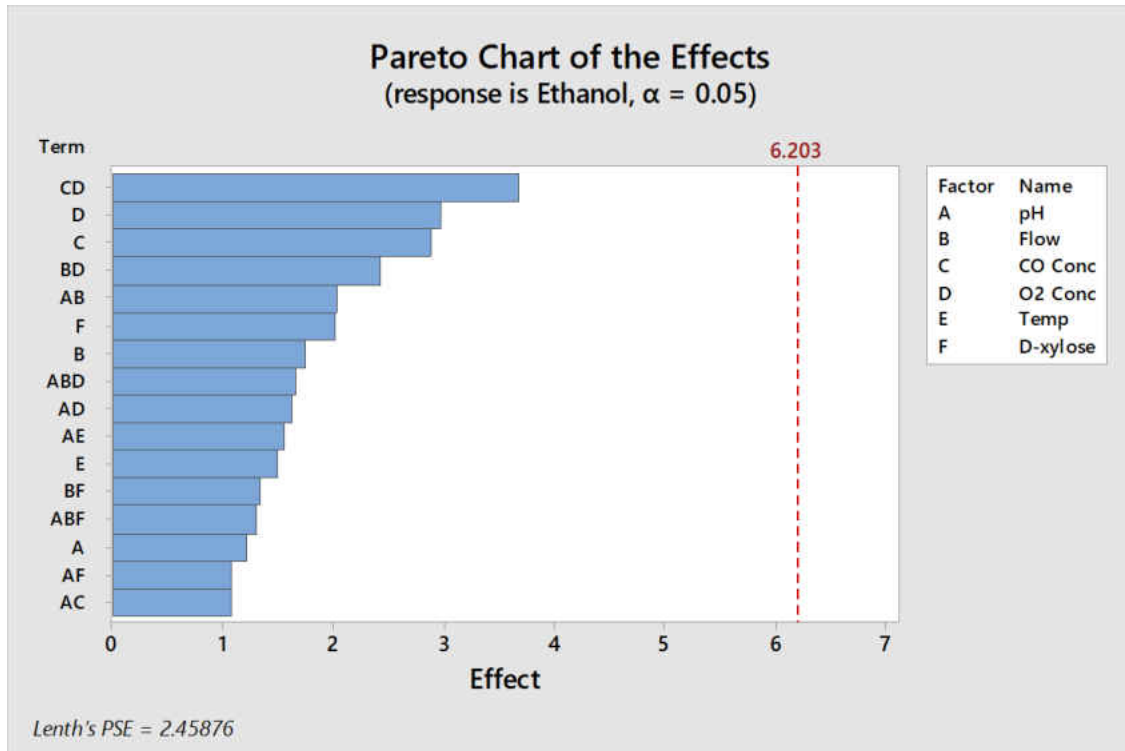


Figure 4-6: Pareto Chart of parameters effect on the formation of ethanol.

From Figure 4-5 there appears to be two interactions that affect 2,3-BDO formation: flow interacting with D-xylose, and carbon monoxide concentration interacting with oxygen concentration. It is believed that the effects are actually two way interactions because the effect from the two way interactions are much greater than the product of the one way effects. The updated coded regression model for 2,3-BDO from this data are shown in Equation 4.4. As expected with more data the updated model for 2,3-BDO better represents the data with an adjusted R^2 of 0.76, while the original $\frac{1}{4}$ fractional factorial design had an adjusted R^2 of 0.44.

$$\begin{aligned}
 [2,3BDO] = & 6.60 - 0.462\dot{V}_{gas} - 0.8054[CO] - 0.4143[O_2] - 2.996[S] + \\
 & 29.14\dot{V}_{gas}[S] - 29.27[CO][O_2]
 \end{aligned}
 \tag{4.4}$$

As with the base $\frac{1}{4}$ fractional factorial design there does not appear to be any significant factors that affect ethanol production at the 95% confidence level. The mean for ethanol production with the additional data point was updated to $2.4 \pm 1.9 \frac{g}{L}$.

The time-based study was conducted to determine whether the products 2,3-BDO and ethanol could be consumed and if there is a local maximum concentration. Figure 4-7 shows the 2,3-BDO and ethanol production over time.

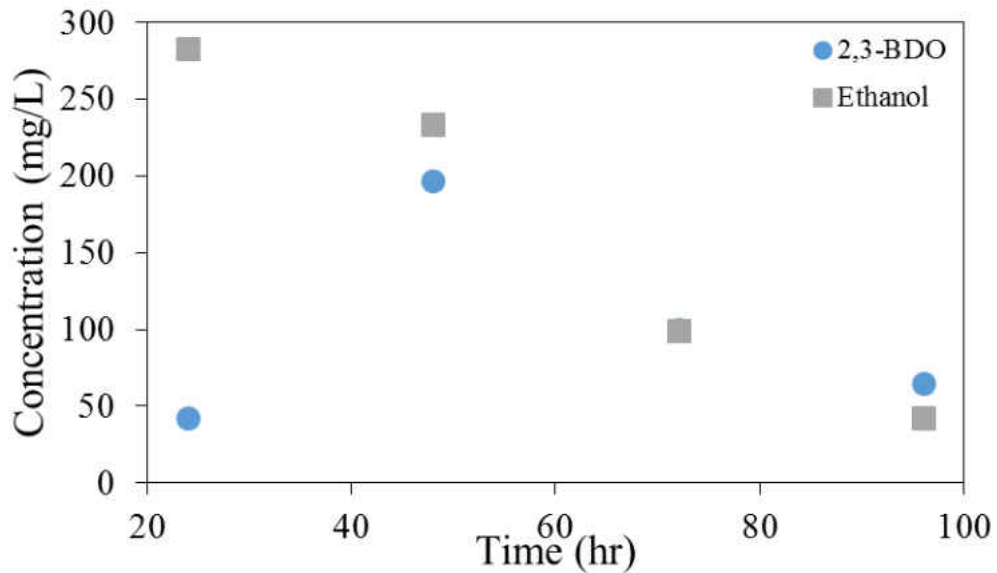


Figure 4-7: 2,3-BDO and ethanol production over 96 hours.

It appears that 2,3-BDO increases for the first 48 hours, but then decreases; whereas, ethanol continually decreases with time. This suggests that 2,3-BDO concentration is greatest between 24 and 72 hours, and ethanol concentration is greatest between 0 and 24 hours. No other studies exhibited a decreased concentration in ethanol or 2,3-BDO. The product could be metabolized by *C. autoethanogenum* as there are certain types of bacteria that can metabolize ethanol and 2,3-BDO[16], but this should be further investigated to verify.

There was a huge difference between product concentrations from what was originally predicted by Equation 4.3 and the experimental data. Ethanol concentration is

below the expected value; whereas, 2,3-BDO concentration is three times greater than provided by the regression model. This suggests that the range of some or all of the parameters are too broad which causes a parabolic representation.

4.3.c 2,3-BDO Rate of Formation Analysis

The measured concentration of 2,3-BDO in the product is quite lower than previous literature values. Table 4-4 provides literature values with the measured value for the formation of 2,3-BDO in batch or semi-batch systems.

Table 4-4: Production of 2,3-BDO from previous researchers.

Author	2,3-BDO ($\frac{mg}{L}$)	TAI (hrs)	Substrate
Köpke et al. (2011)[7]	180	192	Steel Mill Syngas
Kracke et al. (2016)[8]*	66 ± 110	100	Fructose
Liew et al. (2017)[9]*	631 ± 220	312	Carbon Monoxide
Experimental	42	24	Carbon Monoxide

* 95% confidence

Previous literature values for the formation of 2,3-BDO appear to be higher than what was determined; however, the reaction times are quite different for each author. The productivity of 2,3-BDO in the stationary phase within this article was $3.0 \frac{mg}{L-hr}$ after 24 hours where Kracke et al. (2016), Köpke et al. (2011), and Liew et al. (2017) achieved 1.32 ± 2.27 , 1.96, and $3.75 \pm 1.33 \frac{mg}{L-hr}$, respectively. 2,3-BDO productivity was determined after the stationary phase was achieved because the analysis in previous literature suggested that 2,3-BDO is not formed until the stationary phase[7,9]. All of the errors previously listed are with a 95% confidence interval.

4.3.d Ethanol Rate of Formation Analysis

The measured concentration of ethanol in the product is comparable to that of literature values; although there is a significant amount of error due to large variations in the parameters. Table 4-5 provides literature values with the measured value for the

formation of ethanol in batch or semi-batch systems. Ethanol is produced throughout the fermentation process; therefore, the productivity of ethanol, R_E , is also found in Table 4-5.

Table 4-5: Production of ethanol from previous researchers.

Author	Ethanol ($\frac{mg}{L}$)	TAI (hrs)	Substrate	R_E ($\frac{mg}{L-hr}$)
Cotter et al. (2009)[16]	235	48	D-xylose	4.90
Guo et al. (2010)[17]	254	60	D-xylose	4.23
Köpke et al. (2011)[7]	967	192	Steel Mill Syngas	5.04
Kracke et al. (2016)[8]*	812 ± 1220	100	Fructose	8.12 ± 12.2
Liew et al. (2017)[9]*	875 ± 57	312	Carbon Monoxide	2.80 ± 0.18
Xu et al. (2017)[18]	3,380 ± 719	624	Carbon Monoxide	5.42 ± 1.15
Xu et al. (2017)[18]	253 ± 719	624	Synthetic Syngas	0.35 ± 1.15
Experimental*	2,400 ± 1900	24	Carbon Monoxide	100 ± 80

* 95% confidence

From Table 4-5 it appears that Xu et al. (2017) exceeded the production of ethanol compared to other researchers including what was conducted within this research; however, when the rate of ethanol formation is looked at then the ethanol production is consistent with previous researchers. The only literature value for ethanol productivity that is comparable to this study is Kracke et al. (2016)[8] and this may be due to the large error associated from adjusting six parameters.

The dramatic increase in ethanol formation within this thesis is believed to be a result from the increased growth rate experienced. By the time based experiment it appears that the metabolic pathway shifts from the production of ethanol to the production of 2,3-BDO. Although, after 48 hours both metabolites decrease which suggests that the metabolites are being consumed by *C. autoethanogenum*.

4.4 Conclusion

Multiple factors can be experimented with limited experimental runs, and 2,3-BDO can be approximated with a regressed model from those experiments. It appears

that the range chosen for each factor may have been too broad. This broad range posed trouble in narrowing down the local maximum for product formation, especially for ethanol production. The rate of 2,3-BDO and ethanol production exceeded previously literature values with a 2,3-BDO and average ethanol production rate of 5.18 and $100 \pm 80 \frac{mg}{L-hr}$, respectively.

References

- [1] Scientific Research Company (SRC). Environmental Fate/Exposure Summary. HSDB: 2,3-BUTANEDIOL. Retrieved from <https://toxnet.nlm.nih.gov/cgi-bin/sis/search2/r?dbs+hsdb:@term+@rn+@rel+513-85-9>
- [2] Stellman, J. (1998). Glycerols and glycols. In M. McCann, L. Warshaw & C. Brabant (Eds.), *Encyclopaedia of occupational health and safety* (4th ed., pp. 202-203) International Labour Organization.
- [3] Todar, K. (2008-2012). The Embden-Heyerhof Pathway: Butanediol Fermentation. *Diversity of Metabolism in Procaryotes*, pg. 3. Retrieved from http://textbookofbacteriology.net/metabolism_3.html
- [4] Qureshi, S (2016). Epidemiology of Klebsiellae. *Klebsiella Infections*. Retrieved from <http://emedicine.medscape.com/article/219907-overview#showall>
- [5] Janda, J. M. & Abbott, S. L. (2006). *The Enterobacteria* 2nd ed. Washington D.C.: ASM press. Retrieved from https://microbewiki.kenyon.edu/index.php/Enterobacter_aerogenes
- [6] Turnbull P. & Kramer J. M. (1995). *Manual of Clinical Microbiology* 6th ed. Washington D.C.: ASM, pg. 349-356. Retrieved from <https://www.ncbi.nlm.nih.gov/pmc/articles/PMC91618/#B28>
- [7] Köpke, M., Mihalcea, C., Liew, F., Tizard, J. H., Ali, M. S., Conolly, J. J., et al. (2011). 2,3-butanediol production by acetogenic bacteria, an alternative route to

- chemical synthesis, using industrial waste gas. *Applied and Environmental Microbiology*, 77(15), 5467-5475. doi:10.1128/AEM.00355-11 [doi]
- [8] Frauke Kracke, Bernardino Virdis, Paul V. Bernhardt, Korneel Rabaey, and Jens O. Krömer. “Redox Dependent Metabolic Shift in *Clostridium autoethanogenum* by Extracellular Electron Supply.” *Biotechnology for Biofuels*, Vol. 9 (2016): Pgs. 1-12.
- [9] Fungmin Liew, Anne M. Henstra, Michael Köpke, Klaus Winzer, Sean D. Simpson, and Nigel P. Minton. “Metabolic Engineering of *Clostridium autoethanogenum* for Selective Alcohol Production.” *Metabolic Engineering*, Vol. 140 (2017): Pgs. 104-114.
- [10] Haris Nalakath Abubackar, Frank R. Bengelsdorf, Peter Dürre, María C. Veiga, and Christian Kennes. “Improved Operating Strategy for Continuous Fermentation of Carbon Monoxide to Fuel-Ethanol by *Clostridia*.” *Applied Energy*, Vol. 169 (2016): Pgs. 210-217.
- [11] Haris Nalakath Abubackar, Ánxela Fernández-Naveira, María C. Veiga, and Christian Kennes. “Impact of Cyclic pH Shifts on Carbon Monoxide Fermentation to Ethanol by *Clostridium autoethanogenum*.” *Fuel*, Vol. 178 (2016): Pgs. 56-62.
- [12] Munasinghe, P. C., & Khanal, S. K. (2010). Biomass-derived syngas fermentation into biofuels: Opportunities and challenges. *Bioresource Technology*, 101(13), 5013-5022.
- [13] Iowa State University (2006). Guide to Sterilization Times. Retrieved from

<http://agron->

www.agron.iastate.edu/cpandp/SOPs/Equipment/GuidetoSterilizationTimes.pdf

- [14] Taylor, T., & Alshami, A. Biological production of 2,3-butanediol on carbon monoxide and D-xylose with *Clostridium autoethanogenum*. Unpublished Master's, University of North Dakota,
- [15] Goel, A. (2013). Metabolic shifts in microorganisms: The case of *Lactococcus lactis*. Unpublished PhD, Wageningen University,
- [16] Cotter, J. L., Chinn, M. S., & Grunden, A. M. (2009). Ethanol and acetate production by *Clostridium ljungdahlii* and *Clostridium autoethanogenum* using resting cells. *Bioprocess and Biosystems Engineering*, 32(3), 369-380.
- [17] Guo, Y., Xu, J., Zhang, Y., Xu, H., Yuan, Z., & Li, D. (2010). Medium optimization for ethanol production with *Clostridium autoethanogenum* with carbon monoxide as sole carbon source. *Bioresource Technology*, 101(22), 8784-8789.
- [18] Xu, H., Liang, C., Yuan, Z., Xu, J., Hua, Q., & Guo, Y. (2017). A study of CO/syngas bioconversion by *Clostridium autoethanogenum* with a flexible gas-cultivation system. *Enzyme and Microbial Technology*, 101, 24-29.
- [19] Alltech Associates, I. (1998). Quantitation methods in gas chromatography. Unpublished manuscript.

Chapter 5

Conclusions and Prospects

The novel bio-kinetic inhibition model derived is comparable and potentially superior to previous models. This model requires less fitting parameters and thus less data points. The derived model needs to be compared to other bacteria to further justify the superiority.

The production rate of 2,3-BDO can be increased with an experimental design while using carbon monoxide as the primary substrate. From the experimental design, gas flow rate, oxygen, carbon monoxide, and D-xylose concentrations affect the production of 2,3-BDO with 95% confidence; whereas, ethanol production was unaffected. Production of 2,3-BDO does not appear to be significant until the stationary phase according to previous researchers results whereas ethanol production occurs throughout the entire fermentation process. The ethanol productivity experienced was drastically higher than previous literature values with carbon monoxide and syngas derived from coal. 2,3-BDO productivity was comparable to previous literature values at the optimum operating conditions, but was inferior while using syngas derived from coal.

To further study this microbe on real syngas generated from coal it would be desirable to receive bottled syngas from commercialized producers such as the Energy and Environment Research Center (EERC) of Grand Forks, ND or Dakota Gasification Company (DGC) of Beulah, ND.

Appendix A

Raw Data and Figures

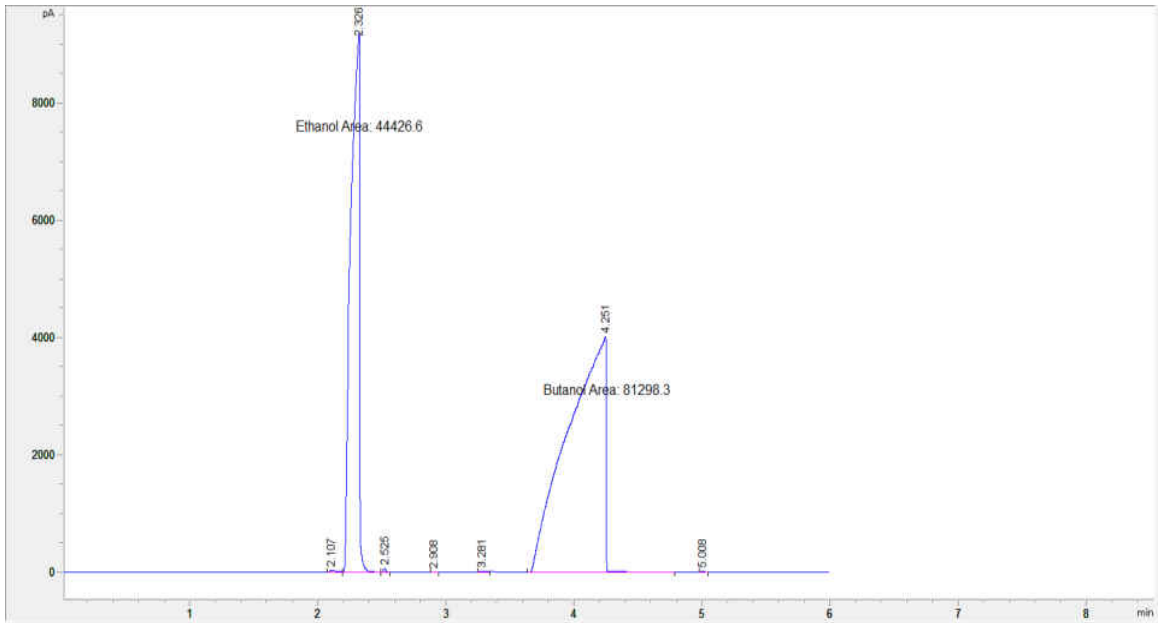


Figure A-1: Calibration run of 30% 2,3-BDO, 30% methanol, and 40% water by volume.

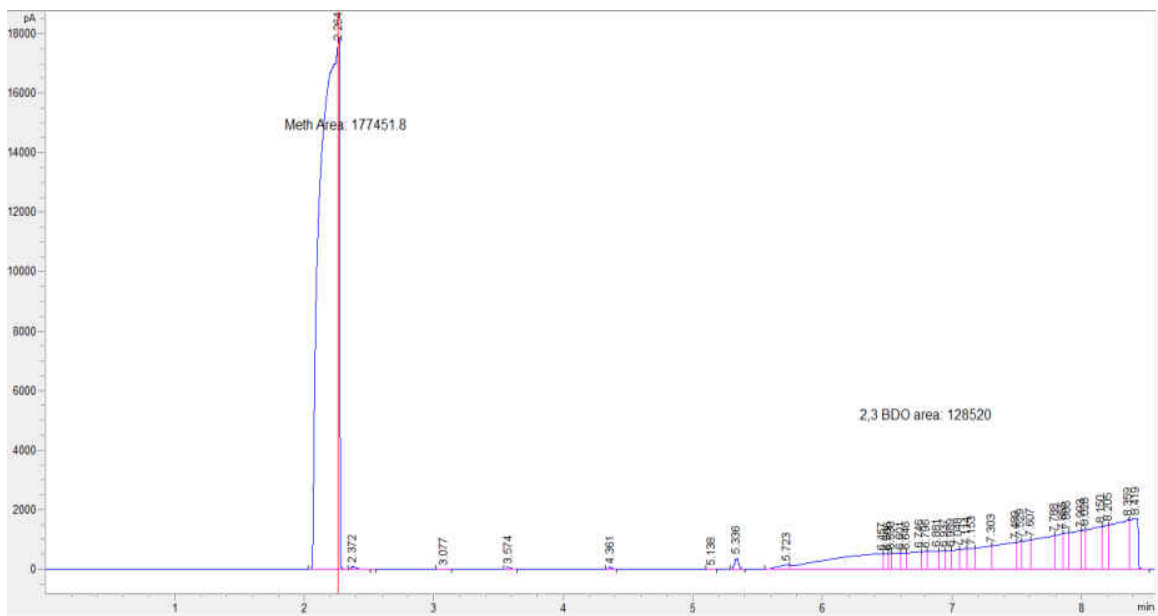


Figure A-2: Calibration run of 30% ethanol, 30% butanol, and 40% water by volume.

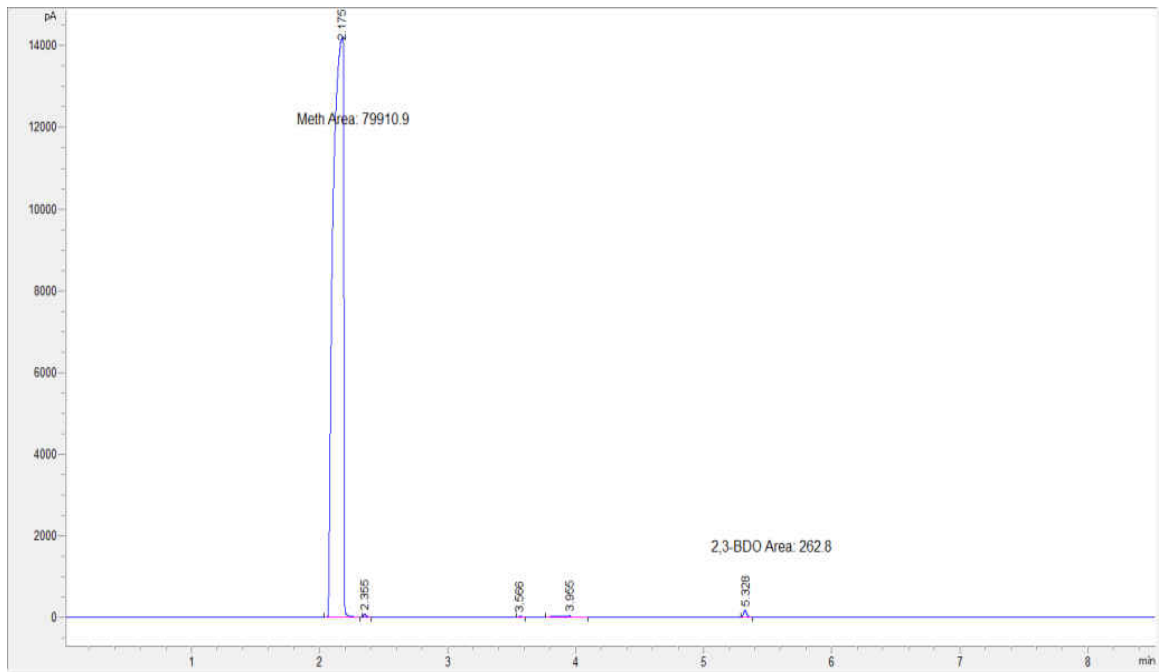


Figure A-3: 2,3-BDO GC analysis standard run order #1.

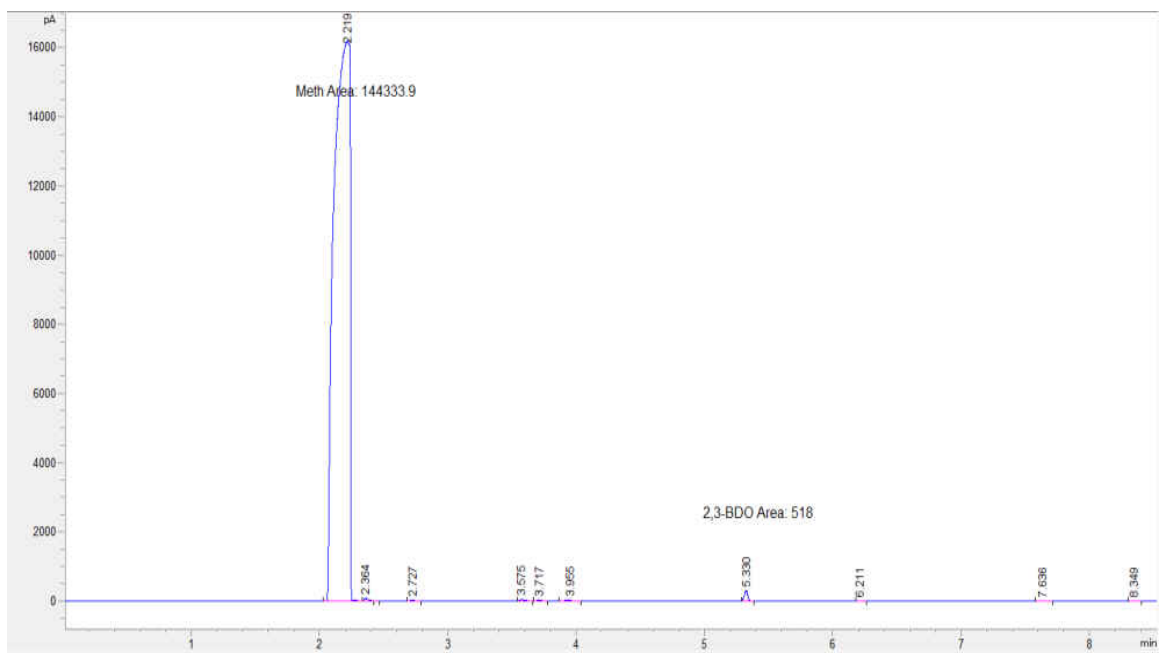


Figure A-4: 2,3-BDO GC analysis standard run order #2.

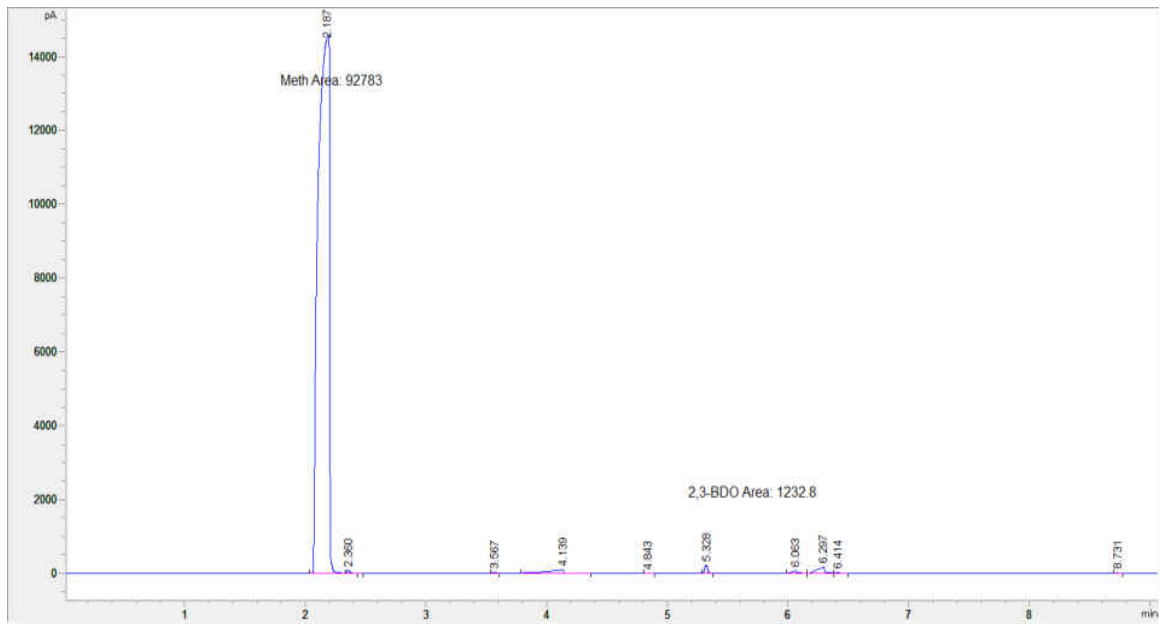


Figure A-5: 2,3-BDO GC analysis standard run order #3.

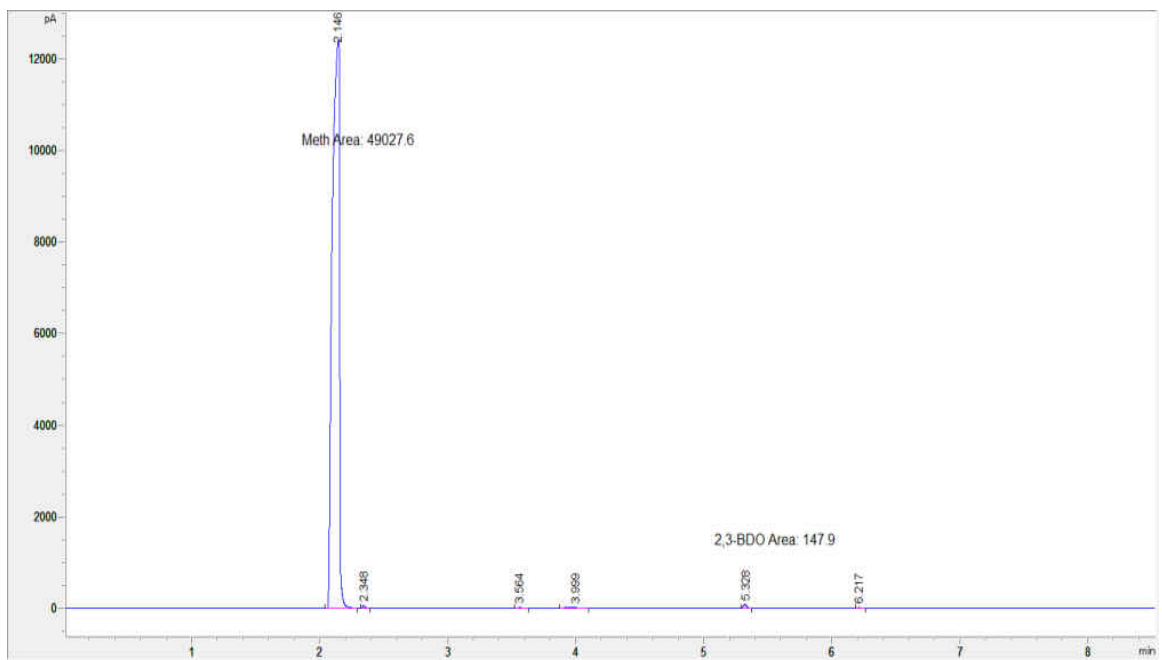


Figure A-6: 2,3-BDO GC analysis standard run order #4.

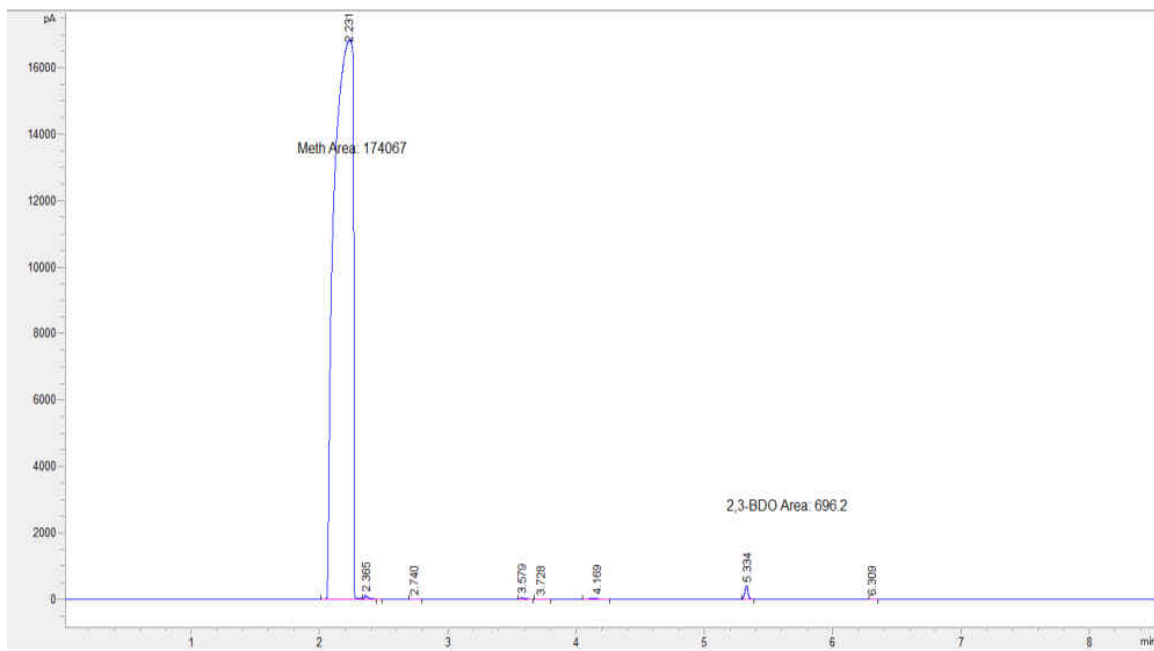


Figure A-7: 2,3-BDO GC analysis standard run order #5.

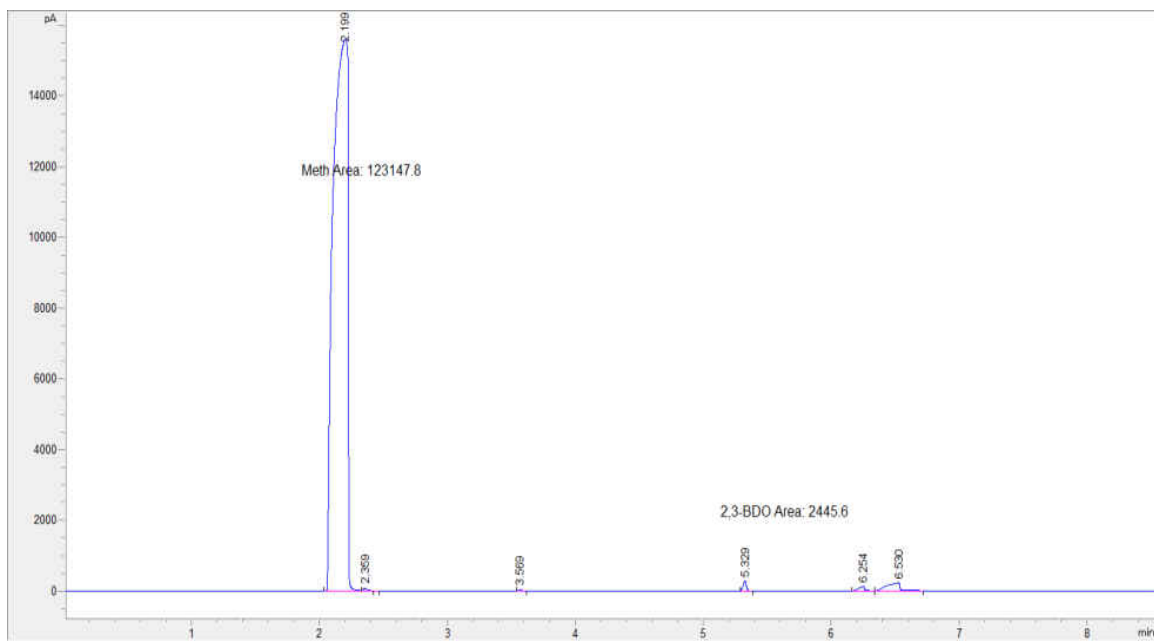


Figure A-8: 2,3-BDO GC analysis standard run order #6.

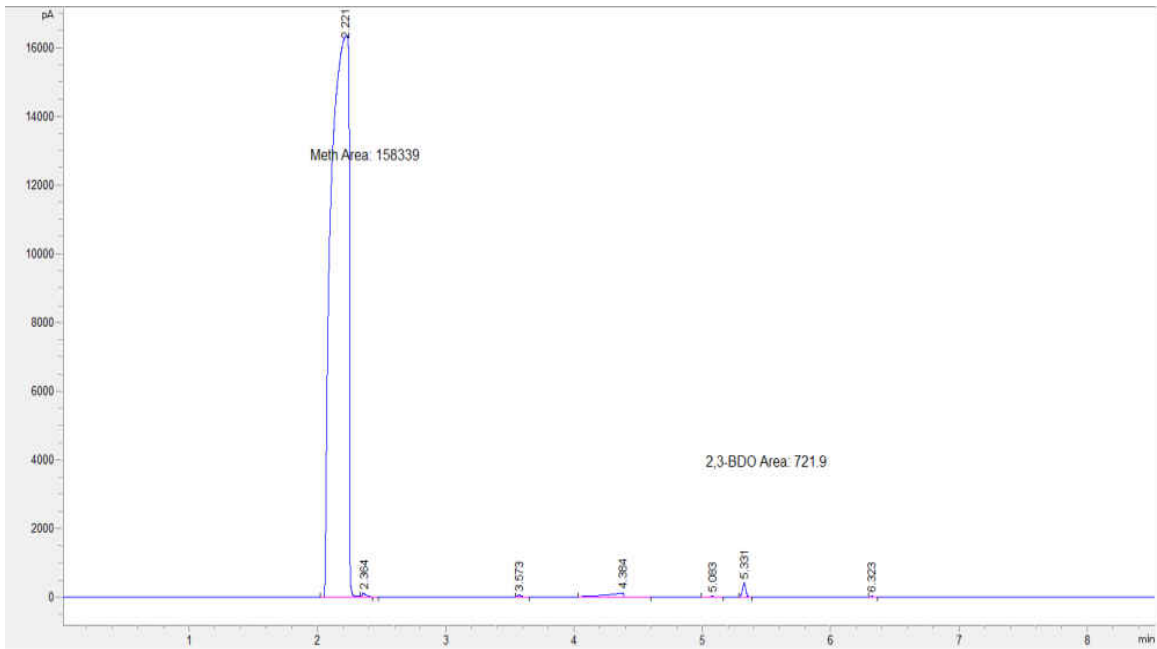


Figure A-9: 2,3-BDO GC analysis standard run order #7.

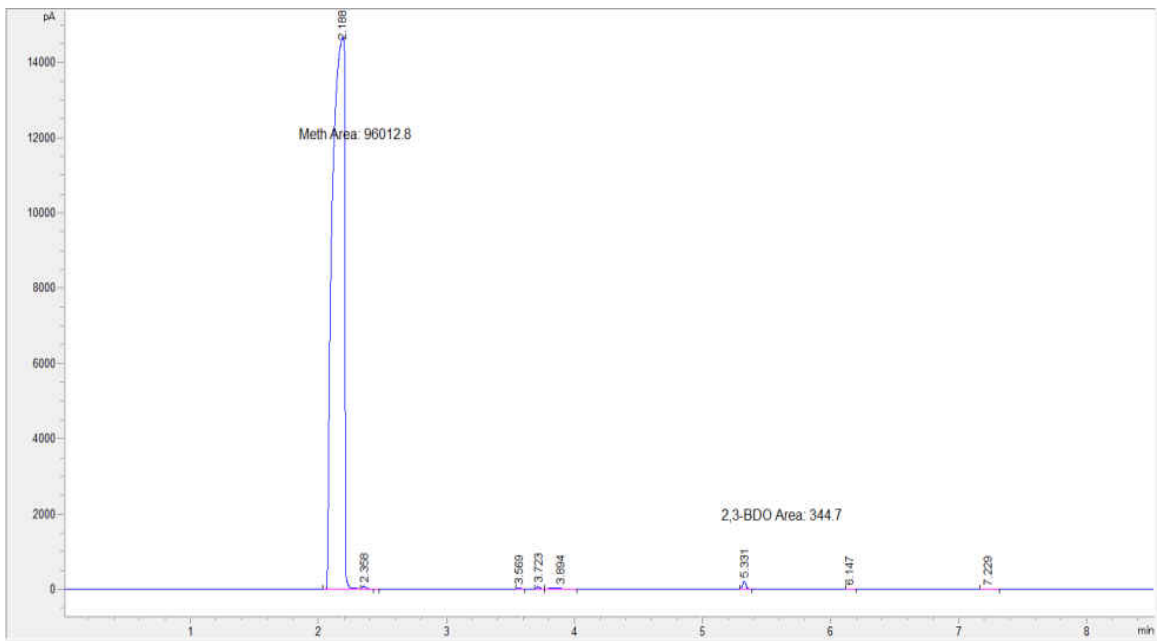


Figure A-10: 2,3-BDO GC analysis standard run order #8.

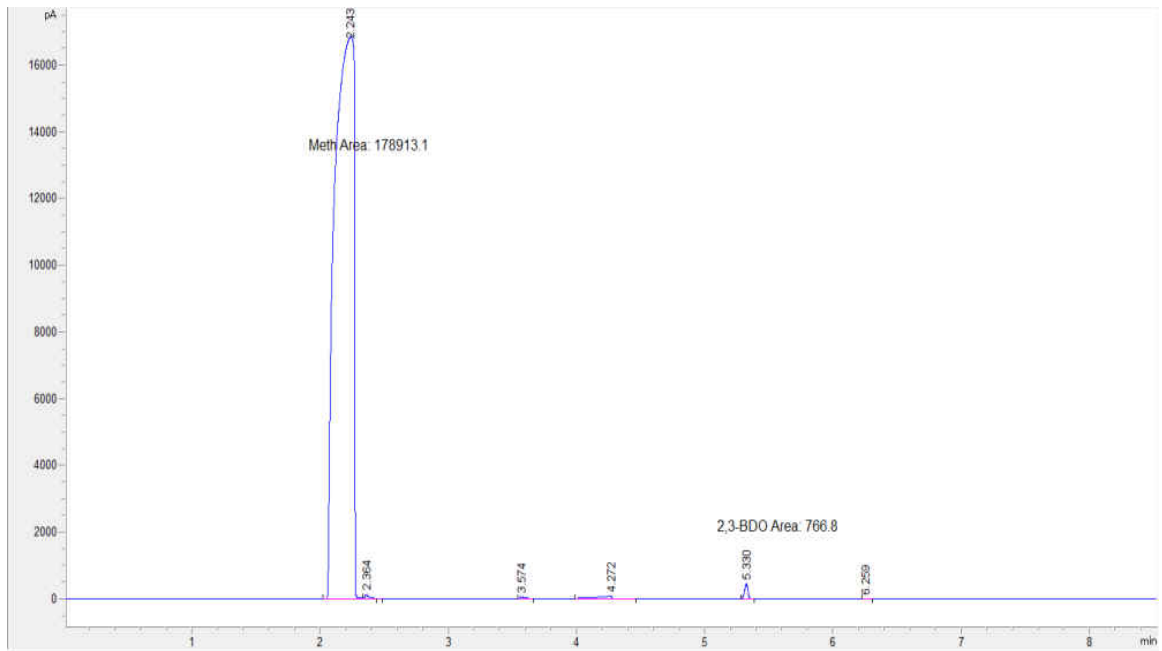


Figure A-11: 2,3-BDO GC analysis standard run order #9.

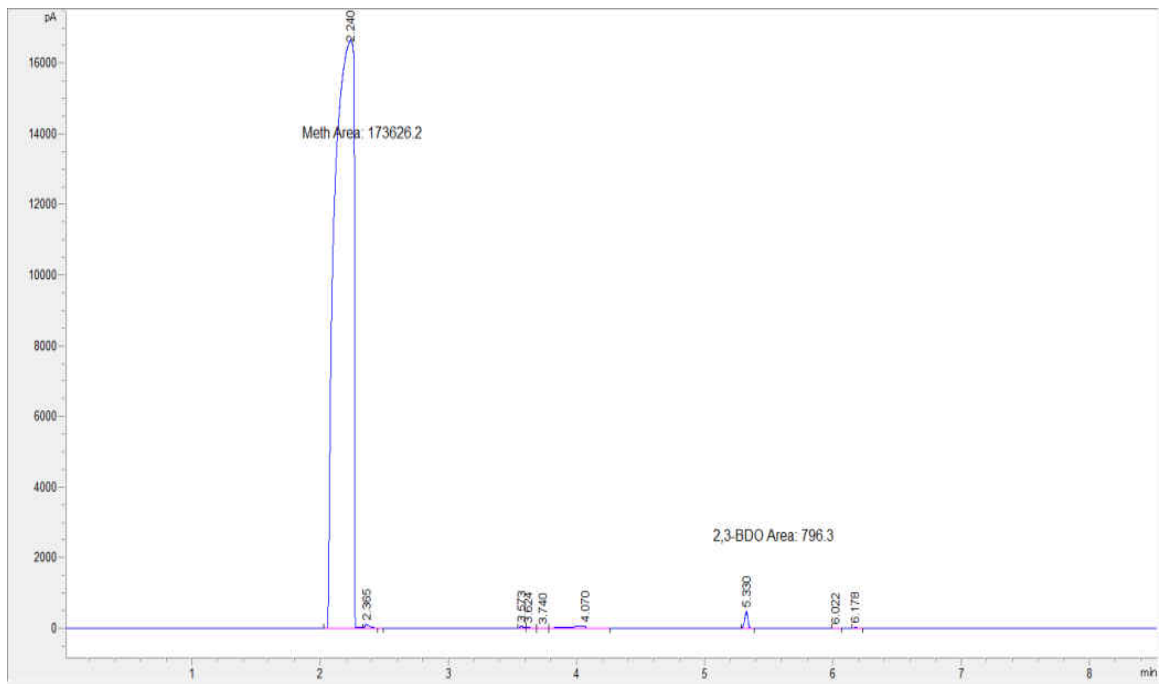


Figure A-12: 2,3-BDO GC analysis standard run order #10.

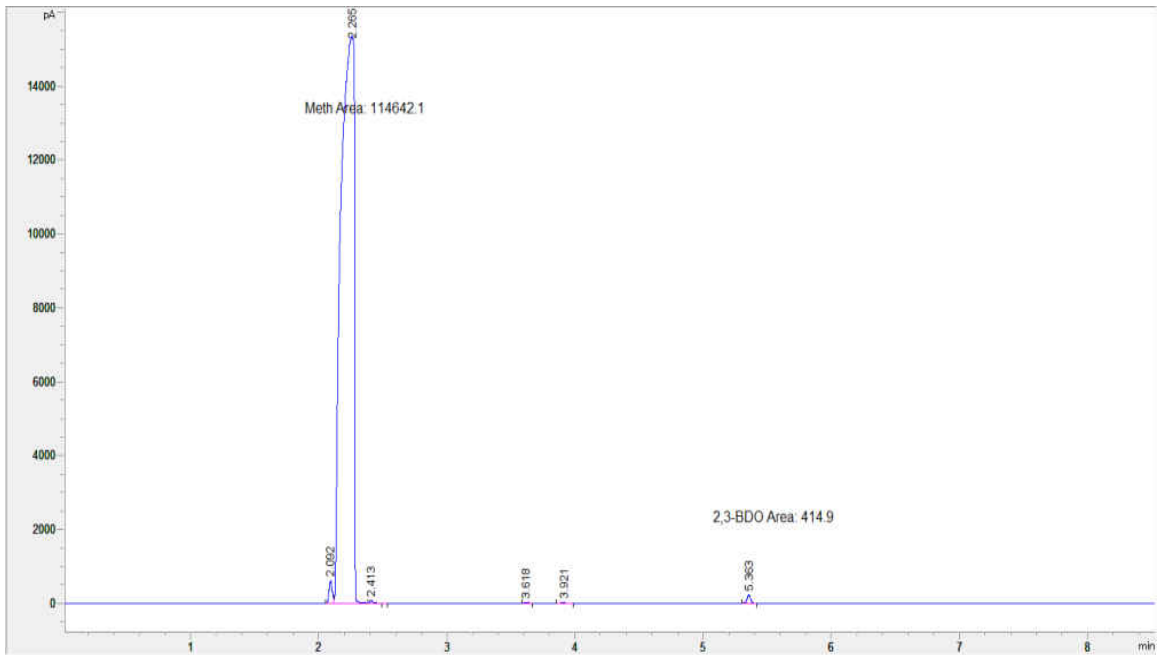


Figure A-13: 2,3-BDO GC analysis standard run order #11.

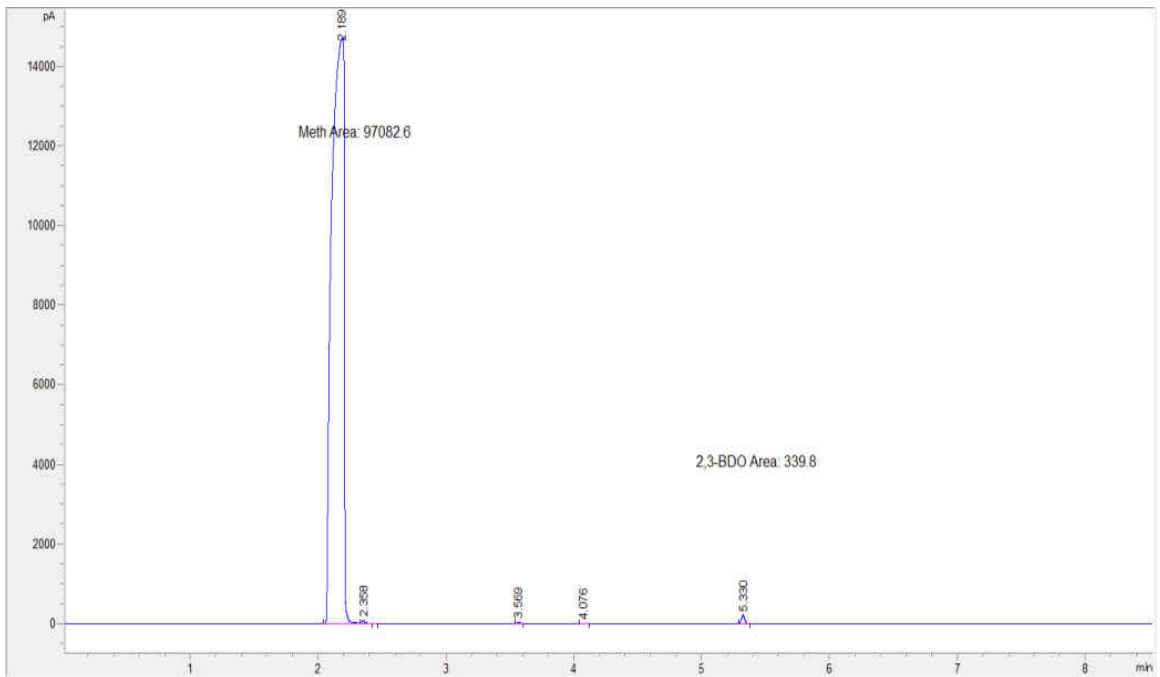


Figure A-14: 2,3-BDO GC analysis standard run order #12.

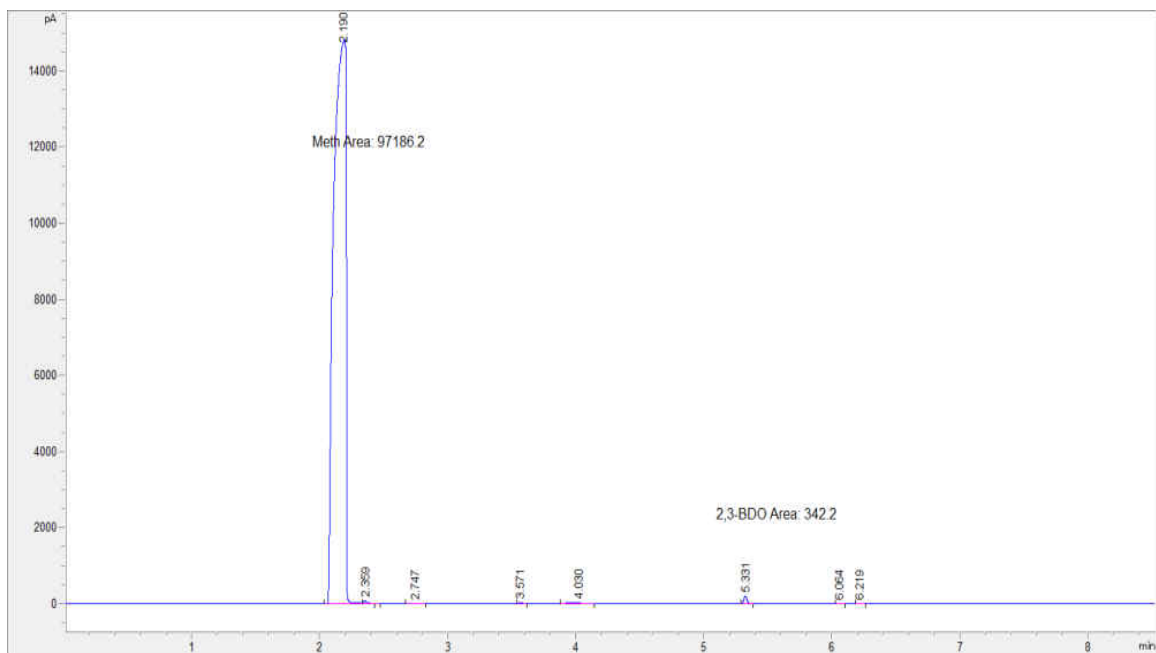


Figure A-15: 2,3-BDO GC analysis standard run order #13.

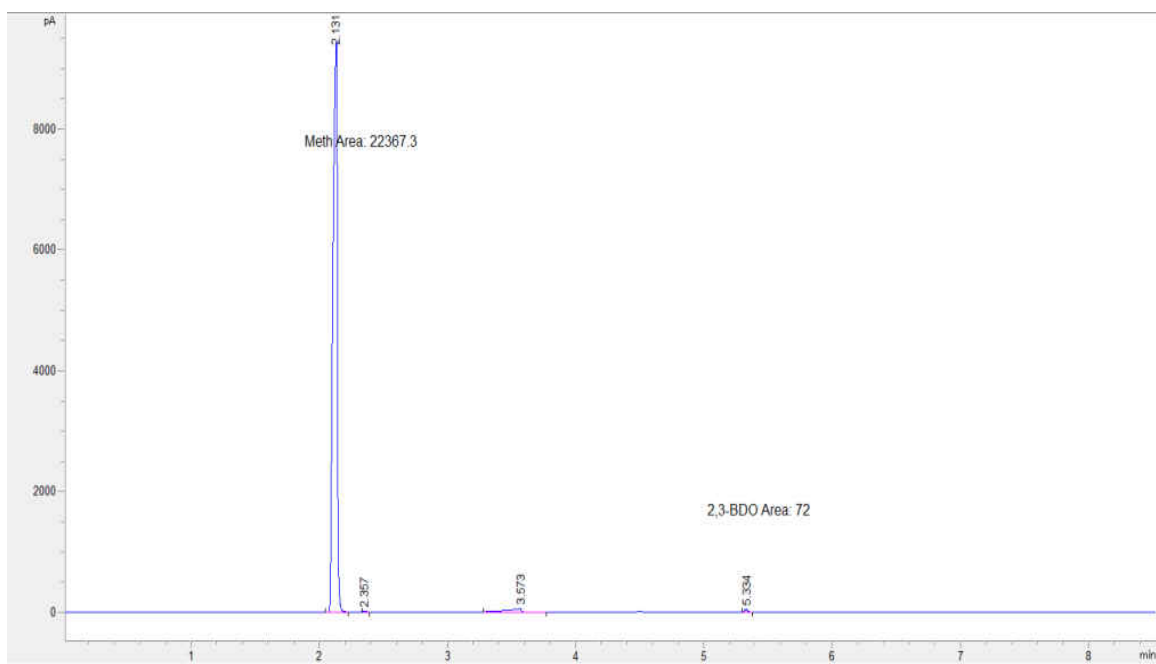


Figure A-16: 2,3-BDO GC analysis standard run order #14.

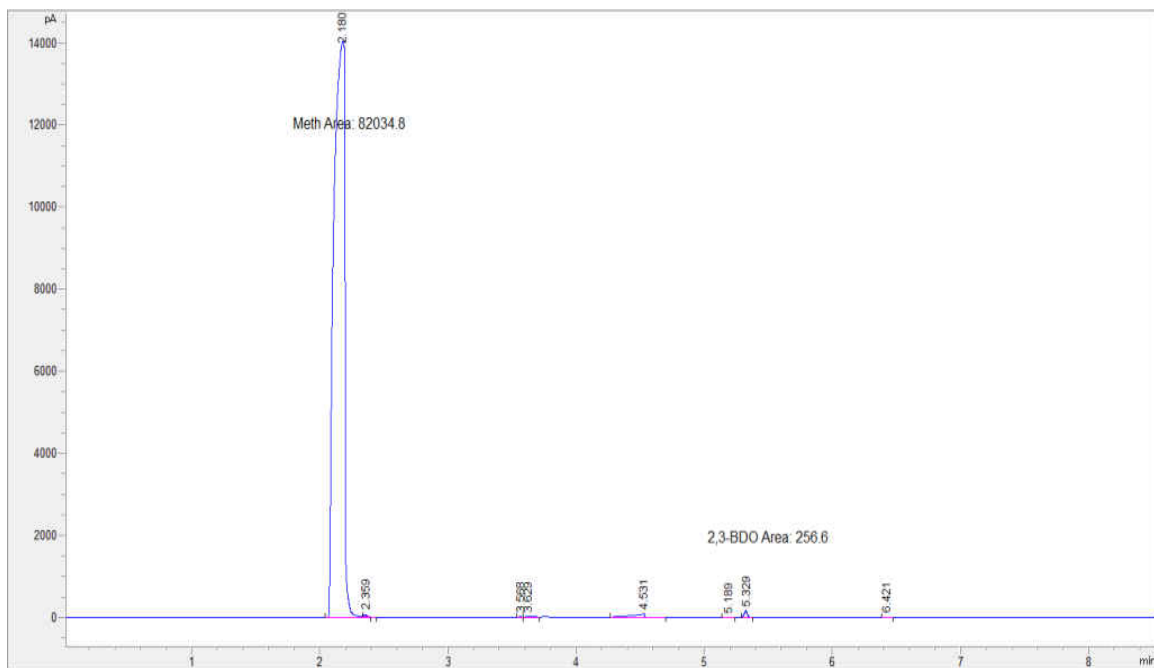


Figure A-17: 2,3-BDO GC analysis standard run order #15.

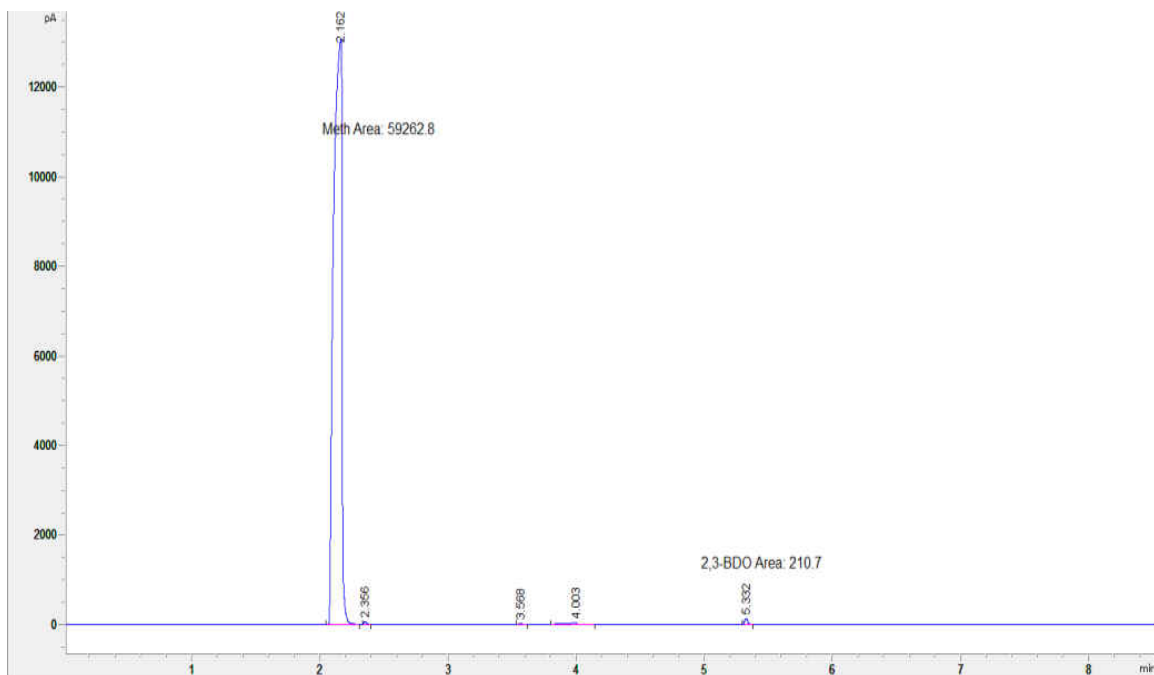


Figure A-18: 2,3-BDO GC analysis standard run order #16.

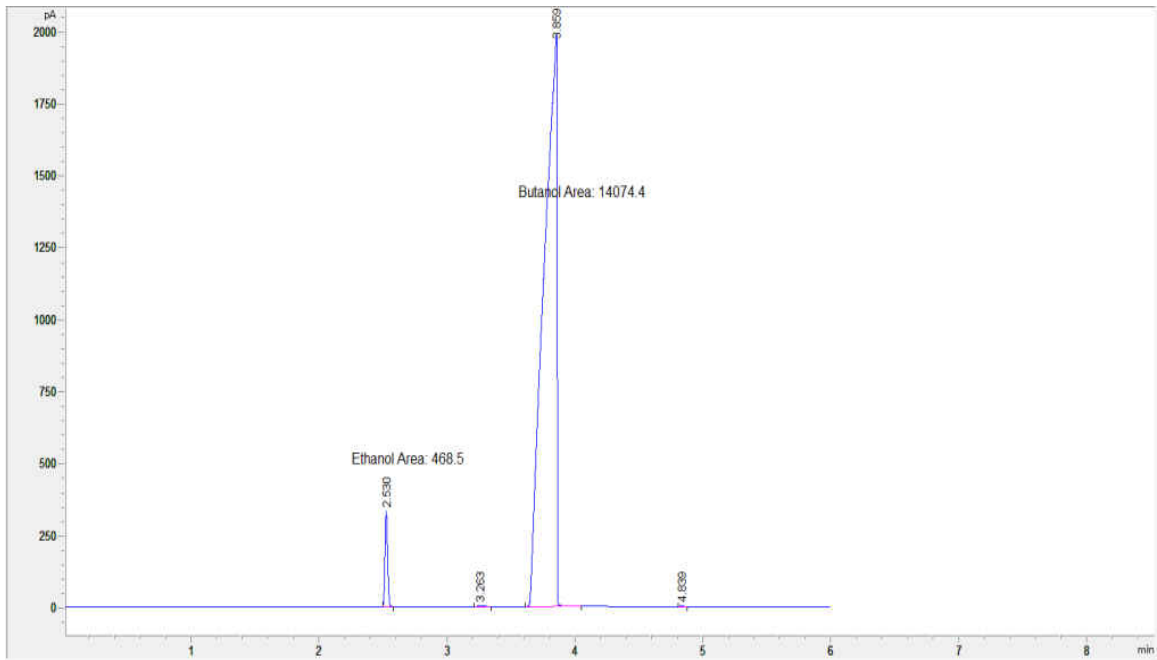


Figure A-19: Ethanol GC analysis standard run order #1.

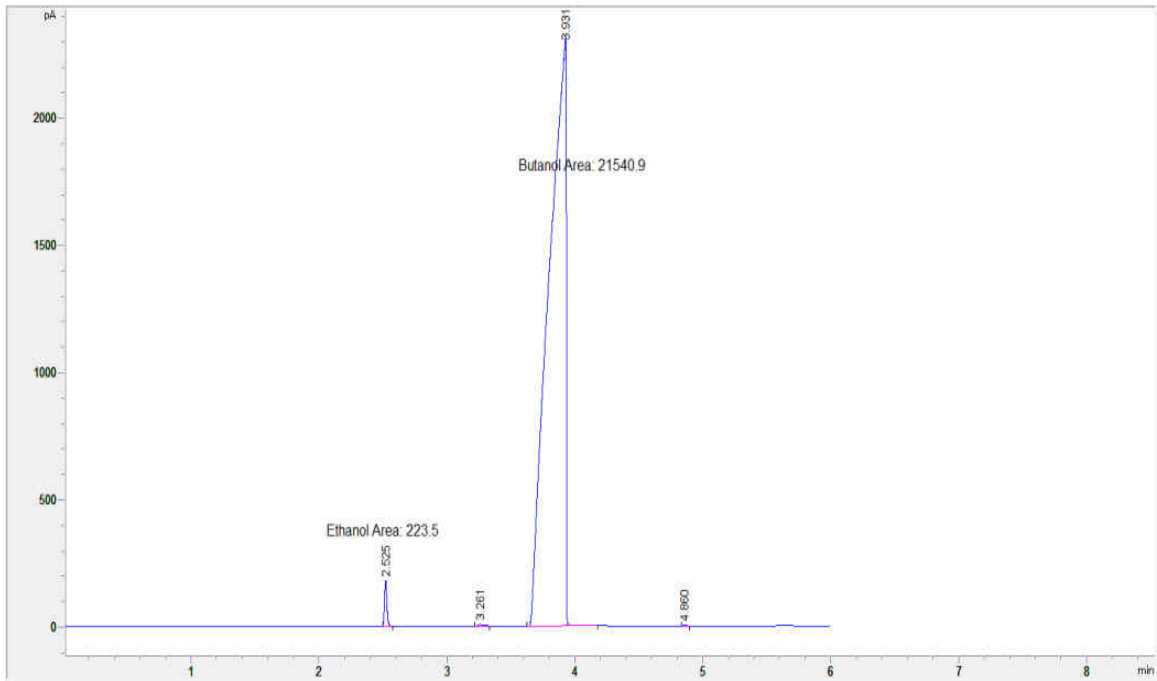


Figure A-20: Ethanol GC analysis standard run order #2.

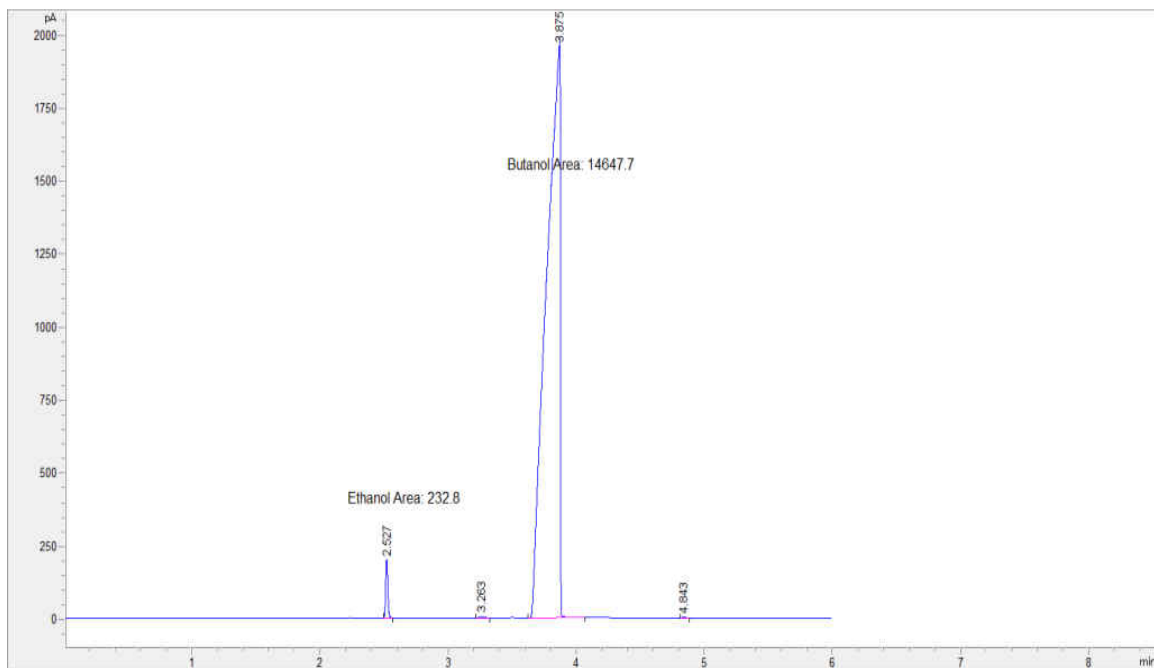


Figure A-21: Ethanol GC analysis standard run order #3.

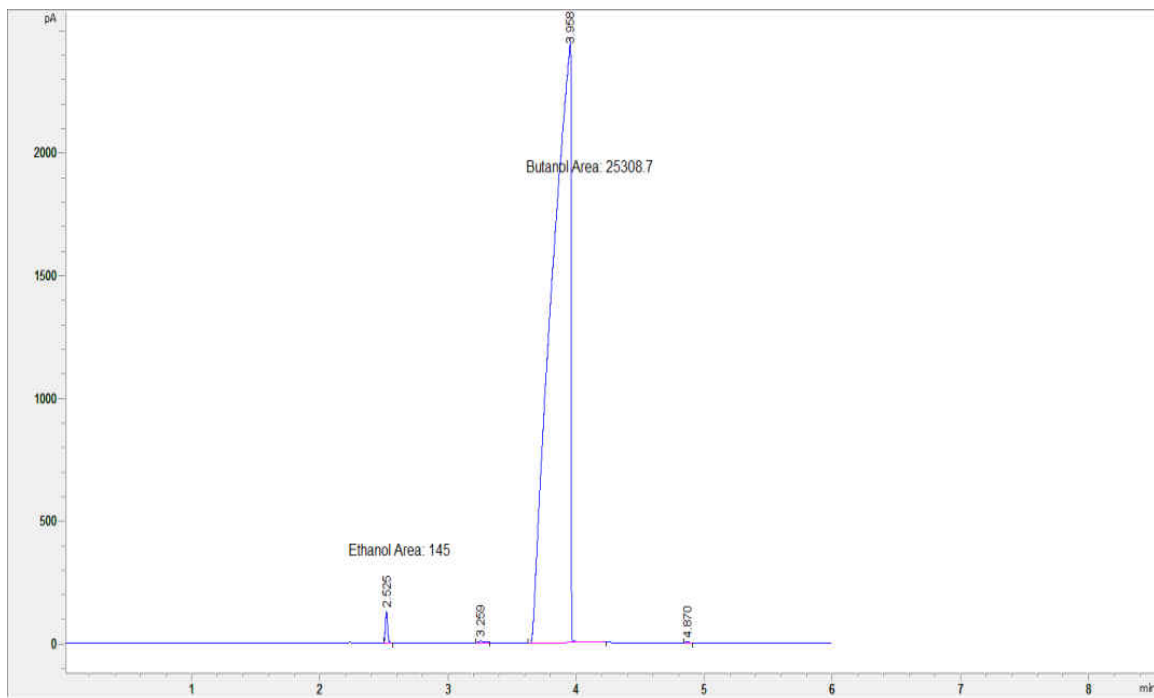


Figure A-22: Ethanol GC analysis standard run order #4.

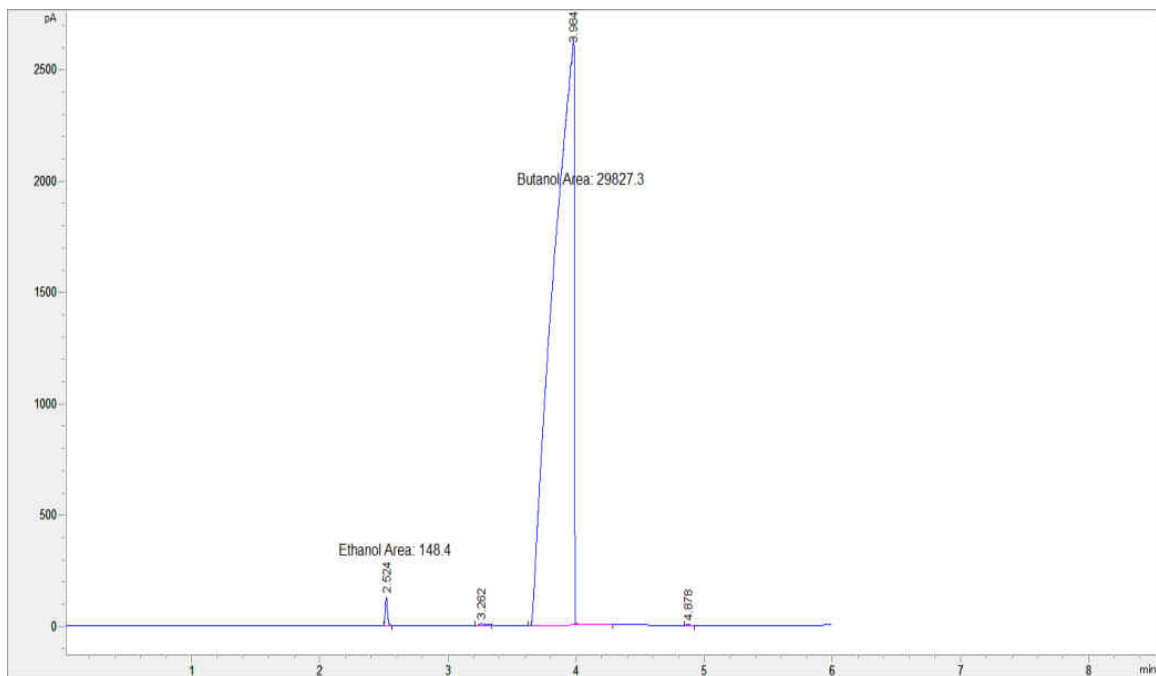


Figure A-23: Ethanol GC analysis standard run order #5.

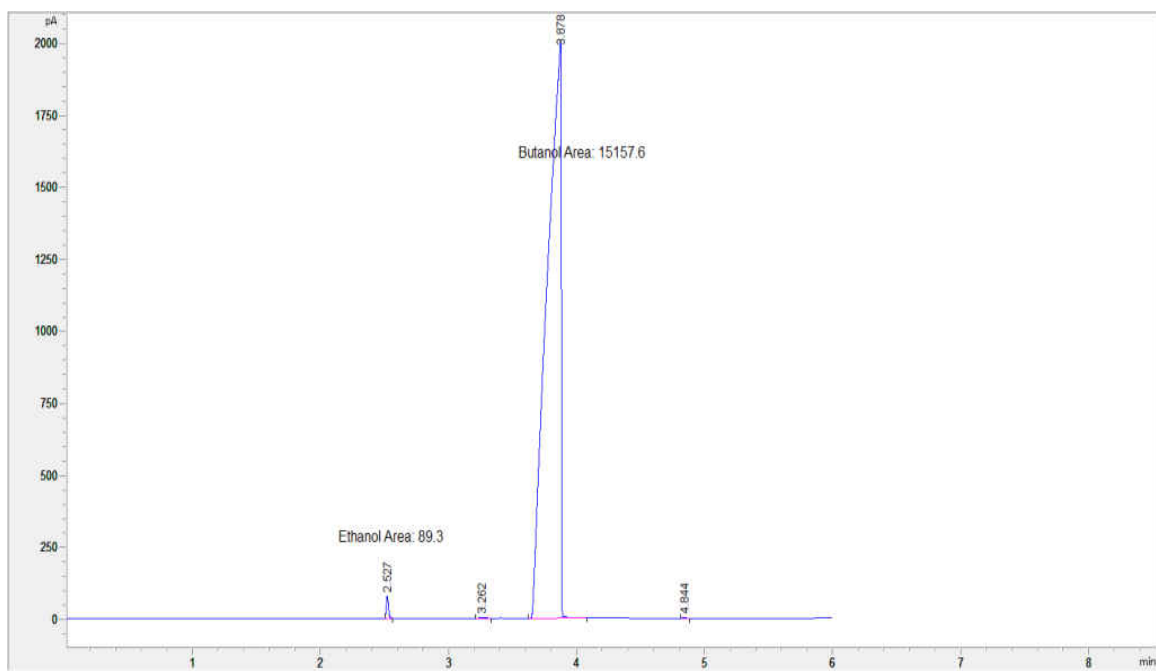


Figure A-24: Ethanol GC analysis standard run order #6.

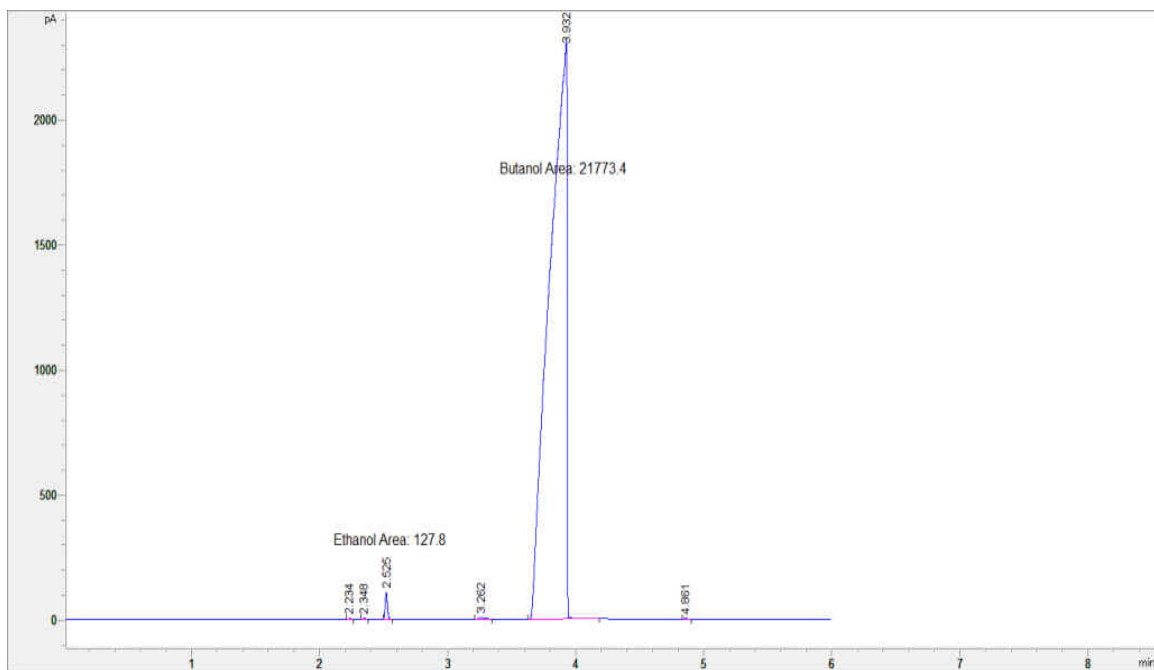


Figure A-25: Ethanol GC analysis standard run order #7.

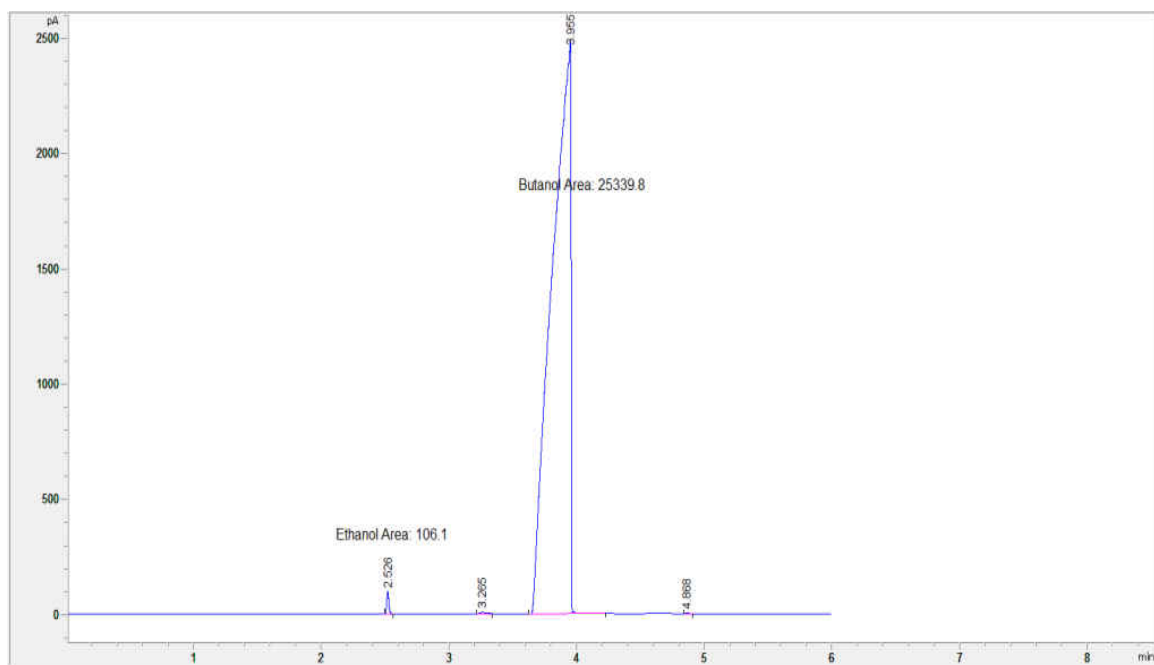


Figure A-26: Ethanol GC analysis standard run order #8.

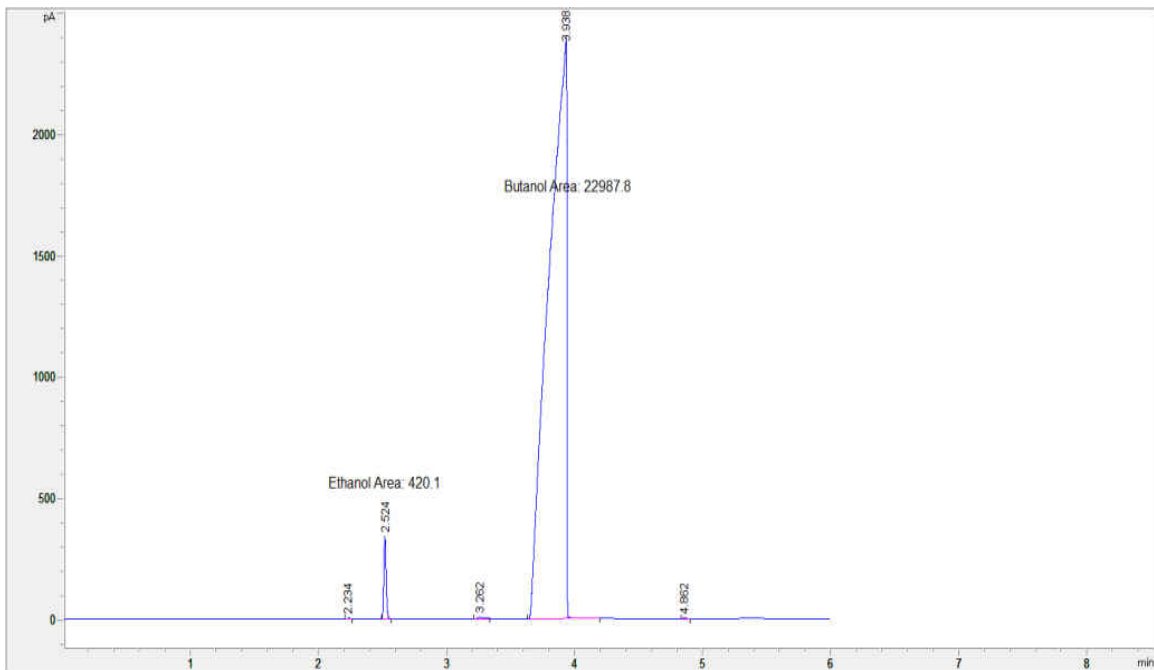


Figure A-27: Ethanol GC analysis standard run order #9.

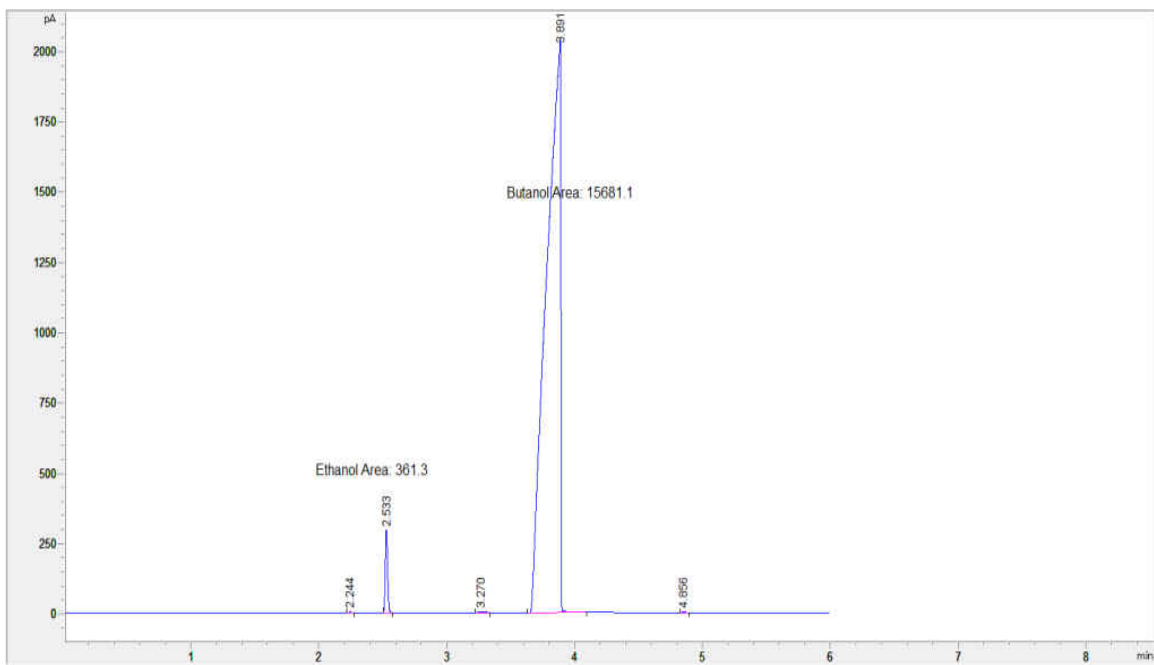


Figure A-28: Ethanol GC analysis standard run order #10.

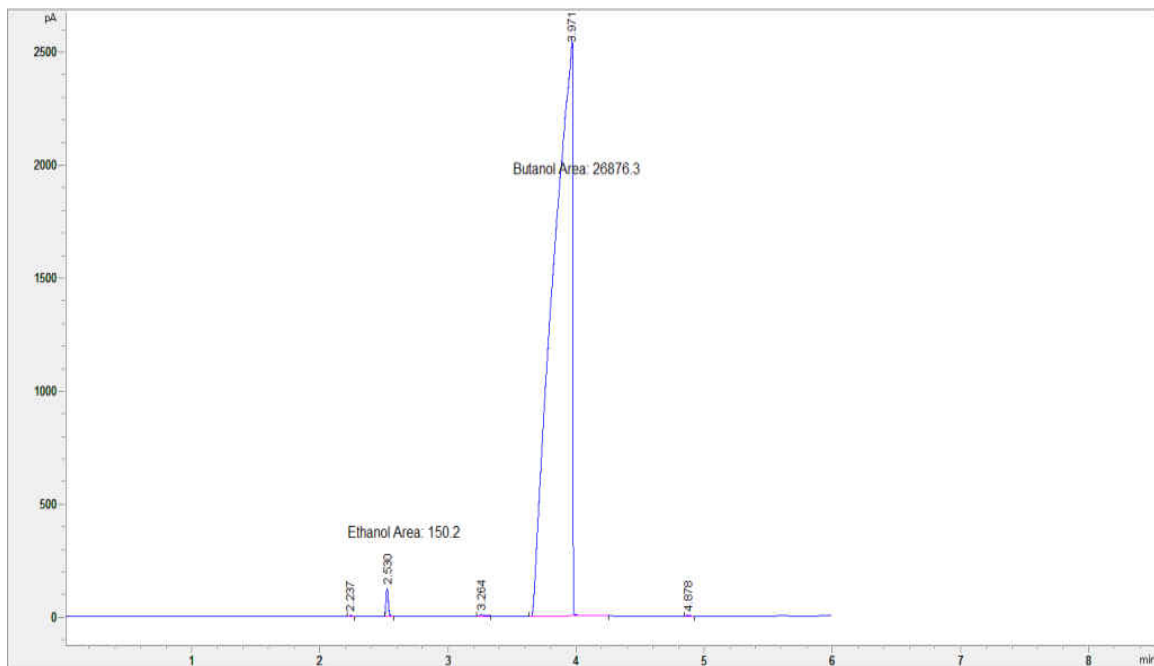


Figure A-29: Ethanol GC analysis standard run order #11.

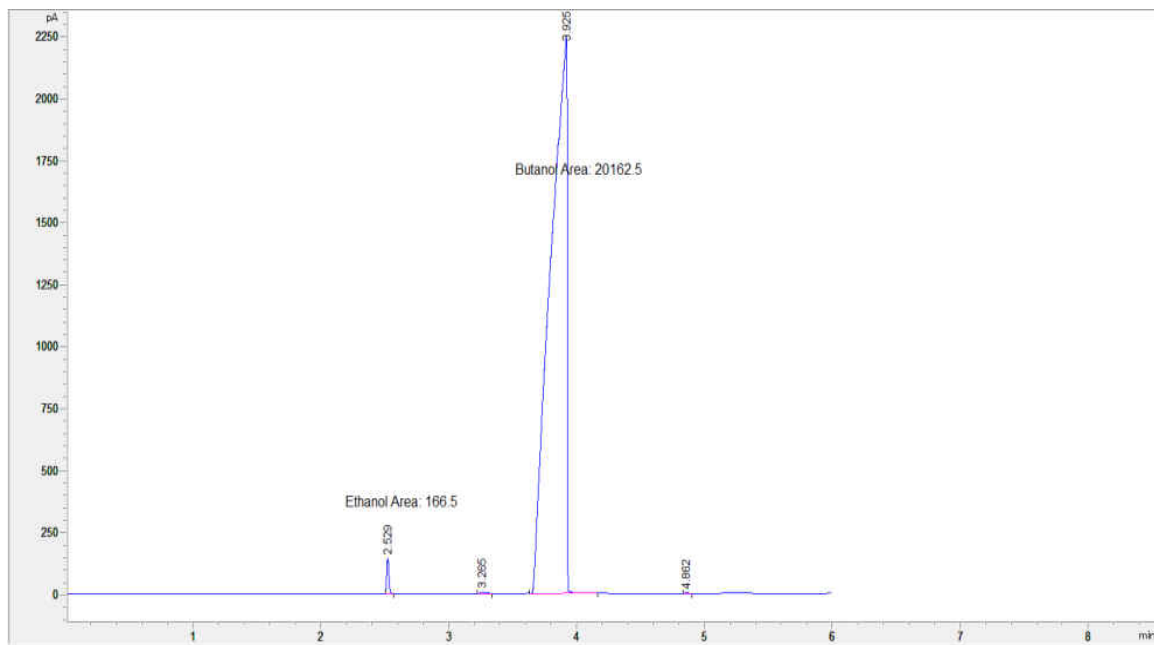


Figure A-30: Ethanol GC analysis standard run order #12.

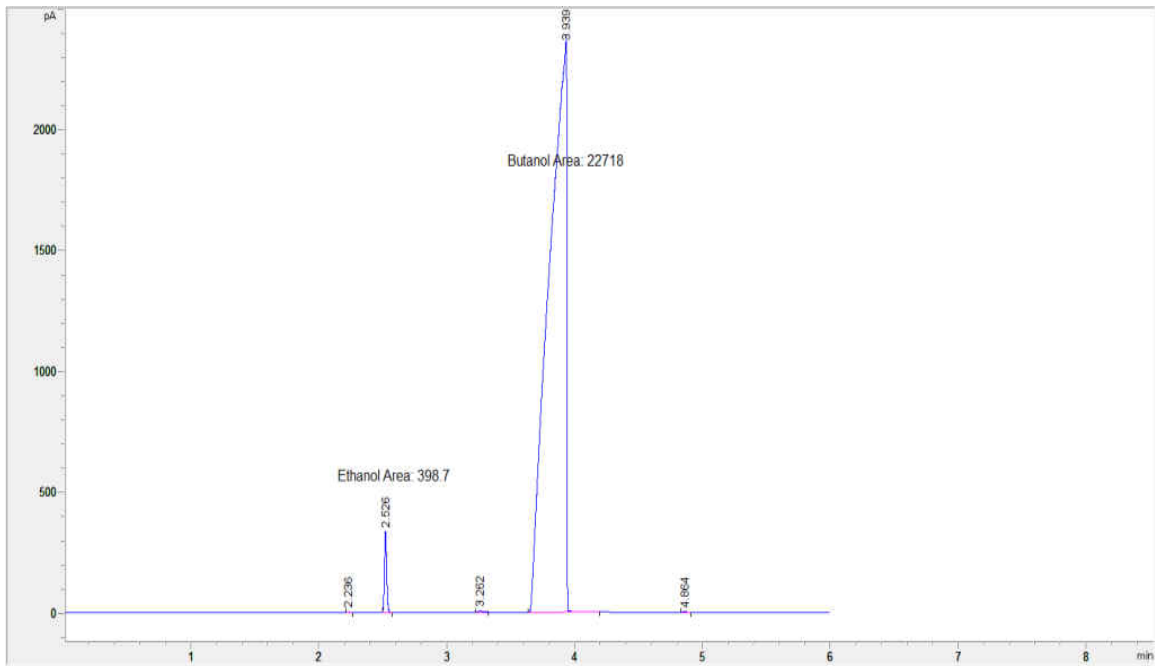


Figure A-31: Ethanol GC analysis standard run order #13.

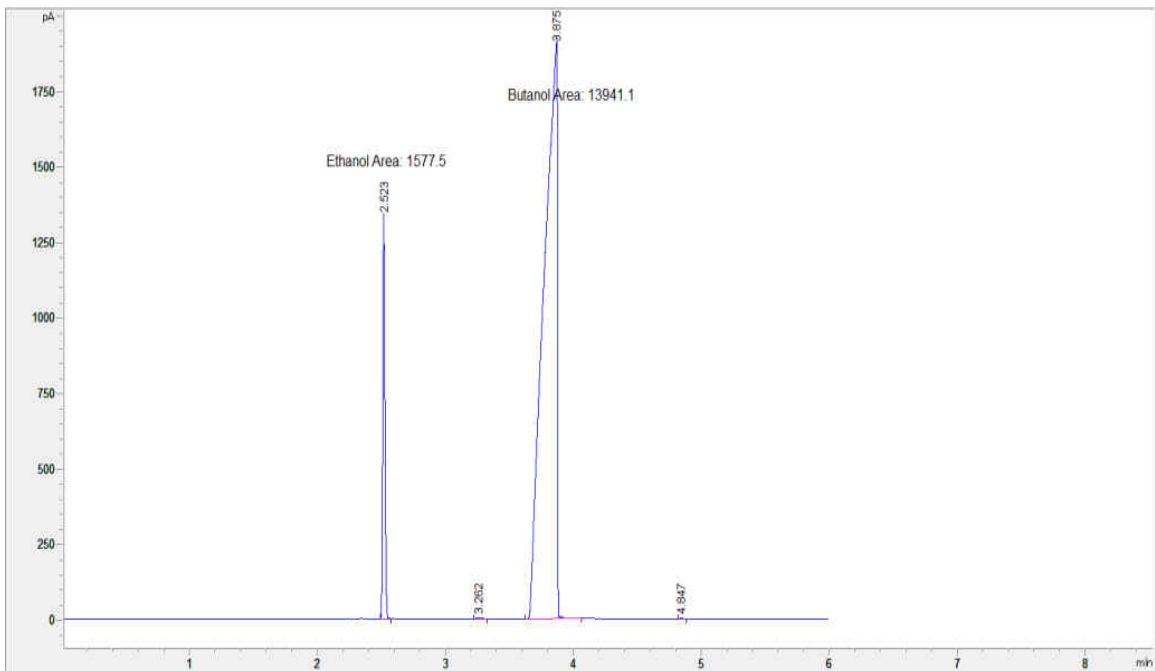


Figure A-32: Ethanol GC analysis standard run order #14.

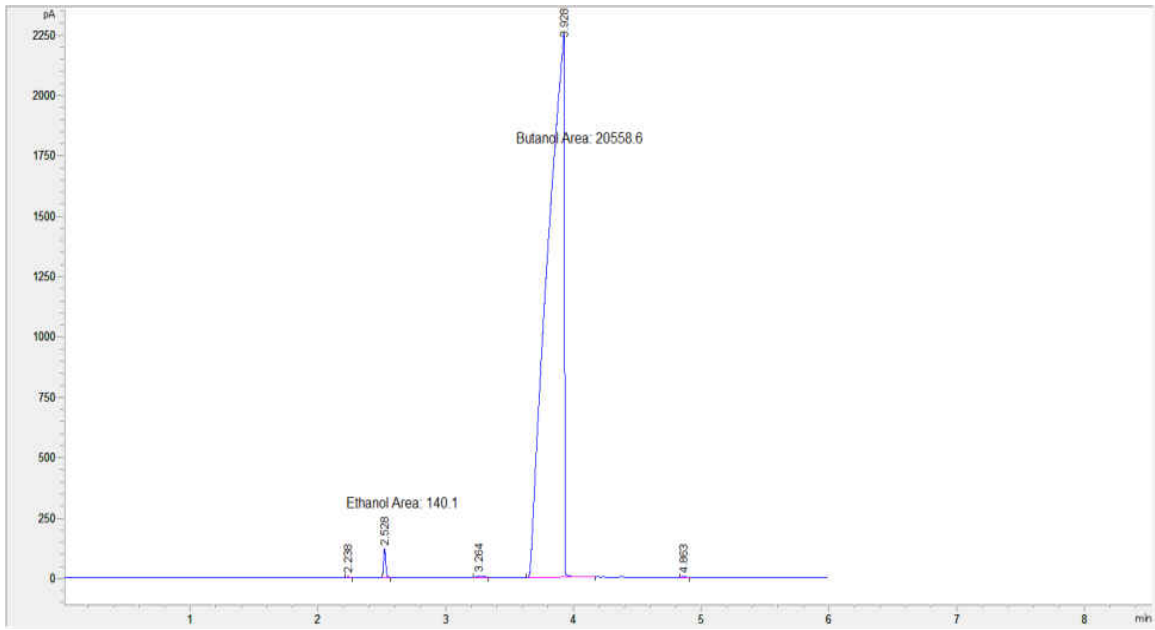


Figure A-33: Ethanol GC analysis standard run order #15.

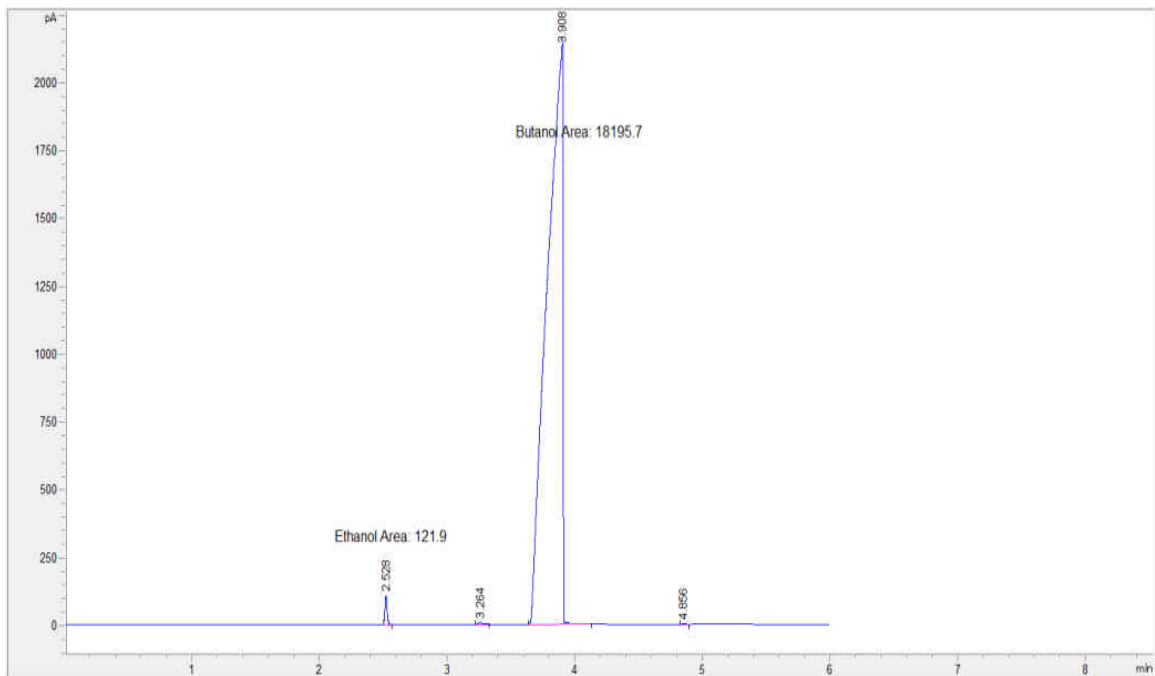


Figure A-34: Ethanol GC analysis standard run order #16.

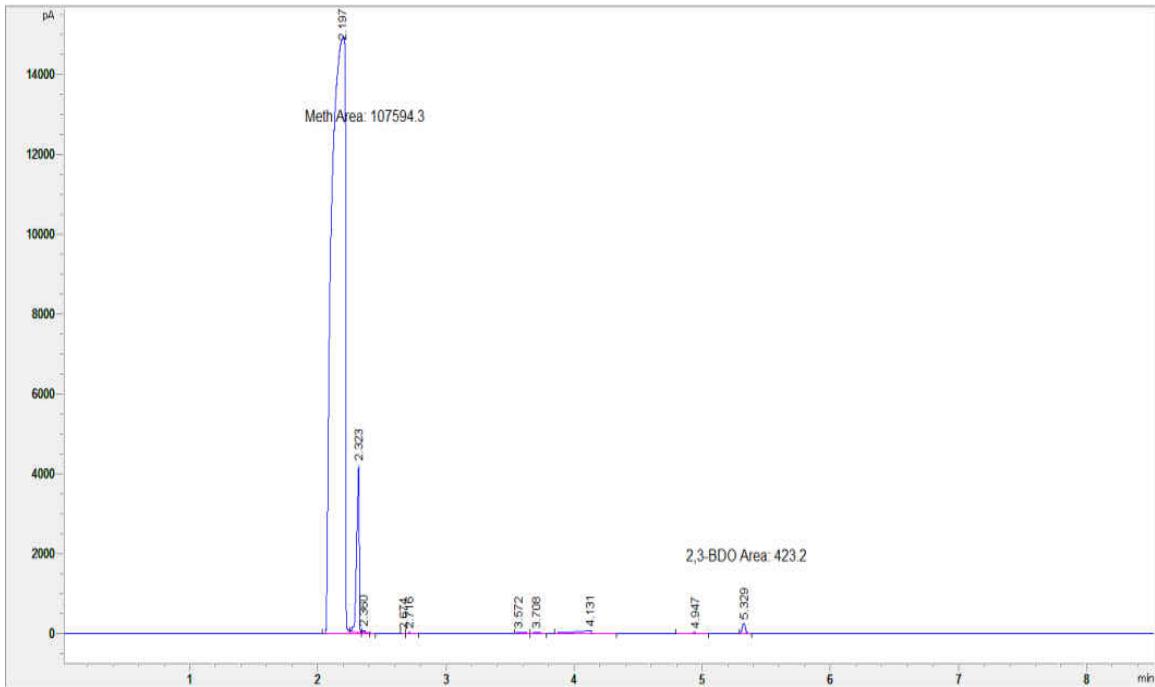


Figure A-35: 2,3-BDO GC analysis from syngas at 24 hours.

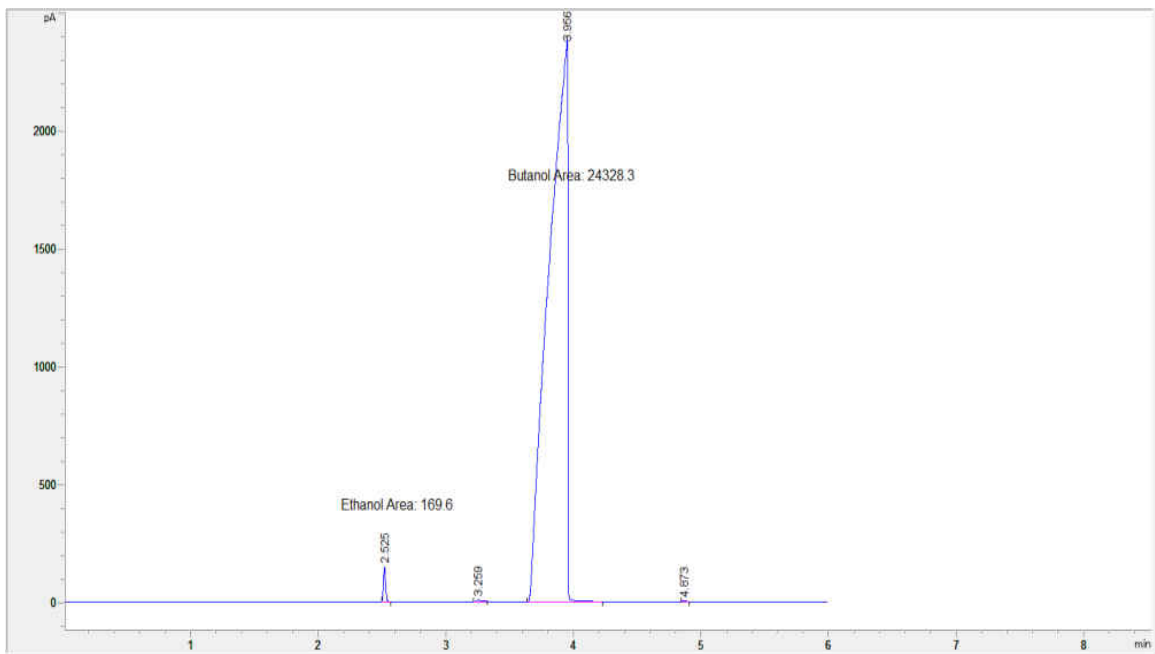


Figure A-36: Ethanol GC analysis from syngas at 24 hours.